National Library of Canada
Bibliothèque nationale du Canada

Canadian Theses Service
Service des thèses canadiennes

Ottawa, Canada
K1A 0N4

NOTICE

The quality of this microform is heavily dependent upon the quality of the original thesis submitted for microfilming. Every effort has been made to ensure the highest quality of reproduction possible.

If pages are missing, contact the university which granted the degree.

Some pages may have indistinct print especially if the original pages were typed with a poor typewriter ribbon or if the university sent us an inferior photocopy.

Previously copyrighted materials (journal articles, published tests, etc.) are not filmed.

Reproduction in full or in part of this microform is governed by the Canadian Copyright Act, R.S.C. 1970, c. C-30.

AVIS

La qualité de cette microforme dépend grandement de la qualité de la thèse soumise au microfilmage. Nous avons tout fait pour assurer une qualité supérieure de reproduction.

S'il manque des pages, veuillez communiquer avec l'université qui a conféré le grade.

La qualité d'impression de certaines pages peut laisser à désirer, surtout si les pages originales ont été dactylographiées à l'aide d'un ruban usé ou si l'université nous a fait parvenir une photocopie de qualité inférieure.

Les documents qui font déjà l'objet d'un droit d'auteur (articles de revue, tests publiés, etc.) ne sont pas microfilmés.

La reproduction, même partielle, de cette microforme est soumise à la Loi canadienne sur le droit d'auteur, SRC 1970, c. C-30.

NL-339 (r. 88/04)

Canada

THE UNIVERSITY OF ALBERTA

PARITY VIOLATION IN NUCLEON-NUCLEON SCATTERING

by

KHALED EZZAT AHMED NEGM

A THESIS

SUBMITTED TO THE FACULTY OF GRADUATE STUDIES AND RESEARCH
IN PARTIAL FULFILMENT FOR THE DEGREE OF MASTER OF SCIENCE

IN

NUCLEAR PHYSICS

DEPARTMENT OF PHYSICS

EDMONTON, ALBERTA

SPRING 1988

Permission has been granted to the National Library of Canada to microfilm this thesis and to lend or sell copies of the film.

The author (copyright owner) has reserved other publication rights, and neither the thesis nor extensive extracts from it may be printed or otherwise reproduced without his/her written permission.

L'autorisation a été accordée à la Bibliothèque nationale du Canada de microfilmer cette thèse et de prêter ou de vendre des exemplaires du film.

L'auteur (titulaire du droit d'auteur) se réserve les autres droits de publication; ni la thèse ni de longs extraits de celle-ci ne doivent être imprimés ou autrement reproduits sans son autorisation écrite.

ISBN 0-315-42804-X

THE UNIVERSITY OF ALBERTA

RELEASE FORM

NAME OF AUTHOR:	KHALED EZZAT AHMED NEGM
TITLE OF THESIS:PARITY	PARITY VIOLATION IN NUCLEON-NUCLEON SCATTERING
DEGREE:	MASTER OF SCIENCE
YEAR THIS DEGREE GRANTED:	1988

Permissionis hereby granted to THE UNIVERSITY OF ALBERTA LIBRARY to reproduce single copies of this thesis and to lend or sell such copies for private, scholarly or scientific resrech purpose only.

The author reserves other publication rights, and neither the thesis nor extensive form it may be printed or otherwise reproduced without the author's written permission.

Signature

Permanent address:
Mohamed Bader Str., #14
Kobry El-Koba,
Cairo, EGYPT.

Date: Dec. 16th, 1987.

THE UNIVERSITY OF ALBERTA

FACULTY OF GRADUATE STUDIES AND RESEARCH

The undersigned certify that they have read, and recommend to the Faculty of Graduate Studies and Research for acceptance, a thesis entitled PARITY VIOLATION IN NUCLEON-NUCLEON SCATTERING submittedby KHALED EZZAT AHMED NEGM in partial fulfilment of the requirements for the degree of MASTER OF SCIENCE in NUCLEAR PHYSICS.

.....

Supervisor

.....

.....

.....

Date: Dec. 16/87

This work is dedicated to

my

Parents, Brother, Uncle, and Aunt.

ABSTRACT

Parity non-conservation (PNC) is always regarded as one of the striking features of symmetry breaking rules. This review, starts with the different forms of symmetry breaking features as observed in nuclear physics. As a major of PNC effect, the scattering asymmetry is represented as an effect influenced by the PNC and parity conserving (PC) effects. Therefore, a detailed review for the different ways of measuring the PC observables and their theoretical significances are introduced. On the other hand, the same thing is represented for the PNC effects as well. As PNC effects are regarded as a common feature of weak interaction, different forms of weak hamiltonians are represented and therefore a detailed study of different ways of representing parity nonconserving potentials is introduced. A complete study for the different ways of theoretical representations for the PNC effects are introduced for different energy ranges are explained. Also, a study of the different forms of weak coupling constants are introduced.

This review tries to introduce an overall review of the present updated state of investigations of PNC effects in nuclei.

ACKNOWLEDGMENTS

I would like to thank my supervisor, Dr. Helmy Sherif, for his guidance and support during the course of this work.

I am grateful to Dr. G. Roy, for helping in the early stages of this work by discussing many important aspects related to this work.

Thanks to Dr. Nathan Rodening, for helping in solving many software problems related to the graphing codes which have been used in this work. Thanks to Dr. R. Sawafta for sharing physics and computer knowledge as well.

To my fellows graduate students, J. Johanson, P. Langill, and G. Lotz for your knowledge and encouragement, I wish you all a happy future.

Thanks to my friends in the M.S.A. and M.C.E. associations for their continues encouragement.

I would like to thank the University of Alberta and the Department of Physics for their continues support in the forms of RA's and TA's during my degree as a graduate student.

Last, by no means least, I'd like to thank my family for their love, patience, support, understanding, and encouragement.

Table of Contents

Chapter		Page
I.	Introduction	1
II.	Review on Parity Non-conservation in Nuclear Physics	5
	II.1. Parity and Time Reversal Invariance	5
	II.2. Electromagnetic Transitions	8
	II.3. Nuclear Wavefunction with Mixed Parity	10
	II.4. Detection of PNC Effect in Strongly Interacting Systems	14
	II.4.a. Longitudinal Analyzing Power	16
	II.4.b. γ-Ray Circular Polarization	17
	II.4.c. γ-Ray Asymmetries	18
	II.5. Parity Non-Conservation in Nuclei	19
	II.5.a. PNC Effect in the $n+p \rightarrow d+\gamma$ Reaction	19
	II.5.b. PNC in α-Decay	21
	II.5.c. PNC Effect in Electromagnetic Nuclear Transitions	22
	II.5.d. PNC Effect in Nuclear Scattering	24
III.	Parity Conserving Nucleon-Nucleon Interaction	26
	III.1. Invariance Principles	26
	III.1.a. Rotational Invariance	28
	III.1.b. Space Reflection Invariance	29
	III.1.c. Time Reversal Invariance	30
	III.1.d. The Exclusion Principle	30
	III.2. The scattering Matrix	31
	III.3. Types of Experiments and their Theoretical Interpretations	34
	III.3.a. Differential Cross Section and Polarization	35
	III.3.b. Polarization Analysis	36
	III.3.c. Use of a Polarized Target	37
	III.3.d. Depolarization and Rotation Parameters	38
	III.3.e. The Spin Correlation Parameters	41

III.3.f. Formulae for Observables 44
III.4. The Phase-Shift Parametrization of the Spin Matrix 44
III.5. Parametrization of the S Matrix in the Coupled States 46
III.6. Separation of Nuclear and Coulomb Contributions 47
III.7. Observables From SAID 48

IV. Parity Non-Conservation in Proton-Proton Scattering 60
IV.1. Parity Nonconseving Nucleon-Nucleon Potentials 61
IV.2. Meson Exchange PNC NN Potential 63
IV.2.a. π,ω,ρ Exchanges 65
IV.2.b. Two-Pion Exchange 66
IV.3. Two-Nucleon S-P Amplitudes 68
IV.4. PNC asymmetry in P-P scattering 70
IV.5. Scattering Asymmetry from 10 MeV and 5.3 GeV 75
IV.6 The Scattering Asymmetry and the Weak Coupling Constants 81

V. Conclusion 84

References 85

Vita 89

List of Tables

Table		Page
I.1	Each Piece of the Weak Interaction Hamlitonian as can be Tested in the Decay or Scattering Experiments (TA80).	3
II.1	P and TRI Selection Rules.	8
II.2	Experimental data and theoretical predictions for various nuclear PNC processes.	20
III.1	Different Combinations of tensors contributing in the scattering amplitude.	28
III.2	Behavior of the rotationally invariant combinations under other transformations.	29
IV.1	Effect of J_w's and J_z's on the Isospin and Strangness.	62
IV.2	Effect of the Charged Current-Current Terms of the Lagrangian on the Isopsin and Strangness.	63
IV.3	Weak Coupling Constants from "Best Value" and "Reseonable Range".	66
IV.4	Nucleon-Nucleon S-P weak scattering ampliutdes and meson-exchange equivlants.	69
IV.5	The Values of Five Parametrs for the Weak NN Vertex.	73
IV.6	Comaprison between experimental reults and calculations for the asymmetry over the energy range from 10 MeV to 5.3 GeV.	78

IV.7 Contributions of 2π and $2\pi+\rho+\omega$ exchanges to the Asymmetry $A_{pp}x10^{-7}$. 81

List of Figures

Figure		Page
I.1	Outline of the theoretical scheme for extracting information on weak interactions from PNC in nuclei.	2
II.1	Classical example of parity and time-reversal transformations for electric (d_e) and magnetic (μ_m) dipole moments.	6
II.2	Graphical description of the total transition rate : (a+b) allowed e.m. transitions in the absence of the weak PNC forces. (c-f) wavefunction admixture contributions, (g) direct effective PNC e.m. transition.	9
II.3	Schematic representation of two classes of PNC experiments: (a) type I, (b) type II.	15
II.4	Schematic explanation of a major source of systematic error in asymmetry measurements.	17
II.5	Valance nucleons are interacting with the core of the nuclei through the action of VPNC. The photon can be emitted in any of the five different ways.	22
II.6	Levels in 181Ta involved in the PNC experiment. Regular [$\mathbb{M}(1)$, $\mathbb{E}(2)$] and irregular $\mathbb{E}'(1)$ multipoles for the 482 KeV transition are indicated together with spins and parities (J^π).	23
III.1	Kinematic diagram for the nucleon-nucleon scattering. The unit vectors $\hat{\mathbf{k}}$, $\hat{\mathbf{N}}$, and $\hat{\mathbf{P}}$ are used in the text.	27
III.2	The scattering of polarized nucleons with their spin along the z-axis.	37

III.3	Directions of polarization vectors in the scattering plane.	40
III.4	The parameter A for pp scattering.	50
III.5	The parametr A for np scattering.	50
III.6	The parameter A_{xx} for pp scattering.	51
III.7	The parameter A_{xx} for np scattering.	51
III.8	The parameter A_{yy} for pp scattering.	52
III.9	The parameter A_{yy} for np scattering.	52
III.10	The parameter A_{zz} for pp scattering.	53
III.11	The parameter A_{zz} for np scattering.	53
III.12	The parameter C_{kk} for pp scattering.	54
III.13	The parameter C_{kk} for np scattering.	54
III.14	The parameter C_{kp} for pp scattering.	55
III.15	The parameter C_{kp} for np scattering.	55
III.16	The parameter C_{pp} for pp scattering.	56
III.17	The parameter C_{pp} for np scattering.	56
III.18	The parameter D for pp scattering.	57
III.19	The parameter D for np scattering.	57
III.20	The parameter P for pp scattering.	58

III.21	The parameter P for np scattering.	58
III.22	The parameter R for pp scattering.	59
III.23	The parameter R for np scattering.	59
IV.1	Contribution to PNC NN forces: (a) point interaction, (b) NN interaction including one-boson-exchange (OBE).	60
IV.2	2π-exchange diagrams (a) ΔI=0, 2 (BLa60), (b) ΔI=1 (DE72), (c) ΔI=0 and other possibilities (MU86).	67
IV.3	The total asymmetry as a function of the center of mass angel.	71
IV.4	The two main contributions to the scattering asymmetry at low energies (the vertical scale is arbitrary).	72
IV.5	Energy dependence of the dominating amplitudes calculated with Paris potential.	74
IV.6	Shape of the major two phase shifts affecting the scattering.	75
IV.7	Comparison between ρ,ω contributions and 2π exchanges to the total asymmetry (vertical scale is arbitrary).	77
IV.8	The scattering asymmetry for different calculations and experiments.	79
IV.9	Comaprison between elastic and total cross sections contributions for the pp interaction.	80
IV.10	Angular distribution for the scattering asymmetry at 230 MeV for the major contributions to the asymmetry.	82
IV.11	Comparison between results and calculations for the weak coupling constants satisfying equations (IV.IIb and c).	82

CHAPTER I

INTRODUCTION

Symmetries have always played a central role in the development of physics. Whenever dynamical laws of motion are not well established, symmetries and their associated conservation laws give useful restrictions on the nature of the forces.

Among the symmetries of physical laws, those associated with space-time have been crucial in classical as well as quantum theories. In addition to the invariance under continuous transformations, there are those related to discrete transformations. Of particular importance are parity (P) or space inversion and time reversal invariance (TRI) or time inversion.

Since the discovery of parity nonconservation (PNC) by Lee and Yang (LE56), it became a fact in nuclear physics and was taken into consideration. As early as 1956, Lee and Yang said: 'If parity is not strictly conserved, all atomic and nuclear states become mixtures consisting mainly of the states they are usually assigned together with small percentages of states possessing the opposite parity...PNC implies the existence of interactions which mix parities....'

Although many properties of the weak interaction are presently under scrutiny via studies at the very highest-energy accelerators, there is also a great deal of interest in experiments which probe the weak forces via low energy, PNC nuclear processes (TA73). Although substantial experimental as well as theoretical efforts have been exerted in this field for well over a decade, there are still some difficulties facing both endeavors.

In most early work on this subject, authors started directly from a model weak Hamiltonian and calculated experimental predictions with which measured results were compared. More recently it has become apparent that a more sensible approach is to break the calculation into two parts. One part involves analyzing the various experimental numbers to produce reliable values for the weak nucleon-nucleon meson vertices. This approach, requiring nuclear physics expertise and detailed nucleon wave function information, has been pioneered by Desplanques and Missimer (DE78) and Box *et al.* (BO76a). The second part is an exercise in elementary particles physics

and attempts to calculate the matrix eléments

$$<MN|\mathcal{H}_w|N>, \qquad (I.1)$$

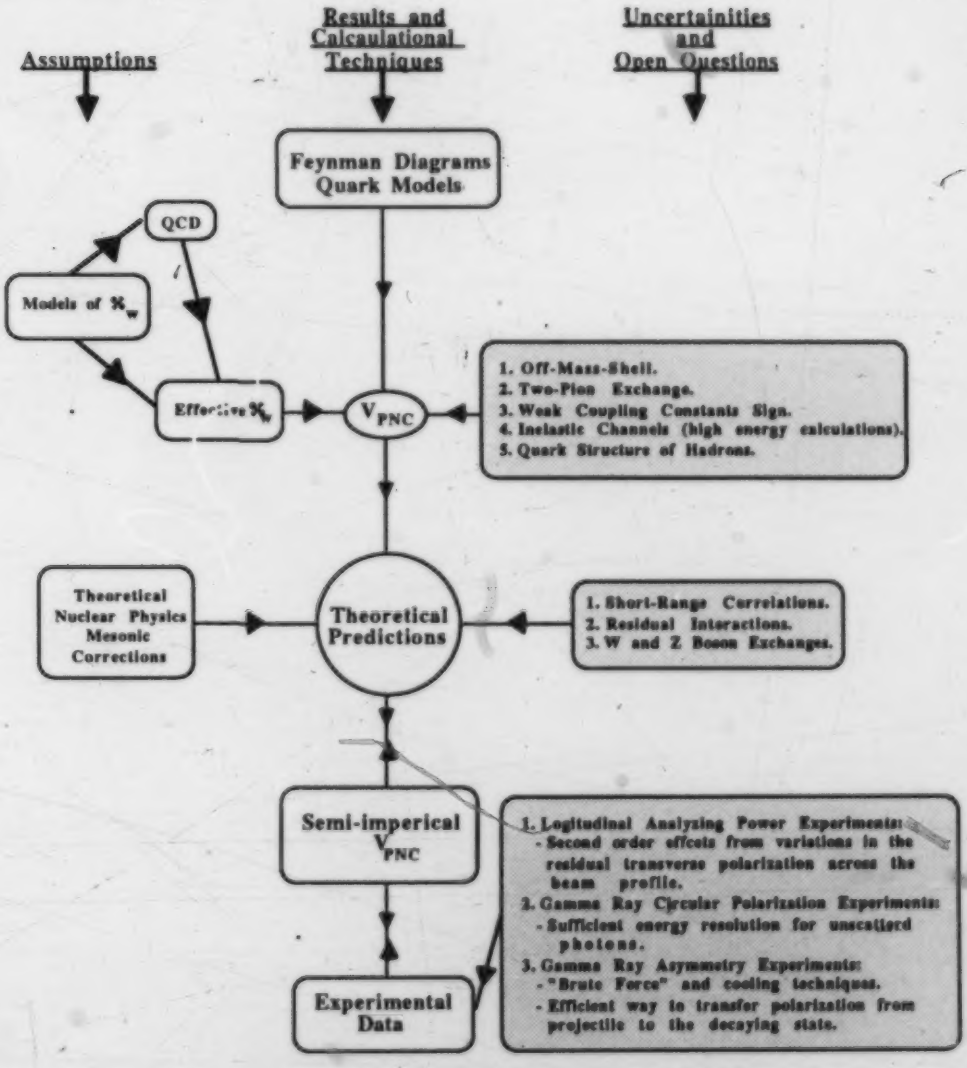
Assumptions
Results and Calcaulational Techniques
Uncertainities and Open Questions
Feynman Diagrams Quark Models
QCD
Models of $\mathcal{H}_w$
Effective $\mathcal{H}_w$
V_{PNC}
1. Off-Mass-Shell.
2. Two-Pion Exchange.
3. Weak Coupling Constants Sign.
4. Inelastic Channels (high energy calculations).
5. Quark Structure of Hadrons.
Theoretical Nuclear Physics Mesonic Corrections
Theoretical Predictions
1. Short-Range Correlations.
2. Residual Interactions.
3. W and Z Boson Exchanges.
Semi-imperical V_{PNC}
Experimental Data
1. Logitudinal Analyzing Power Experiments:
- Second order effects from variations in the residual transverse polarization across the beam profile.
2. Gamma Ray Circular Polarization Experiments:
- Sufficient energy resolution for unscattered photons.
3. Gamma Ray Asymmetry Experiments:
- "Brute Force" and cooling techniques.
- Efficient way to transfer polarization from projectile to the decaying state.

***Figure* I.1. Outline of the theoretical scheme for extracting information on weak interactions from PNC in nuclei .**

starting from the structure of the weak Hamiltonian $\mathcal{H}_w$, in which the weak interaction Hamiltonian can be divided into leptonic (L), semileptonic (SL), strangeness nonconserving nonleptonic ($\Delta S \neq 0$, NL), and strangeness conserving nonleptonic ($\Delta S = 0$, NL) types

$$\mathcal{H}_w = H_L + H_{SL} + H_{NL}^{\Delta S=0} + H_{NL}^{\Delta S=1} . \qquad (I.2)$$

Each term in equation (I.2) corresponds to a particular type of weak process and can be tested either through decay or scattering experiments, as indicated in table I.1. From the very beginning of the discovery of weak interactions, the H_L and H_{SL} terms have been studied through nuclear β-decay, μ-decay and semileptonic decays of strange particles. Nonleptonic decays of strange particles have also yielded valuable information on the $H_{NL}(\Delta S \neq 0)$ term in equation (I.2).

I give a review in the present work, in chapter II, I give a review of the PNC

Table I.1
Each Piece of the Weak Interaction Hamiltonian as can be Tested in the Decay or Scattering Experiments (TA80).

Hamlitonian	Experiment performed : Yes, No	
	Decay	Scattering
H_L	Yes	No
H_{SL}	Yes	Yes
$H_{NL}^{\Delta S=1}$	Yes	No
$H_{NL}^{\Delta S=0}$	Yes	Yes

effects in nuclear physics, restrictions imposed by selection rules on symmetry operations, and how to introduce a wavefunction with mixed parity. A review of the various experimental methods for detecting PNC effects is given as well.

In chapter III, I review on parity conserving nucleon-nucleon interaction, how to represent the scattering matrix and its parametrization in terms of

phaseshifts. Section have been devoted to the use of the computer code SAID, which computes the NN amplitudes and observables.

In chapter IV, I discuss the PNC effects in nucleon-nucleon scattering, particularly proton-proton scattering. Various forms of PNC potentials will be discussed, and the formalism and investigation of the total scattering asymmetry will be introduced. A special section will be devoted to the comparison between experimental data and different types of calculations over a wide range of energy from 10 MeV to 5.3 Gev.

CHAPTER II

REVIEW OF PARITY NON-CONSERVATION EFFECTS IN NUCLEAR PHYSICS

Before 1956 the evidence for the invariance under parity, charge-conjugation, and time-reversal transformations was thought to be extremely strong. All tests in atomic, nuclear and particle physics indicated the validity of these symmetries. However, as Lee and Yang (LEa56) pointed out, there were no tests of these invariances for the weak interactions responsible for β decay and the decays of the strange particles.

In this chapter I will review the selection rules governing the parity (P) and time reversal invariance (TRI) operations in nuclear physics, how to write nuclear wavefunction with mixed parity, and a brief introduction to the PNC effects in nuclei and their possible detection in $n+p \rightarrow d+\gamma$ reaction, α-decay, electromagnetic transitions, and nuclear scattering.

II.1. Parity and Time Reversal Invariance

Here I shall discuss specifically the behavior of the electric and magnetic multipole moments and their selection rules. The quantum mechanical 2^{ℓ} static moment of a distribution of charges and currents; defined as the expectation values of the corresponding operators in a state of angular momentum j and z component m=j; for a system of n particles of 1/2 integer spins, is given by,

$$<\hat{O}(\ell)> = <\beta; j, m=j|\hat{O}(\ell)|\beta; j; m=j> , \qquad (II.1)$$

where β refers to quantum numbers other than angular momentum. One of the restrictions on equation (II.1), arises from angular momentum conservation, thus, 2^{ℓ} poles can only occur for a system with $2j \geq \ell$ (later on we will see that there are other

restrictions for P and TRI)

If parity is conserved, then the expectation value of the multipole operator vanishes unless

$$P\hat{O}(\ell)P^{-1} = \hat{O}(\ell) , \tag{II.2}$$

if we designate electric and magnetic multipoles by $\mathbb{E}$ and $\mathbb{M}$, then because

$$P\,\mathbb{E}(\ell)P^{-1} = (-1)^{\ell}\,\mathbb{E}(\ell) , \tag{II.3a}$$

$$P\,\mathbb{M}(\ell)P^{-1} = (-1)^{\ell+1}\,\mathbb{M}(\ell) , \tag{II.3b}$$

we obtain the selection the selection rules as in table II.1 (see figure II.1). Since it is primarily the low multipole moments which can be measured accurately, we consider for a nonrelativistic system the corresponding dipole operators

$$\mathbb{E}(1) = \sum_i e_i r_i , \tag{II.4a}$$

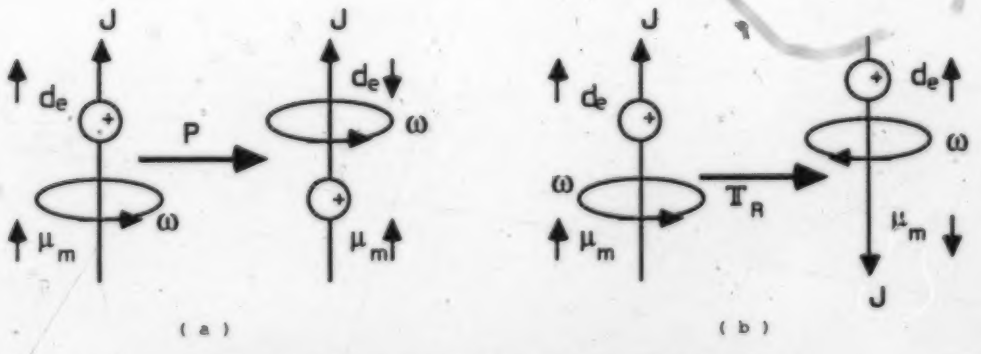

***Figure* II.1. Classical example of parity and time-reversal transformations for electric (d_e) and magnetic (μ_m) dipole moments.**

$$\mathbb{M}(1) = \sum_i (g_{i\ell}\,\ell_i + g_{is}\,s_i) , \tag{II.4b}$$

where the subscripts refer to the particles which make up the system, ℓ and s are orbital and spin angular momentum operators with the corresponding gyromagnetic ratios g. If we use the hermiticity, and the next equation

$$< \mathbb{T}_R \phi | \hat{O} | \mathbb{T}_R \psi > = < \phi(-t) | \hat{O} | \psi(-t) >^* , \tag{II.5}$$

where $\mathbb{T}_R$ is the time reversal operator and we see that TRI requires

$$<\beta; j, j | \hat{O}(\ell) | \beta; j, j > = < \beta; j, -j | \mathbb{T}_R \hat{O}(\ell) \mathbb{T}_R^{-1} | \beta; j, -j > . \tag{II.6}$$

By means of the Wigner-Eckart theorem and the properties of Clebsh-Gordon coefficients, we note that equation (II.6) implies

$$(j \ell; -m\, 0 | j\, -m)\, \mathbb{T}_R \hat{O}(\ell) \mathbb{T}_R^{-1} = (j \ell; m\, 0 | j\, m)\, \hat{O}(\ell) , \tag{II.7}$$

and the TRI requires

$$\mathbb{T}_R \hat{O}(\ell) \mathbb{T}_R^{-1} = (-1)^{\ell} \hat{O}(\ell) . \tag{II.8a}$$

For the electric moments (which arise from the charge distribution of the source), we have,

$$\mathbb{T}_R \mathbb{E}(\ell) \mathbb{T}_R^{-1} = (-1)^{\ell} \mathbb{E}(\ell) , \tag{II.8b}$$

and for magnetic moments (which arise from currents and magnetization), we have,

$$\mathbb{T}_R \mathbb{M}(\ell) \mathbb{T}_R^{-1} = (-1)^{\ell+1} \mathbb{M}(\ell) , \tag{II.8c}$$

from equations (II.3), and equations (II.8), we note that selection rules due to P and TRI

can be classified as in table II.1.

Table 1
P and TRI Selection Rules.

Symmetry	Allowed Multipole moments Electric	Magnetic
Parity (P)	even ℓ	odd ℓ
Time reversal ($\mathbf{T}_R$)	even ℓ	odd ℓ

In summary, we note that the static odd electric moments and even magnetic ones are forbidden by PC (parity conservation) and TRI, and both P and TRI must be violated for such moments to occur in nature.

II.2. Electromagnetic Transitions

Space-time symmetries also restrict the electromagnetic transitions. Such transitions may occur with the emission or absorption of photons and take place between bound states of the system.

There are also restrictions which follow from TRI, in particular to the first order in the fine structure constant, in which the electromagnetic transition matrix elements between bound states can all be chosen to be real. The proof of this assertion makes use of the hermiticity as well as TRI, and therefore requires lowest order perturbation theory to be valid for the transition. Since the fine structure constant, which controls the rate of the transition, is small compared to unity, we have,

$$< \beta'; j', m' | \hat{O}(\ell) | \beta; j, m > = (-)^{j+j'-m-m'} < \beta'; j', m' | \mathbf{T}_R \hat{O}(\ell) \mathbf{T}_R^{-1} | \beta; j, -m >^* . \qquad (II.9)$$

Together with the behavior of the multipoles under $\mathbf{T}_R$, equations (II.8), and the symmetry of the Clebsh-Gorden coefficients under reversal of the magnetic quantum

numbers, we find for the reduced matrix elements as

$$\mathbb{E}(\ell) = \langle j' \| \mathbb{E}(\ell) \| j \rangle = (-)^{\ell} \langle j' \| \mathbb{E}(\ell) \| j \rangle^{*} = (-)^{\ell} \mathbb{E}(\ell)^{*}. \qquad \text{(II.10a)}$$

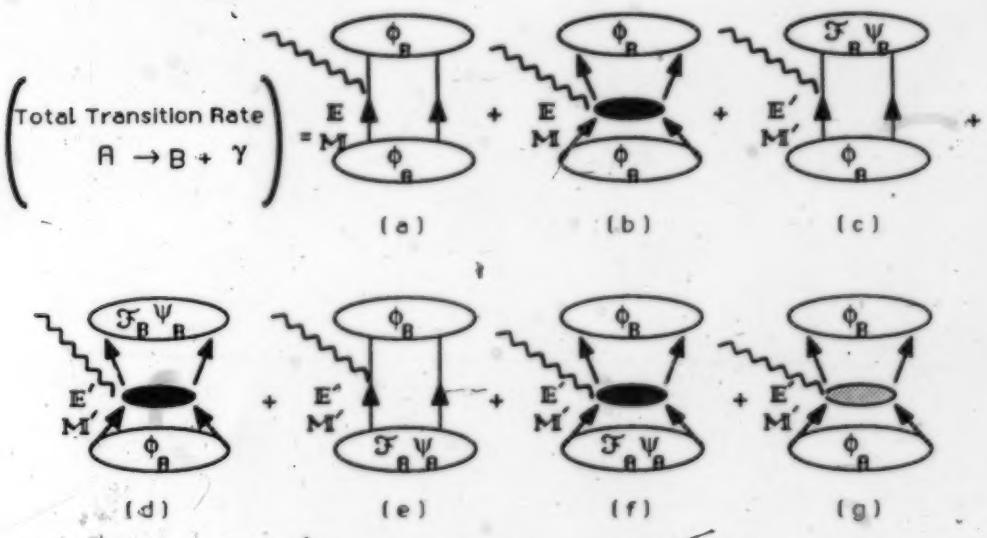

Figure **II.2. Graphical description of the total transition rate : (a+b) allowed e.m. transitions in the absence of the weak PNC forces. (c-f) wavefunction admixture contributions, (g) direct effective PNC e.m. transition (dark and dotted ellipses are PC are PNC ones respectively).**

$$\mathbb{M}(\ell) = \langle j' \| \mathbb{M}(\ell) \| j \rangle = (-)^{\ell+1} \langle j \| \mathbb{M}(\ell) \| j \rangle^{*} = (-)^{\ell+1} \mathbb{M}(\ell)^{*}. \qquad \text{(II.10b)}$$

For a PNC nuclear states A and B, we have,

$$A \overline{\overline{PNC}} \phi_A^{\pi_1} + \mathcal{F}_A \psi_A^{-\pi_1}, \qquad \text{(II.11a)}$$

$$B \overline{\overline{PNC}} \phi_B^{\pi_2} + \mathcal{F}_B \psi_B^{-\pi_2}. \qquad \text{(II.11b)}$$

The total transition T[A(i) → B(j)] is given as a sum of the following form (GA73)

$$\mathcal{T}\,A(i) \rightarrow B(j)\,] = \langle B|H_e|A\rangle$$
$$= \langle \phi_B^{\pi_2}|\mathbb{E}(\mathbf{M})|\phi_A^{\pi_1}\rangle + \mathcal{F}_A \langle \phi_B^{\pi_2}|\mathbb{E}'(\mathbf{M}')|\psi_A^{-\pi_1}\rangle +$$
$$+ \mathcal{F}_B \langle \psi_B^{-\pi_2}|\mathbb{E}'(\mathbf{M}')|\phi_A^{\pi_1}\rangle + \langle \phi_B^{\pi_2}|V_{PNC_e}(\mathbb{E}' \text{ or } \mathbf{M}')|\psi_A^{\pi_1}\rangle . \quad \text{(II.12)}$$

where $\mathbb{E}'$ and $\mathbf{M}'$ (irregular transitions) are the allowed transitions due to PNC effect. The first term of equation (II.12) is the usual allowed transition depending on the parity of the states φ_A and φ_B as shown in figures (II.2a and b). The second and third matrix elements give contributions to $\mathbb{E}'$ or $\mathbf{M}'$, because of the opposite parity of φ with respect to ψ (figures II. c-f) (GA73). The fourth matrix element represents the contributions to $\mathbb{E}$ or $\mathbf{M}$ radiation through effective parity conserving electromagnetic (PNC_e) operators (fig.II.2 g). Owing to PNC forces we have $\mathbb{E}$ and $\mathbf{M}$ transitions (for equal ℓ) between two discrete nuclear states which can lead to interference effects. Such an interference between magnetic and electric multipole radiation of the same multipole order gives rise to a circular polarization P_γ of the emitted photon. P_γ can be written as suggested by R. J. Blin-Stoyle (BL60a) as

$$P_\gamma = 2 \sum_{\ell} \frac{\langle \mathbf{M} \rangle \langle \mathbb{E}' \rangle + \langle \mathbf{M}' \rangle \langle \mathbb{E} \rangle}{\langle \mathbf{M} \rangle^2 + \langle \mathbb{E} \rangle^2} \quad \text{(II.13)}$$

Only one of the two terms in the numerator will contribute depending on the nature of the allowed transition. Note that we have no interference between different orders, e.g., $\mathbf{M}(1)\,\mathbf{M}(2)$.

II.3. Nuclear Wavefunction with Mixed Parity

In the presence of parity non-conservating interactions, we can write the total Hamiltonian of a system of n nucleon system as

$$\mathbb{H} = H_o + V_{PNC} \,, \tag{II.14}$$

where H_o is a PC Hamiltonian, and we can write the total wave function of the system as

$$\Psi_i = \psi_i^{\pi} + \mathcal{F}\, \phi_i^{-\pi}, \tag{II.15}$$

where ψ_i^{π} is the eigenstate of H_o, and $\mathcal{F}$ is the amplitude of the amount of the wavefunction with opposite parity occurring due to the influence of the PNC forces (i.e., PNC amplitude).

We can write the H_o in the form

$$H_o = T + V_{PC} \,, \tag{II.16a}$$

with the spectrum of eigenstates $\{ s(\pi); i\rangle,\ i = 1, 2, 3, \ldots \}$ given through

$$H_o \,|\, s(\pi); i \,\rangle = E_i \,|\, s(\pi); i \,\rangle \,, \tag{II.16b}$$

where s, π are the spin and parity assignment of the states, and i counts the nuclear levels.

Because V_{PNC} is very small compared to V_{PC} ($V_{PNC}/V_{PC} \sim 10^{-7}$), the eigenstate $|s; j\rangle$ of $\mathbb{H}$

$$\mathbb{H} \,|\, s; j \,\rangle = E_j \,|\, s; j \,\rangle \,; \qquad j = 1, 2, 3, \ldots \tag{II.17}$$

can be calculated by the use of the first order perturbation theory

$$|\, s; j \,\rangle = |\, s(\pi); j \,\rangle + \int\!\!\sum_{i}^{all} \mathcal{F}_i \,|\, s(-\pi); i \,\rangle \,, \tag{II.18a}$$

with

$$\mathcal{F}_i = \frac{< s(-\pi); i \mid V_{PNC} \mid s(\pi); j >}{E_j - E_i} \quad . \tag{II.18b}$$

The summation in equation (II.18a) extended over all eigenstates of H_0, say, all bound and continuum states as indicated by $\int$. And in general the summation in equation (II.18a) will be restricted to a finite number of eigenstates of H_0. In actual calculations it is preferred to use the following expression instead of expression (II.18a)

$$| s; j >^m = | s(\pi); j > + \sum_i^m \mathcal{F}_i \, | s(-\pi); i > \, , \tag{II.18c}$$

where m is the number of states actually taken into account. The state $| s; j>^m$, however, is no an longer eigenstate of $\mathbb{H}$,

$$\mathbb{H} \, | s; j >^m \neq E_j \, | s; j >^m , \tag{II.18d}$$

which shows that the wavefunction $< x_1, ..., x_n \mid s; j >^m$ will not have the required asymptotic behavior for large x.

The usual way of calculating nuclear structure properties is to start from a shell model description which makes use of the fact that the interaction between nucleons can be divided into two parts: (i) An average field U_i, and (ii) the residual interaction V_{res},

$$H_o = H + V_{res} \, , \tag{II.19a}$$

with

$$H = \sum_i T_i + \sum_i U_i \, , \tag{II.19b}$$

and

$$V_{res} = -\sum_i U_i + \sum_{ij} V_{PNC_{ij}} , \qquad \text{(II.19c)}$$

where H defines our model space as

$$H(i)|a_i> = \varepsilon_{a_i}|a_i> , \qquad \text{(II.19d)}$$

which describe the bulk properties of the nucleus, while V_{res} contains all parts of the NN interaction which cannot be taken into account into the average filed U_i. Actual calculations are done by the use of oscillator or Woods-Saxon type single particle (s.p.) wavefunctions. The residual interaction is either neglected, or treated in a phenomenological way in the space defined by H. The resulting approximate wavefunctions $\varphi'(1 \ldots n)$ of H_0 are then given by a superposition of s.p. Slater determinants $\varphi(1 \ldots n)$,

$$|\phi> = \prod_{a_i} a^{\dagger}_{a_i} |0> . \qquad \text{(II.20)}$$

The wavefunctions $\varphi'(1 \ldots n)$ then have the disadvantage of having lost all the effects of the NN interaction at small relative distances and thus are highly incorrect for relative distances smaller than 1 fm. Especially those wavefunctions are not zero inside the hard-core region as required by the strong NN interaction.

Also the long range properties of the eigenstate φ' are important and thus V_{res} should not be neglected either as in a pure shell-model description. This is the more important when one does take into account not only the lowest excited states in the equation (II.18a). The most important requirements on the wavefunctions of the strongly interacting system H only, can be summarized as follows: (i) a relativistic description of the bound states, which means good reproduction of the observed energy spectrum and transition probabilities; at least up to few MeV of excitation energies, (ii) good description of the relative motion of two particles inside a nucleus for a small relative distances short-range correlation (SRC); i.e., wavefunctions which include the effect of the strong repulsive core of the strong NN interaction.

II.4. Detection of PNC Effect in Strongly Interacting Systems

The PNC experiments fall into three general classes (WI58): (i)Type I: experiments determine rates of processes that would vanish if parity were exactly conserved. The only practical examples involve α decays. Parity conservation forbids any unnatural parity state from decaying to a 0^+ state by α emission. An example is

$$^{16}O(2^-) \rightarrow {}^{12}C(0^+) + \alpha \ , \qquad \text{(II.21a)}$$

which competes with the PC γ-decay

$$^{16}O(2^-) \rightarrow {}^{16}O + \gamma \ . \qquad \text{(II.21b)}$$

These type of experiments are sensitive to the probability of parity admixture in nuclear states

$$\Gamma_{PNC} \ \alpha \ |\langle f \mid H_{PNC} \mid i \rangle|^2 \ . \qquad \text{(II.22)}$$

(ii) Type II: experiments determine isoscaler observables arising from the interference of PNC and PC matrix elements. One can probe isoscaler interactions in two ways: (a) detecting the longitudinal projection of a particle's spin along its momentum, a common example is the circular polarization $\mathbf{P}_\gamma = \langle \sigma_\gamma \ . \ \mathbf{p}_\gamma \rangle$ of γ-rays emitted by unpolarized nucleus, (b) detecting PNC interactions by orienting a particle's spin perpendicular to its motion. In this case σ precesses around $\mathbf{P}$ in the presence of a PNC interaction that breaks the degeneracy of the states with $\sigma \ . \ \mathbf{p} = \pm 1$.

In all cases isoscaler measurements are proportional to the amplitude of the parity admixtures, e.g., the circular polarization produced by the interference of a PNC $\mathbf{E}(1)$ multipole with a dominant PC $\mathbf{M}(1)$ multipole is

$$\mathbf{P}_\gamma \approx 2 \, \mathrm{Re} \, \frac{\langle f | E(1) | i \rangle}{\langle f | M(1) | i \rangle} \ . \qquad \text{(II.23)}$$

(iii) Type III: experiments determine the interference of PNC and PC matrix elements but the observable is not an isoscaler. As a result the observable is second order in the weak interaction, e.g., odd power of cos θ in the angular distribution of γ-rays emitted by an isolated nuclear state, and in states of good parity, such terms must vanish. One might expect that, from statistical considerations alone, type I (which are sensitive to the square of a very small PNC amplitude) would be greatly inferior to type II (where the effects are linear in the PNC amplitude). However, this is not correct. Consider the two systems in figure (II.3), in the first two processes lead to distinct final states with amplitudes A_{PNC} and A_{PC}, e.g., A_{PNC} could correspond to the first reaction mentioned in type I and A_{PC} to the second reaction. The rate $\Gamma_{PNC} \alpha |A_{PNC}|^2$ is the observable. In the second system, two competing processes with amplitudes A^{PNC} and A_{PC} lead to a single final state, producing an isoscaler observable $P \alpha 2A_{PNC}/A_{PC}$. For definiteness, we take **P** to be γ-ray circular polarization. Assume that in each case we can produce N_0 of the decaying states. For the first system the number of PNC decays is

$$N_{PNC} = N_o \frac{\Gamma_{PNC}}{\Gamma_{PC} + \Gamma_{PNC}} \approx N_o \frac{\Gamma_{PNC}}{\Gamma_{PC}} \alpha N_o \frac{|A_{PNC}|^2}{|A_{PC}|^2} . \qquad \text{(II.24)}$$

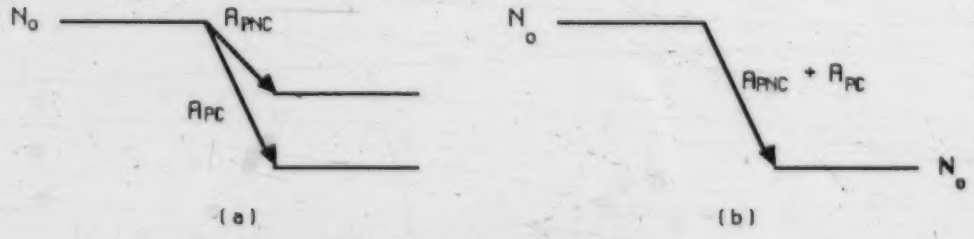

***Figure* II.3. Schematic representation of two classes of PNC experiments: (a) type I, (b) type II.**

We infer A_{PNC} from the relation $|A_{PNC}|^2=|A_{PC}|^2 N_{PNC}/N_o$. The statistical uncertainty in N_{PNC} leads to a corresponding statistical uncertainty in A_{PNC} as

$$\Delta A_{PNC} = \frac{1}{2A_{PNC}} |A_{PC}|^2 \frac{\Delta N_{PNC}}{N_o} = \frac{A_{PC}}{2\sqrt{N_o}} . \qquad (II.25)$$

For the second system assume that **P** can be detected with 100% efficiency (not necessarily a realistic assumption!). The statistical error in **P** (assuming $P \ll 1$) is $\Delta P = (N_o)^{-1/2}$. We obtain ΔA_{PNC} from equation (II.25). Therefore on statistical grounds neither class of experiments is preferred. In fact, if **P** is a γ-ray circular polarization and one includes a realistic value for the analyzing power of the circular polarimeter, the type I experiments is statistically superior (of course, in practical cases systematic errors are as important as statistical uncertainties.).

The main distinction between type I and type II is flexibility. Type I experiments are restricted to the α−decay of unnatural parity states. The process typically involves highly excited states that are difficult to describe with confidence in nuclear models. Type II experiments have been carried out in the two-nucleon and few-nucleon systems, and in many complex nuclei (the observables being linear in the weak amplitude, provide information on the sign of the weak amplitude).

II.4.a. Longitudinal Analyzing Power

The longitudinal analyzing power for reactions induced by polarized nucleons is defined by

$$A_L(\theta) = \frac{1}{P_z} \frac{\sigma^+(\theta) - \sigma^-(\theta)}{\sigma^+(\theta) + \sigma^-(\theta)} , \qquad (II.26)$$

where P_z is the longitudinal polarization of the beam and σ^+ and σ^- are cross sections for positive and negative helicity projectiles, respectively.

In polarized proton experiments the dominant systematic error are usually associated with residual transverse components of the polarization. The most difficult problems are not due to beam misalignment or to a nonzero mean transverse polarization, but to the second order effect arising from variations in the residual

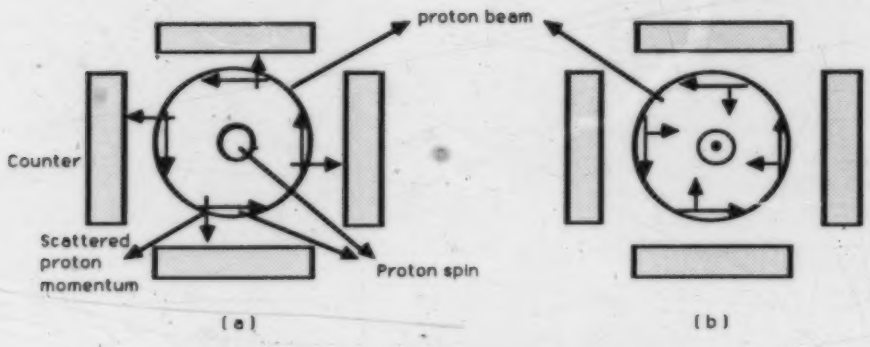

***Figure* II.4. Schematic explanation of a major source of systematic error in asymmetry measurements.**

transverse polarization across the beam profile. This is illustrated in figure (II.4). Suppose that, for positive-helicity protons, there exists on the fringes of the beam a small component of transverse polarization directed clockwise (figure II.4a). In addition, suppose that the proton scattering has a strong transverse analyzing power, A_T, so that spin-up protons scatter preferentially to the left. Then the protons scatter preferentially toward the nearer counter. Assume, that, on reversing the helicity of the beam, the transverse polarization also reverses and is directed counterclockwise (figure II.4b). Because of the transverse analyzing power, the protons scatter preferentially toward the more distant counter. This second-order solid angle effect is proportional to $\langle xp_y \rangle$ and $\langle yp_x \rangle$ and minimizes a PNC helicity dependence.

II.4.b. γ-Ray Circular Polarization

There are no efficient analyzers of γ-ray circular polarizations. Essentially all polarimeters are based on the dependence of Compton scattering by polarized electrons in magnetized Fe. Because only ≈2/26 of the electrons in Fe are polarized at saturation, the analyzing power of this polarimeter cannot exceed ≈8%. Two different geometries are employed. In the transmission geometry one looks for a small change in the transmitted γ-ray fraction when the magnetization of the Fe is reversed. Large

solid angles and good γ-ray energy resolution can be obtained with this method. In the forward scattering geometry one detects the scattered γ-ray. Energy resolution and solid angle are sacrificed for a higher analyzing power.

It is easy to compute the analyzing power for the transmission polarimeter if the γ-ray detector has sufficient energy resolution to identify the unscattered photons. For photons with circular polarization **P** incident on magnetized Fe with the electron spins parallel (s=+1) or antiparallel (s=-1) to the incident photon momentum, the Compton cross section is

$$\sigma(E_\gamma) = \sigma_o(E_\gamma) + s\,P\,\sigma_1(E_\gamma), \qquad \text{(II.27)}$$

where σ_1 is the spin dependent cross section. The polarimeter analyzing power is

$$\eta = \frac{N_R - N_L}{N_R + N_L}, \qquad \text{(II.28)}$$

where $N_R(N_L)$ is the number of right-handed (left-handed) photons transmitted by the polarimeter when the electron spins are parallel to the incident photon momentum, thus

$$\eta = \frac{\exp[-(\sigma_o + f\sigma_1)nt] - \exp[-(\sigma_o - f\sigma_1)nt]}{\exp[-(\sigma_o + f\sigma_1)nt] + \exp[-(\sigma_o - f\sigma_1)nt]} = -\tanh(f\sigma_1 nt) \approx -f\sigma_1 nt, \qquad \text{(II.29)}$$

where f is the number of polarized electrons per Fe atom, n is the number of Fe atoms per unit volume, and t is the polarimeter thickness.

II.4.c. γ-Ray Asymmetries

Asymmetry measurements are generally favored over circular polarization measurements whenever the initial state can be produced with a polarization greater than the analyzing power of the appropriate circular polarimeter. Two methods are used to polarize the initial, excited nuclear state: (i) production of the state in a reaction

induced by polarized projectile or by using a polarized targets, (ii) "brute force" polarization generated by strong crystalline fields at very low temperatures.

The "brute force" technique is possible only for levels fed in β-decay of moderately long-lived activities because of the time required to cool a sample. On the other hand, the production of polarized, excited nuclei in reactions involving polarized particles is, in principle, widely applicable. The difficulty lies in finding an efficient way to transfer the polarization from the projectile to the decaying state. In general this is maximal when the spins of the target and residual nuclei are low.

II.5. Parity Non-Conservation in Nuclei

Weak interactions in nuclei lead to the mixing of nuclear states of the opposite parity. Once weak PNC potentials are given, whether theoretical or semi-empirical, they are treated as a perturbation for the nuclear physics problem. PNC potentials determine the opposite-parity admixture to the particular nuclear state, say ψ_i. Then the new state , of undetermined parity, is (which is another form for equation II.15)

$$\Psi_i = \psi_i + \sum_{k \neq i} \frac{\langle k | V_{PNC} | i \rangle}{E_i - E_k} \psi_k = \psi_i + \mathcal{F} \phi_i . \qquad (II.30)$$

In case of complex nuclei, an accurate expression for the unperturbed state ψ_i will, in general, not available. Further, the summation should be performed over all k states that can contribute.

II.5.a. PNC Effect in the n+p→d+γ Reaction

Two PNC quantities connected with this reaction have been measured: (i) the emitted photon shows circular polarization (LOa72) and (ii) when one of the initial nucleons is polarized, γ-emission is asymmetric with respect to its spin (CAb77). An important theorems shows that the first process depends only on the ΔI=0,2

short-range part of the PNC potential, while the second process depends on the ΔI=1 term in the weak potential (DA65,71,72). The proof of the theorem depends entirely on the spin and isospin properties of the two-nucleon systems. The only assumption needed is that the weak NN interaction can be treated as a first order perturbation. Thus this reaction is important for testing the strangeness-conserving non-leptonic weak interaction. The experimental values (see table II.2) can be explained only by assuming that the vector-meson-exchange PNC potential (ΔI=0,2) is much stronger than predicated theoretically. However, if this particular result is excluded, much weaker ΔI=0,2 potentials of the theoretically predicted strength could explain other experiments.

Table II.2
Experimental data and theoretical predictions for various nuclear PNC processes.

Experiment	Result	ΔI	Theory
1. $n+p \rightarrow d+\gamma$ Circular Polarization	$P_\gamma=-(1.3\pm0.45)\times10^{-6}$ (LOa72, CA77)	0, 2	$P_\gamma=+2\times10^{-8}$
Asymmetry	$A_\gamma=(6\pm21)\times10^{-8}$	1	$A_\gamma=0.5\times10^{-8}$ (DA65,71,72, EP67,LA74)
2. $^{19}F^* \rightarrow {}^{19}F+\gamma$ 110 KeV $1/2^- \rightarrow 1/2^+$	$A_\gamma=(114\pm70)\times10^{-6}$ (EP75)	0,1	$A_\gamma=-(110\pm70)\times10^{-8}$ (HE78,BO76a,b)
3. $^{41}K^* \rightarrow {}^{41}K+\gamma$ 1.29 MeV $7/2^- \rightarrow 3/2^+$	$P_\gamma=(2.0\pm0.4)\times10^{-5}$ (LOa72)	0,1,2	$P_\gamma=-4.4\times10^{-6}$ (DE73,78)
4. $^{175}Lu^* \rightarrow {}^{175}Lu+\gamma$ 396 KeV $9/2^- \rightarrow 7/2^+$	$P_\gamma=(5.5\pm0.5)\times10^{-5}$ (LOa72)	0,1,2	$P_\gamma=-1.5\times10^{-5}$ (DE73,78)
5. $^{181}Ta^* \rightarrow {}^{181}Ta+\gamma$ 482 KeV $5/2^+ \rightarrow 7/2^+$	$P_\gamma=-(5.2\pm0.5)\times10^{-6}$ (LOa72)	0,1,2	$P_\gamma=(0.5\text{-}1.0)\times10^{-6}$ (GA73)

Although this is a two-body problem, theoretical analysis is still sufficiently involved (LA74, EP76, and CR76). For some time, existing theoretical calculations were at variance with each other. However, they have now settled at an approximate value $P\approx2\times10^{-8}$. This value takes into account all corrections including the relativistic

ones and was obtained using PNC potentials. This value is in strong disagreement with the experimental data ($P_\gamma = -(1.3\pm0.45)\times10^{-6}$ (see table II.2).

The experiment with polarized neutrons yields information on V_{PNC} which is not too dependent on the vagaries of the theoretical calculations. The asymmetry A_γ depends mostly on the long-range PNC π-exchange. Even when the short-range $\Delta I=1$ term of the PNC potential becomes strong, as in the case of semi-imperical potentials, this does not influence the result by more than 20%. The theoretical predictions of the one π-exchange contributions to A_γ seem to be rather independent of the calculational method used. The published values for A_γ are in the range $A_\gamma \approx k_\pi(0.5\text{-}0.6)\times10^{-8}$. Here k_π measures the strength of the pion potential, being unity for PNC potentials. The existing experimental value ($A_\gamma = (6\pm21)\times10^{-8}$, see table II.2) carries an error which is too large to draw any definite conclusion.

II.5.b. PNC in α-Decay

The α-decay of the 2^- state in ^{16}O (NE74) is important because it involves only the $\Delta I=0$ part of the weak interaction. The theory of α-decay is not sufficiently understood to allow precise calculations of α-decay widths. Estimates were made by calculating the ratio of irregular and regular decay widths; they did not aim at reproducing absolute values. The results depend strongly on accounting for short-range hard-core effects. In view of such calculational complications (HE69b and APa76) errors of factors of 4 for the rate are possible (BO76a,b).

Some comfort can be taken from the fact that the existing theoretical calculations agree approximately. They seem to indicate the strength of the $\Delta I=0$ PNC potential. This is supported by one analysis (BO76a) made using semi-empirical PNC potentials, another group (DE78) has drawn a different conclusion, due to the richer isospin structure of their semi-empirical potential.

II.5.c. PNC Effect in Electromagnetic Nuclear Transitions

There are three kinds of PNC effect in heavier nuclei: (i) circular polarization of γ-radiation from unpolarized nuclei, (ii) angular distribution of γ-radiation from polarized nuclei, and (iii) up-down asymmetry of γ-radiation following the capture of polarized thermal neutrons.

The theoretical analysis of processes (i) and (ii) is rather more complicated than in the two-body case because the result is affected in an important way by the PNC interaction of the valence nucleon with the nucleons in the core (see figureII.5). This effect is proportional to the product of matrix elements such as in figure (II.15b), with the summation running over all nucleons in the nucleus. As every contribution is important, the wavefunction not only must include core effects but must be known more accurately than when calculating processes in which valence nucleons are of primary importance, noting that core excitations also influence the result (DE73). The result also depends on short-range NN correlations and on pairing corrections. The correlations responsible for the existence of the giant dipole resonance can introduce additional factors.

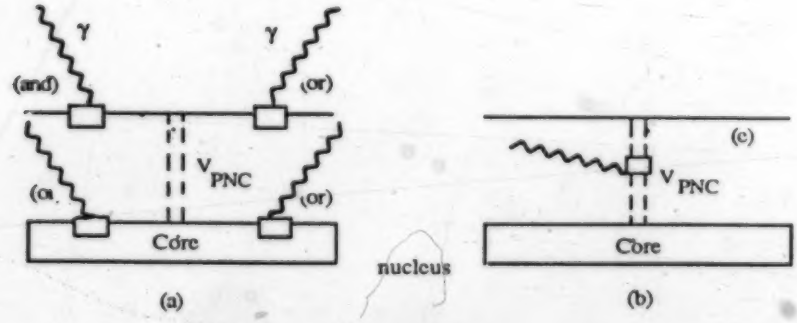

***Figur* II.5. Valance nucleons are interacting with the core of the nuclei through the action of V_{PNC}. The photon can be emitted in any of the five different ways.**

Calculations have been performed for several nuclei, including ^{19}F, ^{41}K, ^{175}Lu and ^{181}Ta. The corresponding references are listed in table II.2. The decay of ^{181}Ta

has been investigated extensively both experimentaly and theoretically. Important energy levels and PNC transitions are shown in figure (II.6). Theoretical analyses seem to indicate the need for stronger I=0,2 terms in the weak potential than predicted by the PC approximations. There have been claims stating that if the $\Delta I=1$ term of V_{PNC} is sufficiently strong, the experimental date are explainable (CU77). The ^{181}Ta experiment played an important rule in a semi-empirical determination of the strength of the π-exchange PNC force (DE78). However, another analysis (DE79) indicates that experiments in complex nuclei are not really suitable for the determination of that strength.

Investigations of several transitions performed using semi-empirical potentials seems to indicate that all terms ($\Delta I=0,1,2$) could be appreciably larger than the first theoretical estimates (DE78). The sign of $\Delta I=0,2$ terms in the semi-empirical potential V_{PNC} disagrees with the theoretical predictions. Such puzzling results stress the importance of the isospin analysis of nuclear PNC effect and the need of more experiments.

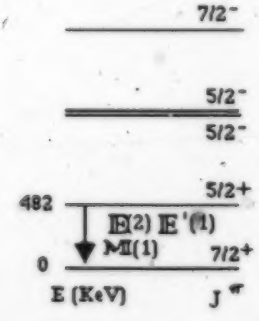

***Figure* II.6. Levels in ^{181}Ta involved in the PNC experiment. Regular [M(1), E(2)] and irregular E'(1) multipoles for the 482 KeV transition are indicated together with spins and parities (J^{π}).**

II.5.d. PNC Effect in Nuclear Scattering

Nucleon scattering goes through spin-isospin states which do not occur in decay experiments. PNC amplitudes for NN scattering at low energies emerge as a useful by-product of the calculations for the n-p→d+γ reaction (MIb76). Analysis shows that the experiments depend on six matrix elements of V_{PNC} (more details in chapter IV). They are usually calculated in the distorted-wave-Born approximation (DWBA), by which the total scattering amplitude can be written as

$$\mathbb{F}_{s's} = \mathcal{G}_{s's} + \mathcal{F}_{s's} , \qquad \text{(II.31)}$$

where $\mathcal{G}^{\circ}_{s's}$ is the normal hadronic scattering amplitude (i.e.due to strong interaction), while s and s' are the total spins. The PNC part is calculated using distorted waves $\psi_s^{(\pm)}$ which are computed for some set of strong potentials

$$\mathcal{F}_{ss} \alpha \ < \psi_{s'}^{(-)} | V_{PNC} | \psi_s^{(+)} > . \qquad \text{(II.32)}$$

The differential asymmetry $A(\theta)$ depending on the helicity of the incident nucleon is given by

$$A(\theta) = \frac{\frac{d\sigma^{+}}{d\Omega} - \frac{d\sigma^{-}}{d\Omega}}{\frac{d\sigma^{+}}{d\Omega} + \frac{d\sigma^{-}}{d\Omega}} , \qquad \text{(II.33a)}$$

where $d\sigma^{+}/d\Omega$ are the differential cross sections for the positive and negative helicities, respectively. The differential helicity is a function of the scattering amplitudes introduced in (II.31)

$$A(\theta) = \frac{2\,\mathrm{Re}\,| \mathcal{F}^{\circ}_{00} \mathcal{G}^{\circ}_{01} + \mathcal{F}^{\circ}_{11} \mathcal{G}_{10} |}{|\mathcal{G}_{00}|^2 + |\mathcal{G}_{11}|^2} . \qquad \text{(II.33b)}$$

If the total cross sections $\overline{\sigma^+}$ ($\overline{\sigma^-}$) are measured, then the asymmetry caused by PNC forces is

$$A = \frac{\sigma^+ - \sigma^-}{\sigma^+ + \sigma^-} . \qquad \text{(II.34)}$$

Theoretical studies indicated that the study of PNC thermal neutron scattering might help to fix some, as yet arbitrary, parameters of semi-empirical potential (TA78). The effect depends again on the matrix elements of V_{PNC}. As a transversely polarized beam of thermal neutrons of momentum **k** travels a distance x through a medium of density ρ, PNC interactions with nuclei in the medium will rotate the neutron's spin about the direction of propagation by an angle

$$\Omega = \frac{4\pi}{|k|} \rho \times \mathcal{g} , \qquad \text{(II.35)}$$

where $\mathcal{g}$ is the PNC part of the forward scattering amplitude. The scattering amplitude receives contributions from three processes: (i) direct scattering by V_{PNC}, (ii) scattering on parity impurities in the nuclear wavefunction, and (iii) scattering by atomic electrons if there are weak neutral PNC semi-leptonic interactions.

For medium and high energy regions, the effect coming from short-range weak interactions might become more observable if investigated at large momentum transfers. Then weak interactions, may be, eventually become dominant. A chosen model for weak interactions will fix the strength of the parameters. In chapter IV a brief review will be discussed about these models and their parameters, namely the ones affecting the V_{PNC} potentials.

CHAPTER III

PARITY CONSERVING NUCLEON-NUCLEON INTERACTION

The two-nucleon problem was born in the first half of the decade of the 1930's. While the proton had been known for some time, a proton beam in the modern sense was not feasible before the invention of the various particle accelerators at the end of the 1920's and the beginning of the 1930's. The neutron was discovered in 1932 and was soon postulated to serve together with the proton, one of the building blocks of nuclei. It was established early that the force between two protons is different from a pure Coulomb force, and the total cross section for neutrons scattering on protons was soon measured.

In 1935 Yukawa (YUb35) made his fundamental assumption that the forces between two nucleons are due to the exchange of a new particle, the meson. The fact remains, however, that the development of the subject of the two-nucleon interaction has been ever since the bigining along two parallel lines: expirements coupled with phenomenological considerations, and meson theory.

In this chapter I will review on some invariance principles governing the nucleon-nucleon interaction, density matrix formalism, parity conserving nucleon-nucleon (NN) obeservables; their experimental and theoretical interpretations, and the use of SAID programme to get an output representing the strong parity conserving amplitudes (see equations II.31 and II.33b) considered in the present work.

III.1. Invariance Principles

In quantum mechanics a scattering process is described by the scattering amplitude. This amplitude depends on the kinematical variables, such as the scattering angle and energy, and also on quantum numbers describing the states of the particles participating in the collision process. The dependence of the scattering amplitude on these latter quantities is greatly connected with conservation laws.

these latter quantities is greatly connected with conservation laws.

In the case of NN interactions, the scattering amplitude may depend on the spin states of the two nucleons and on their charges. Thus, the scattering amplitude is likely to be a matrix in spin and charge spaces. The two spaces are independent of each other (except for some overall requirements of the exclusion principle).

The amplitude in terms of the kinematic variables and spin, will depend on $\mathbf{k}_i$ and $\mathbf{k}_f$, the incoming and outgoing momenta in the centre of mass system (since we are discussing elastic scattering, we have $|\mathbf{k}_i| = |\mathbf{k}_f|$), and on the two spin vector operators $\sigma^{(1)}$ and $\sigma^{(1)}$. The geometrical arrangements of the kinematical variables are shown in figure(III.1). It is evident that for elastic scattering the unit vectors

$$\hat{\mathbf{P}} = \frac{\mathbf{k}_i + \mathbf{k}_f}{|\mathbf{k}_i + \mathbf{k}_f|}, \quad \hat{\mathbf{N}} = \frac{\mathbf{k}_i \times \mathbf{k}_f}{|\mathbf{k}_i \times \mathbf{k}_f|}, \quad \hat{\mathbf{K}} = \frac{\mathbf{k}_f - \mathbf{k}_i}{|\mathbf{k}_f - \mathbf{k}_i|} = \hat{\mathbf{N}} \times \hat{\mathbf{P}}, \qquad \text{(III.1)}$$

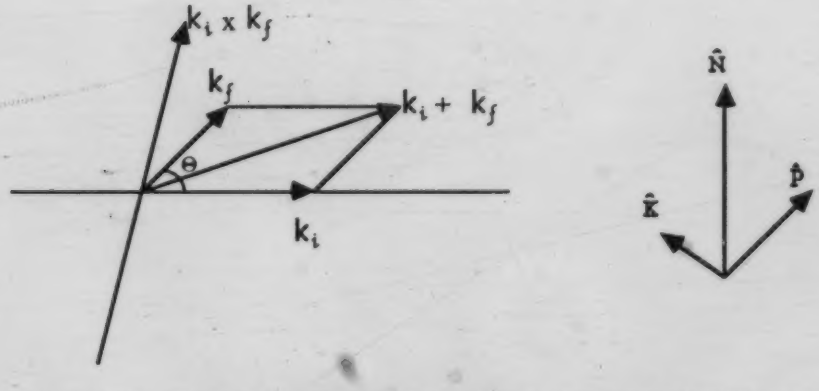

Figure **III.1. Kinematic diagram for the nucleon-nucleon scattering (the unit vectors $\hat{K}$, $\hat{N}$, and $\hat{P}$ are used in the text).**

form a Cartesian coordinate system. It is also clear that assuming non-relativistic kinematics, these three unit vectors have a very convenient meaning in the laboratory system, since they represent the direction of the outgoing momentum, the direction perpendicular to the scattering plane, and the direction perpendicular to the first two.

We can now write down separately the various tensors that can be formed of

the two spin vectors and of the kinematic vectors. From these we can figure out contributions of these tensors, which are invariant under transformations, corresponding to certain conservation laws. The general form of the scattering amplitude can then be expressed in terms of these combinations.

III.1.a. Rotational Invariance

This requires that the resulting expressions be tensors of the zeroth rank (i.e. scalars or pseudoscalars). We can form 17 such combinations; they are given in table III.1. Only 16 of them are independent because

$$\sigma^{(1)} \cdot \sigma^{(2)} = \sigma^{(1)} \cdot \hat{K}\, \sigma^{(2)} \cdot \hat{K} + \sigma^{(1)} \cdot \hat{P}\, \sigma^{(2)} \cdot \hat{P} + \sigma^{(1)} \cdot \hat{N}\, \sigma^{(2)} \cdot \hat{N} \quad . \qquad \text{(III.2)}$$

The combinations $\hat{K} \cdot \hat{P}$, $\hat{K} \cdot \hat{N}$, and $\hat{P} \cdot \hat{N}$ are zero and hence do not have to be taken into account in forming these expressions.

Table III.1
Different Combinations of tensors contributing in the scattering amplitude.

Rank	Tensors of the spin vectors	Kinematic tensors
0	1	1
	$\sigma^{(1)} \cdot \sigma^{(2)}$	$\hat{K} \cdot \hat{P}$
		$\hat{P} \cdot \hat{N}$
		$\hat{N} \cdot \hat{K}$
1	$\sigma^{(1)} + \sigma^{(2)}$	$\hat{K}$
	$\sigma^{(1)} - \sigma^{(2)}$	$\hat{N}$
	$\sigma^{(1)} \times \sigma^{(2)}$	$\hat{P}$
2	$\sigma_i^{(1)} \sigma_j^{(2)} + \sigma_j^{(1)} \sigma_i^{(2)}$	$K_i K_j$
		$P_i P_j$
		$K_i P_j + K_j P_i$
		$K_i N_j + K_j N_i$
		$P_i N_j + P_j N_i$

III.1.b. Space Reflection Invariance

This requires that the expressions remain unchanged if all the vectors they contain change signs and all the axial vectors remain the same. $\hat{\mathbf{P}}$ and $\hat{\mathbf{K}}$ are vectors while $\hat{\mathbf{N}}$, which is the cross product of the other two, is an axial vector. The spin vectors are also axial vectors since they can be thought of as a cross product of a coordinate vector and a momentum. Thus the transformation is

Table III.2
Behavior of the rotationally invariant combinations under other transformations

Rotational invariant	1	$\sigma^{(1)}\cdot\sigma^{(2)}$	$(\sigma^{(1)}+\sigma^{(2)})\cdot\hat{\mathbf{K}}$	$\hat{\mathbf{N}}$	$\hat{\mathbf{P}}$	$(\sigma^{(1)}-\sigma^{(2)})\cdot\hat{\mathbf{K}}$	$\hat{\mathbf{N}}$	$\hat{\mathbf{P}}$	$(\sigma^{(1)}\times\sigma^{(2)})\cdot\hat{\mathbf{K}}$	$\hat{\mathbf{N}}$	$\hat{\mathbf{P}}$
Space reflection	Y	Y	N	Y	N	N	Y	N	N	Y	N
Time reversal	Y	Y	N	Y	Y	N	Y	Y	Y	N	N
Exclusion principle	Y	Y	Y	Y	Y	N	N	N	N	N	N

Rotational invariant	K_iK_j	N_iN_j	P_iP_j	$\sigma_i^{(1)}\sigma_j^{(2)}+\sigma_j^{(1)}\sigma_i^{(2)}$ $K_iP_j+K_jP_i$	$K_iN_j+K_jN_i$	$P_iN_j+P_jN_i$
Space reflection	Y	Y	Y	Y	N	N
Time reversal	Y	Y	Y	N	N	N
Exclusion principle	Y	Y	Y	Y	Y	Y

$$\hat{\mathbf{P}}\to-\hat{\mathbf{P}},\quad \hat{\mathbf{K}}\to-\hat{\mathbf{K}},\quad \hat{\mathbf{N}}\to\hat{\mathbf{N}},\quad \sigma\to\sigma\ . \tag{III.3a}$$

The behavior of the 17 rotation-invariants under this transformation is shown in Table III.2.

III.1.c. Time Reversal Invariance

This requires that the expressions remain unchanged if the direction of time is reversed. This reverses all velocities and hence changes the signs of all momenta. The spin vectors also change their signs since they are products of a coordinate vector and a momentum. Thus the transformation is

$$\hat{P} \rightarrow -\hat{P}, \quad \hat{K} \rightarrow \hat{K}, \quad \hat{N} \rightarrow -\hat{N}, \quad \sigma \rightarrow -\sigma , \tag{III.3b}$$

and we can see the behavior of these expressions in Table III.2.

III.1.d. The Exclusion Principle

This requires that if we deal with identical particles, the interchange of the labels (1) and (2) leave the expressions unchanged. This transformation affects only the spin vectors

$$\sigma^{(1)} \leftrightarrow \sigma^{(2)} . \tag{III.3c}$$

We see that the first three requirements reduce the number of expressions from 16 to 6. The exclusion principle eliminates one more combination. Thus for proton-proton (pp) scattering we have five, and for neutron-proton (np) scattering six expressions. If charge independence is assumed, we can describe both scatterings in terms of two amplitudes, both consisting of five expressions. The coefficients of these expressions are all functions of the energy and angle of the scattering process, and are in general complex numbers.

III.2. The scattering Matrix

Let $\chi^{(n)}$ be a vector with four components representing one of the initial spin states n, then the scattering state wavefunction may be written as

$$\psi^{(n)} = e^{i(k_i \cdot r)} \chi^{(n)} + f^{(n)} \frac{e^{ikr}}{r} , \qquad \text{(III.4a)}$$

$$f^{(n)} = M \chi^{(n)} . \qquad \text{(III.4b)}$$

Here, M is a 4x4 matrix operating on the initial spin state and in general it is a scaler in ordinary space. Its general form is

$$M = a + c(\sigma_{\hat{N}}^{(1)} + \sigma_{\hat{N}}^{(2)}) + m\,\sigma_{\hat{N}}^{(1)}\sigma_{\hat{N}}^{(2)} + g(\sigma_{\hat{P}}^{(1)}\sigma_{\hat{P}}^{(2)} + \sigma_{\hat{K}}^{(1)}\sigma_{\hat{K}}^{(2)}) + h(\sigma_{\hat{P}}^{(1)}\sigma_{\hat{P}}^{(2)} - \sigma_{\hat{K}}^{(1)}\sigma_{\hat{K}}^{(2)}) . \qquad \text{(III.5)}$$

In a scattering experiment, one prepares the two particles in certain spin states prior to scattering and subsequently measures the states of the particles after scattering. Thus, if the initial polarized state is specified, the general scattering problem is that of finding the final spin expectation values

$$\langle \sigma_\alpha^{(1)} \sigma_\beta^{(2)} \rangle_f \qquad (\alpha, \beta = 0, 1, 2, 3) , \qquad \text{(III.6)}$$

with σ_0=1, corresponds to a measurement where the spin direction is not detected.

This problem can be conveniently formulated in terms of the density matrix rather than wavefunctions. For a given pure spin state $\chi^{(n)}$, the density matrix is defined as

$$\rho_{i,j} = \chi_i^{(n)} \chi_j^{(n)\dagger} , \qquad \text{(III.7a)}$$

where $\chi_i^{(n)}$ is the i^{th} component of the column vector $\chi_i^{(n)}$; $\chi_j^{(n)\dagger}$ is the j^{th}

component of the adjoint row vector $\chi^{(n)\dagger}$. Actually we are dealing with an incoherent mixture of pure spin states, as in the case of a nucleon beam from the accelerator, then the density matrix is

$$\rho_{ij} = \sum_n P_n \chi_i^{(n)} \chi_j^{(n)*} , \qquad \text{(III.7b)}$$

where P_n is the relative probability of finding the system in state $\chi^{(n)}$. For a beam of particles, the sum may be considered as a sum over the states of the individual particles in the beam.

Given the density matrix ρ, the average value $\langle S^\mu \rangle$ of any spin operator S^μ is written as

$$\langle S^\mu \rangle = \frac{\sum_n P_n (\chi^{(n)}, S^\mu \chi^{(n)})}{\sum_n P_n (\chi^{(n)}, \chi^{(n)})} = \frac{\sum\sum_{n\,i,j} P_n \chi_i^{(n)*} S_{ij}^\mu \chi_j^{(n)}}{\sum\sum_{n\,i} P_n \chi_i^{(n)*} \chi_i^{(n)}} = \frac{\mathrm{Tr}(\rho S^\mu)}{\mathrm{Tr}\,\rho} . \qquad \text{(III.8a)}$$

Thus, the quantities (III.8a) are given by (ρ_f is the spin-density matrix for the final states)

$$\langle S^\mu \rangle_f = \frac{\mathrm{Tr}(\rho_f S^\mu)}{\mathrm{Tr}\,\rho_f} , \qquad \text{(III.8b)}$$

with

$$S^\mu \equiv \sigma_\alpha^{(1)} \sigma_\beta^{(2)} , \qquad [\mu = (\alpha, \beta) = 1, 2, \ldots, 16] \qquad \text{(III.8c)}$$

We now rewrite this expression so that the unknown ρ_f is replaced by ρ_i which describes the known initial preparation of the system. By using equations (III.4) we have

$$\rho_f = \sum_n P_n M \chi^{(n)} \chi^{(n)\dagger} M^\dagger = M \rho_i M^\dagger , \qquad \text{(III.9)}$$

and equation (III.8b) becomes

$$\langle S^\mu \rangle_f = \frac{Tr(M \rho_i M^\dagger S^\mu)}{Tr(M \rho_i M^\dagger)} . \qquad \text{(III.10)}$$

The initial polarized state is completely specified by the expectation value $\langle S^\mu \rangle_i$ of S^μ given by equation (III.8c). The 4x4 matrix density ρ_i for the initial NN system is then given by

$$\rho_i = \sum_{\mu=1}^{16} \frac{Tr(\rho_i S^\mu)}{Tr(S^\mu S^{\mu\dagger})} = \frac{1}{4} \sum_{\mu=1}^{16} Tr(\rho_i) \langle S^\mu \rangle_i S^\mu . \qquad \text{(III.11)}$$

where S^μ's are given by equation (III.8c), being considered as base matrices with the orthogonality relation

$$Tr(S^\mu S^\nu) = 4 \delta_{\mu\nu} . \qquad \text{(III.12)}$$

By substituting (III.11) into (III.10), we get a basic relation between incident and final polarized states (WO52),

$$\frac{d\sigma}{d\Omega})_p \langle S^\mu \rangle_f = \frac{1}{4} \sum_{\nu=1}^{16} \langle S^\nu \rangle_i \, Tr(M S^\nu M^\dagger S^\nu) , \qquad \text{(III.13a)}$$

where

$$\frac{d\sigma}{d\Omega})_p = \frac{Tr(M \rho_i M^\dagger)}{Tr \rho_i} = \frac{1}{4} \sum_{\nu=1}^{16} \langle S^\nu \rangle_i \, Tr(M S^\nu M^\dagger) , \qquad \text{(III.13b)}$$

is the differential cross section at the scattering angle considered.

III.3. Types of Experiments and their Theoretical Interpretations

In principle, there are 16^2 (=256) different experiments possible at a single scattering angle. For, 16 incident polarized states with $\langle S^{\mu} \rangle_i$ (μ=1, 2, ..., 16) can be prepared, and in the final state 16 measurements of $\langle S^{\upsilon} \rangle_f$ (υ=1, 2, ..., 16) are possible. In more physical terms, one can prepare one unpolarized and three unpolarized states for each of an incoming beam and a target. For each of these preparations, one can measure the differential cross section, the 3+3(=6) polarized components of the scattered beam and recoil particles, and the 3^2(=9) correlations of spins of the two outgoing nucleons.

Although all of these experiments are presumably independent, there are many theoretical relationships between them. For example, half of the 256 observables are pseudoscalars, and hence vanish identically if parity is conserved. In the following we will discuss some typical experiments and introduce the observables associated with them.

We begin by defining the laboratory coordinate system. let $\hat{L}_i$, $\hat{L}_f$ and $\hat{L}_r$ be the incident, outgoing and recoil momentum vectors in the laboratory system, then we define three sets of the orthogonal unit vectors

$$\hat{L}_i = \frac{L_i}{|L_i|}, \qquad \hat{n} = \frac{L_i \times L_f}{|L_i \times L_f|}, \qquad \hat{s}_i = \hat{n} \times \hat{L}_i , \tag{III.14a}$$

$$\hat{L}_f = \frac{L_f}{|L_f|}, \qquad \hat{n}, \qquad \hat{s}_f = \hat{n} \times \hat{L}_f , \tag{III.14b}$$

and

$$\hat{L}_r = \frac{L_r}{|L_r|}, \qquad \hat{n}, \qquad \hat{s}_r = \hat{n} \times \hat{L}_r . \tag{III.14c}$$

III.3.a. Differential Cross Section and Polarization

Consider the scattering of an unpolarized beam (UB) on an unpolarized target (UT). All $<S^{\nu}>_i$'s equal zero in equations (III.13) except for $<\sigma_0^{(1)}\sigma_0^{(2)}>_i=1$, and hence the differential cross section for the scattering of a UB on a UT is given by

$$\frac{d\sigma}{d\Omega})_{up} = \frac{1}{4}\,\mathrm{Tr}(M M^{\dagger}) , \tag{III.15}$$

and $<\sigma^{(1)}>_f$, the polarization vector of particle 1 produced by UB-UT scattering, is

$$\frac{d\sigma}{d\Omega})_{up}<\sigma^{(1)}>_f = \frac{1}{4}\mathrm{Tr}(M M^{\dagger}\sigma^{(1)}) . \tag{III.16}$$

The axial vector $<\sigma^{(1)}>_f$ is along the direction normal to the scattering plane. For, after we take the indicated trace in (III.16), we are left with functions of $\hat{L}_i$ and $\hat{L}_f$. The only axis we can form from $\hat{L}_i$ and $\hat{L}_f$ is $\hat{L}_i \times \hat{L}_f$, which is along the direction mentioned above. Thus, in UB-UT scattering,

$$<\sigma^{(1)}>_f = P\,\hat{n} , \tag{III.17a}$$

where P is given by

$$\frac{d\sigma}{d\Omega})_{up} P = \frac{1}{4}\mathrm{Tr}(M M^{\dagger}\sigma_{\hat{n}}^{(1)}) , \tag{III.17b}$$

$\sigma_{\hat{n}}^{(1)}$ is the normal component of $\sigma^{(1)}$.

The following symmetry properties hold true when the two outgoing particles are identical (e.g. for the p-p system)

$$\frac{d\sigma}{d\Omega})_{up}(\theta) = \frac{d\sigma}{d\Omega})_{up}(\pi-\theta) , \tag{III.18a}$$

$$P_0(\theta) = -P_0(\pi - \theta). \qquad \text{(III.18b)}$$

Next we consider the scattering of a polarized beam by a UT. The differential cross section is, by equations (III.13),

$$\frac{d\sigma}{d\Omega})_p = \frac{1}{4}\mathrm{Tr}(M M^\dagger) + \frac{1}{4}<\sigma^{(1)}>_i \cdot \mathrm{Tr}(M\sigma^{(1)}M^\dagger). \qquad \text{(III.19)}$$

The first term on the right-hand side is the differential cross section $d\sigma/d\Omega)_{up}$ for UB-UT scattering, and the second is the contribution due to initial polarization $<\sigma^{(1)}>_i$. On the basis of invariance under time reversal, we have the relation

$$\mathrm{Tr}(M\sigma^{(i)}M^\dagger) = \mathrm{Tr}(M M^\dagger \sigma^{(i)}), \qquad (i = 1, 2) \qquad \text{(III.20)}$$

Therefore, equation (III.19) becomes

$$\frac{d\sigma}{d\Omega})_p = \frac{d\sigma}{d\Omega})_{up}(1 + P_i P\cos\phi), \qquad \text{(III.21)}$$

where $P_i = |<\sigma^{(i)}>_i|$ is the incident polarization of the particle 1 and P is the polarization of the particle 1 produced in UB-UT scattering, given equation (III.17b). ϕ is the angle between $<\sigma^{(1)}>_i$ and $\hat{n}$.

III.3.b. Polarization Analysis

Equation (III.21) involves the principle of the polarization analysis, Noting that it is independent on the spin of the target particles and hence holds true for any such particles. Let us consider the scattering of a polarized beam by an unpolarized nucleus. We are trying to measure the polarization P_i of the beam. In order to use the nucleus as an analyzer, the polarization P of an initially unpolarized beam scattered by this nucleus is assumed to be already known. We take the coordinate axes so

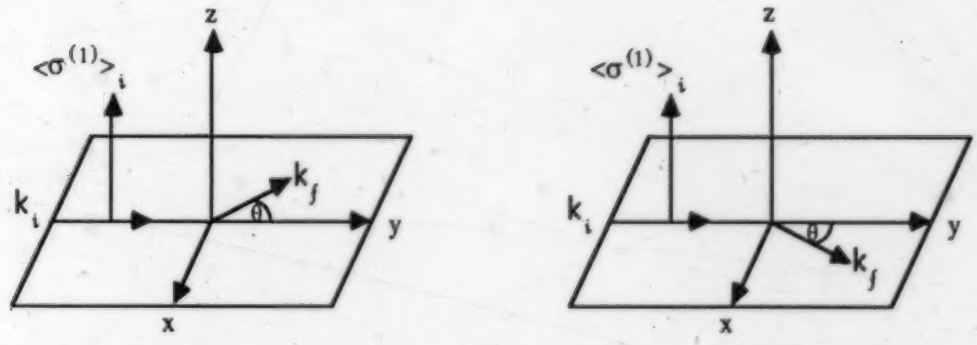

***Figure* III.2. The scattering of polarized nucleons with their spin along the z-axis.**

that the initial polarization $\langle\sigma^{(1)}\rangle_i$ is parallel to the z-axis, and assume that the scattering plane is set in the xy-plane (see figure III.2). If the particles 1 arescattered left (right) with respect to their direction, the angle ϕ between $\langle\sigma^{(1)}\rangle_i$ and $\hat{\mathbf{n}}$ is $\phi=0$ (π), and equation (III.21) becomes

$$\sigma_L \equiv \frac{d\sigma}{d\Omega})_p(\theta,\phi) = \frac{d\sigma}{d\Omega})_{up}(\theta)(1 + P_i P) , \qquad \text{(III.22a)}$$

$$\sigma_R \equiv \frac{d\sigma}{d\Omega})_p(\theta,\phi_0+\pi) = \frac{d\sigma}{d\Omega})_{up}(\theta)(1 - P_i P) , \qquad \text{(III.22b)}$$

where (θ, ϕ_0) is the c.m. scattering angle with the polar axis along the direction of the incident beam. The cross section $d\sigma/d\Omega)_{up}$ for an initially unpolarized beam does not depend on the azimuthal angle ϕ, if parity is conserved.

III.3.c. Use of a Polarized Target

The polarization experiments as described above require double scatterings: the scattering to produce polarization and its subsequent scattering for polarization

analysis. However, the polarization can be measured in only a single scattering, if a polarized target (PT) is available. Consider a scattering of a UB on a PT with $\langle\sigma^{(2)}\rangle_i = P_i$ being given . We are trying to gain the polarization P to be produced in the corresponding UB-UT scattering. The previous discussion of the PB-UT scattering holds also in the present case, since the matrix M is symmetric with respect to $\sigma^{(1)}$ and $\sigma^{(2)}$. Thus, the cross section for the UB-PT scattering is given by equation (III.21), where P_i is now the polarization intensity of the target and P is the polarization in question. Hence, by measuring the cross section $d\sigma/d\Omega$ we can obtain P from equation (III.21).

III.3.d. Depolarization and Rotation Parameters

If an incident beam is prepared with a polarization $\langle\sigma^{(1)}\rangle_i$, and the target is unpolarized, the polarization $\langle\sigma^{(1)}\rangle_f$ of the scattered particles or $\langle\sigma^{(2)}\rangle_f$ transferred to particles 2 is obtained from equation (III.13a) (W54) as

$$\frac{d\sigma}{d\Omega})_p \langle\sigma_\beta^{(i)}\rangle_f = \frac{1}{4}\mathrm{Tr}(M M^\dagger \sigma_\beta^{(i)}) + \frac{1}{4}\sum_{\alpha=1}^{3}\mathrm{Tr}(M\sigma_\alpha^{(1)}M^\dagger\sigma_\beta^{(i)})\langle\sigma_\alpha^{(i)}\rangle_i \quad , \qquad \text{(III.23a)}$$

and i=1, 2, with

$$\frac{d\sigma}{d\Omega})_p = \frac{1}{4}\mathrm{Tr}(M M^\dagger) + \sum_{\alpha=1}^{3}\frac{1}{4}\mathrm{Tr}(M\sigma_\alpha^{(1)}M^\dagger)\langle\sigma_\alpha^{(1)}\rangle_i \quad . \qquad \text{(III.23b)}$$

For experimental reasons we rewrite equation (III.23a), referring to the laboratory coordinate system given by equation (III.23a)

$$\frac{d\sigma}{d\Omega})_p \langle\sigma^{(1)}\rangle_f = \frac{d\sigma}{d\Omega})_{up}\{(P + D\langle\sigma_{\hat{n}}^{(1)}\rangle_i)\hat{n} + (A\langle\sigma_{\hat{L}_i}^{(1)}\rangle_i + R\langle\sigma_{\hat{s}_i}^{(1)}\rangle_i)\hat{s}_f +$$

$$+ (A'\langle\sigma_{\hat{L}_i}^{(1)}\rangle_i + R'\langle\sigma_{\hat{s}_i}^{(1)}\rangle_i)\hat{L}_f\} \quad , \qquad \text{(III.24)}$$

where

$$\frac{d\sigma}{d\Omega})_{up} D = \frac{1}{4} Tr(M \sigma^{(1)}_{\hat{n}} M^{\dagger} \sigma^{(1)}_{\hat{n}}) , \tag{III.25a}$$

$$\frac{d\sigma}{d\Omega})_{up} R = \frac{1}{4} Tr(M \sigma^{(1)}_{\hat{s}_i} M^{\dagger} \sigma^{(1)}_{\hat{s}_f}) , \tag{III.25b}$$

$$\frac{d\sigma}{d\Omega})_{up} A = \frac{1}{4} Tr(M \sigma^{(1)}_{\hat{L}_i} M^{\dagger} \sigma^{(1)}_{\hat{s}_f}) , \tag{III.25c}$$

$$\frac{d\sigma}{d\Omega})_{up} R' = \frac{1}{4} Tr(M \sigma^{(1)}_{\hat{s}_i} M^{\dagger} \sigma^{(1)}_{\hat{L}_f}) , \tag{III.25d}$$

$$\frac{d\sigma}{d\Omega})_{up} A' = \frac{1}{4} Tr(M \sigma^{(1)}_{\hat{L}_i} M^{\dagger} \sigma^{(1)}_{\hat{L}_f}) , \tag{III.25e}$$

The parameter D is called the depolarization, and the R, R', A, A', are the rotation and asymmetry parameters. They have the following physical meaning.

D: consider a beam is prepared with its intial polarization component P_i along $\hat{n}$. Then equation (III.24) becomes

$$\langle \sigma^{(1)}_{\hat{n}} \rangle_f = \pm \frac{P + D P_i}{1 + P P_i} , \tag{III.26a}$$

where P is the polarization produced by UB-UT scattering at the same scattering angle. Equation (III.26a) allows us to measure D. Consider a completly polarized beam, $P_i = \pm 1$, then

$$\langle \sigma^{(1)}_{\hat{n}} \rangle_f = \pm \frac{D \pm P}{1 \pm P} . \tag{III.26b}$$

If D=1, we have $\langle \sigma^{(1)} \rangle_f = \pm 1$, i.e. the scattered beam remains completely polarized. If D<1, we obtain $\langle \sigma^{(1)} \rangle_f < 1$, thus the initial beam is depolarized by scattering.

R and R': A beam is prepared with its polarization P_i in the direction $\hat{s}_i$. Equation (III.25) reduces to

$$\langle \sigma^{(1)} \rangle_f = P\hat{n} + RP_i\,\hat{s}_f + R'P_i\,\hat{L}_f\,, \qquad \text{(III.27)}$$

and we have $\langle \sigma_{\hat{n}}^{(1)} \rangle_f = P$, $\langle \sigma_{\hat{s}(f)}^{(1)} \rangle_f = RP_i$ and $\langle \sigma_{\hat{L}(f)}^{(1)} \rangle_f = R'P_i$. Let us take for simplicity $P_i=1$, and first measure P, and then R and R'. As seen from figure (III.3) the following relations hold true

$$R = \sqrt{(1 - P^2)}\,\cos(\theta_L - \beta)\,, \qquad \text{(III.28a)}$$

$$R' = \sqrt{(1 - P^2)}\,\sin(\theta_L - \beta)\,. \qquad \text{(III.28b)}$$

transverse rotation parameters. The following relation holds between the A's and R's as therefore, measurements of R and R' give β, the angle of rotation of the polarization vector in the scattering plane.

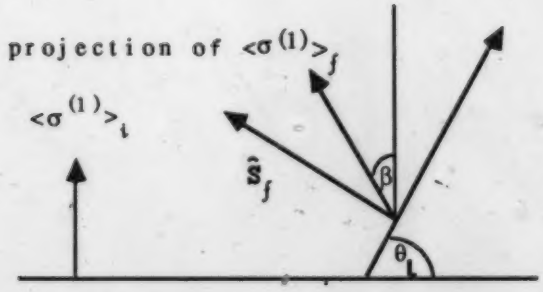

Figure **III.3. Directions of polarization vectors in the scattering plane.**

A and A': In the same way, the parameters A and A' can be interpreted as giving the angle of rotation of the polarization vector in the scattering plane. To distinguish between the parameters R, and R' and A, A', the former ones are called

$$\frac{A + R'}{A' - R} = \tan\frac{\theta}{2}\,, \qquad \text{(III.29)}$$

and hence only three of the rotation parameters are independent.

III.3.e. The Spin Correlation Parameters

Consider the simultaneous measurement of the polarization of the scattered beam and recoil particles $\langle\sigma_\alpha^{(1)}\sigma_\beta^{(2)}\rangle_f$ produced by UB-UT scattering. Note that, in general, $\langle\sigma_\alpha^{(1)}\sigma_\beta^{(2)}\rangle_f \neq \langle\sigma_\alpha^{(1)}\rangle_f \langle\sigma_\beta^{(2)}\rangle_f$, thus these measurements can give further new information on the M matrix.

By referring to the Laboratory coordinate system , we define (WO56)

$$\frac{d\sigma}{d\Omega})_{up} C_{nn} = \frac{1}{4}\mathrm{Tr}\left(M M^\dagger \sigma_{\hat{n}}^{(1)} \sigma_{\hat{n}}^{(2)}\right), \qquad \text{(III.30a)}$$

$$\frac{d\sigma}{d\Omega})_{up} C_{kp} = \frac{1}{4}\mathrm{Tr}\left(M M^\dagger \sigma_{\hat{k}_f}^{(1)} \sigma_{\hat{k}_r}^{(2)}\right), \qquad \text{(III.30b)}$$

$$\frac{d\sigma}{d\Omega})_{up} C_{pp} = \frac{1}{4}\mathrm{Tr}\left(M M^\dagger \sigma_{\hat{L}_f}^{(1)} \sigma_{\hat{k}_r}^{(2)}\right), \qquad \text{(III.30c)}$$

III.3.f. Formulae for Observables

It can be seen from table III.3 that some observables depend only on the amplitudes in the spin-triplet states, while others, with the spin singlet states. The quantities c, h, a+m and a+g are the triplet amplitudes, as will be shown in the next section. Thus the following observables can give information on the triplet amplitudes

$$\frac{d\sigma}{d\Omega})_{up} P,\ \frac{d\sigma}{d\Omega})_{up} C_{kp},\ \frac{d\sigma}{d\Omega})_{up} (C_{pp}^n - C_{kk}^n),\ \frac{d\sigma}{d\Omega})_{up} (C_{kp}^n + C_{pk}^n),\ \frac{d\sigma}{d\Omega})_{up} C_{np}^n. \qquad \text{(III.31a)}$$

Other observables are generally related to both of the triplet amplitudes.

Table III.3
Nonrelativistic expressions for observables in terms of the coefficient of the matrix M.

$$\frac{d\sigma}{d\Omega})_{up} = |a|^2 - |m|^2 - 2|c|^2 - 2|g|^2 - 2|h|^2$$

$$A = -\left[\left[|a|^2 - |m|^2 - 4\,\mathrm{Re}(gh^*)\right]\sin(\theta/2) + 2\,\mathrm{Re}\{i(a-m)^*c\}\cos(\theta/2)\right] / \left[d\sigma/d\Omega)_{up}\right]$$

$$A' = \left[\left[2\,\mathrm{Re}\{i\,(a-m)^*c\}\sin(\theta/2) + \{|a|^2 - |m|^2 + 4\,\mathrm{Re}(gh^*)\}\cos(\theta/2)\right] / \left[d\sigma/d\Omega)_{up}\right]\right]$$

$$A_{xx} = \left[\left[2\,\mathrm{Re}\{(a-m)g^* - (a-m)h^*\cos\theta - 2ich^*\sin\theta\}\right] / \left[d\sigma/d\Omega)_{up}\right]\right]$$

$$A_{zz} = \left[\left[2\,\mathrm{Re}\{(a-m)g^* + (a-m)h^*\cos\theta + 2ich^*\sin\theta\}\right] / \left[d\sigma/d\Omega)_{up}\right]\right]$$

$$C_{kk} = \left[\left[2\,\mathrm{Re}\{(a-m)g^* - (a+m)h^*\}\right] / \left[d\sigma/d\Omega)_{up}\right]\right]$$

$$C_{kp} = \left[\left[4\,\mathrm{Re}(ich^*)\right] / \left[d\sigma/d\Omega)_{up}\right]\right]$$

$$C_{pp} = \left[\left[2\,\mathrm{Re}\{(a-m)g^* + (a+m)h^*\}\right] / \left[d\sigma/d\Omega)_{up}\right]\right]$$

$$C_{nn} = 1 - \left[\left[|a-m|^2 + 4|g|^2\right] / \left[d\sigma/d\Omega)_{up}\right]\right]$$

$$D = 1 - \left[\left[4|g|^2 - 4|h|^2\right] / \left[d\sigma/d\Omega)_{up}\right]\right]$$

$$P = \left[2\,\mathrm{Re}\{(a+m)c^*\}\right] / \left[d\sigma/d\Omega)_{up}\right]$$

$$R = \left[\left[\{|a|^2 - |m|^2 - 4\,\mathrm{Re}(gh^*)\}\cos(\theta/2) - 2\,\mathrm{Re}\{i\,(a-m)^*c\}\sin(\theta/2)\right] / \left[d\sigma/d\Omega)_{up}\right]\right]$$

$$R' = -\left[\left[2\,\mathrm{Re}\{i\,(a-m)^*c\}\cos(\theta/2) + \{|a|^2 - |m|^2 + 4\,\mathrm{Re}(gh^*)\}\sin(\theta/2)\right] / \left[d\sigma/d\Omega)_{up}\right]\right]$$

For p-p scattering at $90^0_{c.m.}$, the triplet amplitudes $(a+m)_{90^0}$ and $g(90^0)$ are zero, and the amplitudes $(a - m)_{90^0}$ and $g(90^0)$ become the singlet ones. Thus, the

observables in (II.31b) measure the singlet amplitudes at $90^0_{c.m.}$, and the quantities in (III.31c)

$$\frac{d\sigma}{d\Omega})_{up}(1 - C_{nn}),\ \frac{d\sigma}{d\Omega})_{up}(C_{pp} + C_{kk}) , \tag{III.31b}$$

$$\frac{d\sigma}{d\Omega})_{up} R,\ \frac{d\sigma}{d\Omega})_{up} A,\ \frac{d\sigma}{d\Omega})_{up} R',\ \frac{d\sigma}{d\Omega})_{up} A' ,$$

$$\frac{d\sigma}{d\Omega})_{up} C^q_{kn},\ \frac{d\sigma}{d\Omega})_{up} C^q_{pn},\ \frac{d\sigma}{d\Omega})_{up} C^p_{kn},\ \frac{d\sigma}{d\Omega})_{up} C^p_{pn} , \tag{III.31c}$$

give information on the singlet-triplet interference effects.

The spin-scattering matrix M is related to the usual scattering matrix **S** by

$$M(k_f, k_i) = \frac{2\pi}{ik} < \theta_f \phi_f | S - 1 | \theta_i \phi_i > , \tag{III.32}$$

where k is the wave number of the relative motion. The bra and ket vectors on the right-hand side specify the directions of motion of the outgoing and the incoming nucleons, respectively. If equation (III.32) is expressed in the angular momentum representation, we get a familiar formula for the scattering amplitude expanded into spherical harmonics as

$$\mathrm{Im}\, a(\theta) = \frac{k}{4\pi}\int \frac{1}{4}\mathrm{Tr}(M^\dagger M)\, d\Omega , \tag{III.33a}$$

$$\mathrm{Re}\, c(\theta) = \frac{ik}{4\pi}\int \frac{1}{8}\mathrm{Tr}\{M^\dagger M(\sigma^{(1)} + \sigma^{(2)})\hat{N}\}\, dW , \tag{III.33b}$$

$$\mathrm{Im}\, m(\theta) = \frac{k}{4\pi}\int \frac{1}{4}\mathrm{Tr}(M^\dagger M \sigma^{(1)} \cdot \hat{N} \sigma^{(2)} \cdot \hat{N})\, d\Omega , \tag{III.33c}$$

$$\mathrm{Im}(g(\theta) + h(\theta)) = \frac{k}{4\pi}\int \frac{1}{4}\mathrm{Tr}(M^\dagger M \sigma^{(1)} \cdot \hat{P} \sigma^{(2)} \cdot \hat{P})\, d\Omega , \tag{III.33d}$$

$$\mathrm{Im}(g(\theta) - h(\theta)) = \frac{k}{4\pi}\int \frac{1}{4}\mathrm{Tr}(M^\dagger M \sigma^{(1)} \cdot \hat{K} \sigma^{(2)} \cdot \hat{K})\, d\Omega , \tag{III.33e}$$

III.4. The Phase-Shift Parametrization of the Spin Matrix

Results of the scattering experiments are usually analyzed in terms of partial waves. Their phase shifts $\delta_{\ell J}$ are closely related to information on the inner, intermediate and outer regions of nuclear forces depending on ℓ. This is immediately seen, if we note the relation $k_i b=(\ell+1/2)\hbar$ between the angular momentum ℓ and the impact parameter b. The phase shifts can provide, therefore, the necessary insight for the construction of particular models.

The phase-shift operator δ is defined as

$$\mathbf{S} = e^{2i\delta}, \tag{III.34}$$

where $\mathbf{S}$ is the scattering operator. In collision processes of the two nucleons, total angular momentum J, total spin S and parity $\pi=(-)^{\ell}$ are conserved, and hence it is most convenient to discuss in the representation in which J, S and π are diagonal. In the charge independent formalism, total isospin T is also conserved, and takes the values of 0 or 1. However, the Pauli exclusion principle gives the condition of antisymmetry of the states as

$$(-)^{S+1}(-)^{T+1}\pi = (-)^{S+T+1} = -1, \tag{III.35}$$

and hence, if S and L are used for specifying states, T is unnecessary.

By using equations (III.32) and (III.34) the M matrix could be expressed in spin space in terms of phase shifts as

$$\langle S m_s | M(k_f, k_i) | S' m'_s \rangle = \frac{2\pi}{ik} \langle \theta_f \phi_f, S m_s | e^{2i\delta} - 1 | S' m'_s, \theta_i \phi_i \rangle$$

$$= \frac{2\pi}{ik} \sum \langle \theta_f \phi_f | \ell m_\ell \rangle \langle \ell m_\ell S m_s | \ell S J m_J \rangle \langle \ell S J m_J | e^{2i\delta} - 1 |$$
$$\ell' S' J' m'_J \rangle \langle \ell' S' J' m'_J | \ell' m'_\ell S' m'_s \rangle \langle \ell' m'_\ell | \theta_i \phi_i \rangle, \tag{III.36a}$$

where

$$<\theta\phi|\ell m_\ell> = Y_\ell^{m_\ell}(\theta,\phi) \ . \qquad \text{(III.36b)}$$

$<\ell m_\ell S m_s|LSJm_J>$ are Clebsch-Gordan coefficients, which will be deoted as $(\ell S; m_\ell m_s|J\ m_J>$ below.

If the quantization axis is taken along the direction of motion of incident nucleons (z-axis), then $(\theta_i\phi_i)=0$ and $(\theta_f\phi_f)$ becomes the scattering angle (θ, ϕ). By noting that S, J and m_J are good quantum numbers, equation (III.36a) becomes

$$<S\,m_s|M|S'\,m'_s> = \delta_{ss'}\frac{4\pi}{2ik}\sum_{\ell}\sum_{J=|\ell-S|}^{\ell+S}\sqrt{\frac{2\ell'+1}{4\pi}}\,Y_\ell^{m'_s-m_s}(\theta,\phi)$$

$$(\ell S; m'_s-m_s\,m_s|J\,m'_s)(\ell S; 0\,m_s|J\,m_s)<\ell S J m'_s|e^{2i\delta}-1|\ell' S J m'_s>, \qquad \text{(III.36c)}$$

where the summations over ℓ and ℓ' are to be taken so that the condition (III.34) is satisfied. Because of rotation invariance the matrix elements are independent of the projection quantum number m_J of the total angular momentum J. By considering this, we introduce the following notations for the nonvanishing matrix elements of S-1

$$<\ell 0\,\ell m_J|e^{2i\delta}-1|\ell 0\,\ell m_J> = R_\ell \ , \qquad \text{(III.37a)}$$

$$<\ell 1\,\ell m_J|e^{2i\delta}-1|\ell 1\,\ell m_J> = R_{J\ell} \ , \qquad \text{(III.37b)}$$

$$<J\pm1\ 1\ J m_J|e^{2i\delta}-1|J\mp1\ 1\ J m_J> = -R_\pm^J = -R^J \ , \qquad \text{(III.37c)}$$

where the symmetry relation $R^J{}_+=R^J{}_-$ is a consequence of time reversal invariance.

Furthermore, for brevity we write the matrix elements for the spin-singlet and spin-triplet states as

$$M_{ss'} = <00|M|00> \ , \qquad \text{(III.38a)}$$

$$M_{m_s m'_s} = <1\,m_s|M|1\,m'_s> , \qquad \text{(III.38b)}$$

respectively. Then, the nonvanishing matrix elements are (ST57)

$$M_{ss} = \frac{4\pi}{2ik} \sum_{\ell} \sqrt{\frac{(2\ell+1)}{4\pi}}\, R_{\ell}\, Y^{0}_{\ell}(\theta,\phi)\,, \qquad \text{(III.38c)}$$

$$M_{m_s m'_s} = \frac{4\pi}{2ik} \sum_{\ell} \{ \sum_{J=|\ell-1|}^{\ell+1} \sqrt{\frac{(2\ell+1)}{4\pi}}\, (\ell\, S; m'_s - m_s \mid J\, m'_s - m_s)(\ell\, S; m'_s\, 0 \mid J\, m'_s) \times$$
$$R_{\ell J} - \sum_{\ell=\ell\pm1} \sqrt{\frac{(2\ell'+1)}{4\pi}}\, (\ell\ S; m'_s - m_s \mid J\, m'_s - m_s)\, R^{J} \}\, Y_{\ell}^{m'_s - m_s}(\theta,\phi), \qquad \text{(III.38d)}$$

with $\ell' = 2J - \ell$.

When these formulae are applied to the p-p system, the antisymmetry condition (III.35) should be taken into account. This requires that ℓ must be even (odd) for the singlet states (triplet) states. Furthermore, an additional factor of two must be multiplied on the right-hand side of equation (III.38c) and equation (III.38d), because the detecting apparatus measures both protons from beam and target. The relation between $\sigma_{pp}(\theta)$ and σ_{pp} total is then given by $2\,\sigma_{pp} = \int \sigma_{pp}(\theta)\, d\Omega$.

III.5. Parametrization of the S Matrix in the Coupled States

In collisions of two nucleons, the orbital angular momentum ℓ is not a good quantum number. The S matrix is, therefore, not diagonal with respect to ℓ. For a given total J, the two triplet states with $\ell = J \pm 1$ couple to each other (HO69). Let S_J be the submatrix of S for the triplet state with a given J, which may be written as

$$S_J - 1 = \begin{bmatrix} R_{J-1,\ell} & -R^{J} \\ -R^{J} & R_{J+1,J} \end{bmatrix}. \qquad \text{(III.39a)}$$

If inelastic processes are absent, the S_J is a symmetric, unitary 2x2 matrix, and hence can be expressed in terms of three real parameters. This way of parametrization is not unique. One way is to diagonalize S_J in terms of a unitary transformation

$$\mathbb{S}_J = \begin{bmatrix} \cos\varepsilon_J & -\sin\varepsilon_J \\ \sin\varepsilon_J & \cos\varepsilon_J \end{bmatrix} \begin{bmatrix} e^{2i\delta_{J-1,J}} & 0 \\ 0 & e^{2i\delta_{J+1,J}} \end{bmatrix} \begin{bmatrix} \cos\varepsilon_J & \sin\varepsilon_J \\ -\sin\varepsilon_J & \cos\varepsilon_J \end{bmatrix} . \qquad \text{(III.39b)}$$

The phase shifts $\delta_{J\mp1,J}$ thus defined are called Blatt-Biedenharn's eign-phase shifts, and ε_J, the mixing parameter. Physically, this parametrization can be considered as signifying that the two states are mixed in the asymptotic region.

III.6. Separation of Nuclear and Coulomb Contributions

The phase shifts defined by (III.37) and (III.39b) include both nuclear and Coulomb contributions for the pp system (ST57). To get information on nuclear interactions, Coulomb effects have to be removed from the phase shifts. The Coulomb force mainly acts outside the region about the origin in which the nuclear effects occur. Therefore, nuclear phase shifts and Coulomb ones can be regarded as almost additive. The phase shifts defined by

$$\delta_\ell^N = \delta_\ell - \Phi_\ell , \qquad \text{(III.40a)}$$

$$\delta_{\ell J}^N = \delta_{\ell J} - \Phi_\ell , \qquad \text{(III.40b)}$$

$$\varepsilon_J^N = \varepsilon_J , \qquad \text{(III.40c)}$$

are called nuclear phase shifts, where

$$\Phi_\ell = \eta_\ell - \eta_0 = \sum_{x=1}^{\ell} \tan^{-1}\left(\frac{n}{x}\right) , \qquad \text{(III.40d)}$$

are the Coulomb phase shifts. $n=e^2/\hbar v$, v being the relative velocity.

Let $\mathbb{S}_c=1+R_c$ be the pure Coulomb scattering matrix. Then R the matrix is

$$R = S - 1 = \alpha + R_c , \qquad \text{(III.41a)}$$

$$\alpha = S - S_c , \qquad \text{(III.41b)}$$

and the matrix α can be analyzed in terms of partial waves. The R_c, on the other hand, is treated excately

$$\langle f | R_c | i \rangle = \frac{ik}{2\pi} f_c(\theta) , \qquad \text{(III.42a)}$$

$$f_c = - \frac{n}{k(1 - \cos\theta)} \exp\{ - i n \log[\frac{1 - \cos\theta}{2}]\} , \qquad \text{(III.42b)}$$

where $f_c(\theta)$ is the Coulomb scattering amplitude.

III.7. Observables from SAID

In SAID (Scattering Analysis in the Interactive Dial-In) is basically a system for displaying the partial-wave solutions obtained from analyses of these predictions and for displaying the data bases from which solutions were derived, the programme can provide a comprehensive analyses of the NN elastic and inelastic data below 1.3 GeV (this is the last version of SAID July 1987) laboratory kinetic energy are presented. It can display and analyze nucleon-nucleon, nucleon-pion and nucleon-kaon solutions. The data base from an energy dependent and twenty-three single-energy solutions are obtained consists of 9778 pp data and 5729 np data all below 1.3 GeV. The solutions are characterized by tightly constrained "resonance-like" structure in the $^1D_2$ and $^3F_2$ partial waves. No other partial waves exhibit such structure below 1.3 GeV. It describes the full data base and solution files, in which it could be used to modify solutions, plan experiments, and obtain any multitude of predictions which derive from partial-wave analyses of the world data. The amplitudes used in SAID analyses are related to those used by Bystricky (BY78) and by Hoshizaki (HO68) (see AR87). Users can also enter their own solutions and/or data and can conduct parameter studies.

In the following figures we see a typical output from SAID for Wolfenstein parameters and many other observables (energy dependent) as well (making use of SM87 solution in SAID). Comparison with experiment is provided. The output for angle range $0^{o} \rightarrow 180^{o}$ could be achieved for pitches larger than 2.61^{o}. Some observables have not determined experimentally yet in the given energy ranges.

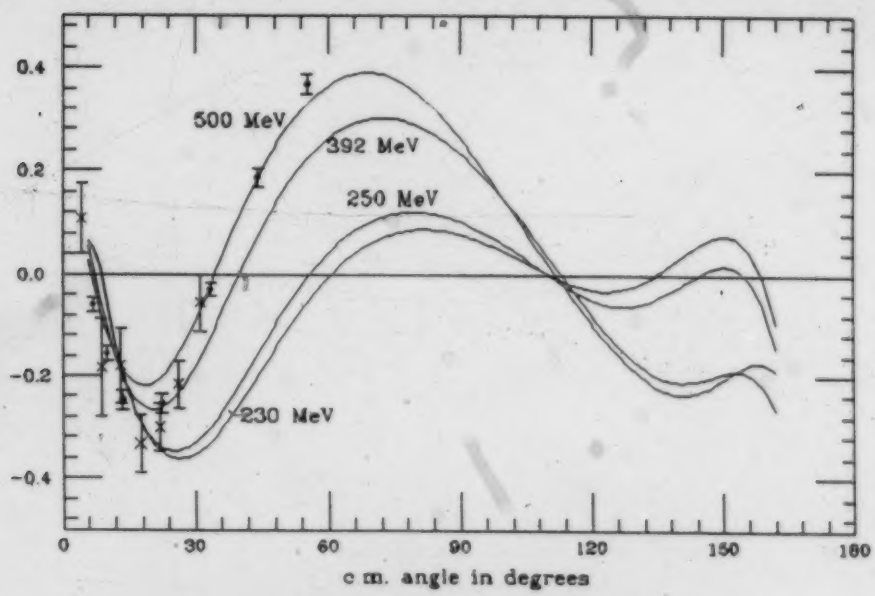

Figure III.4. The parameter A for pp scattering (× for 392 MeV (BE80a) and • for 500 MeV (MA86)).

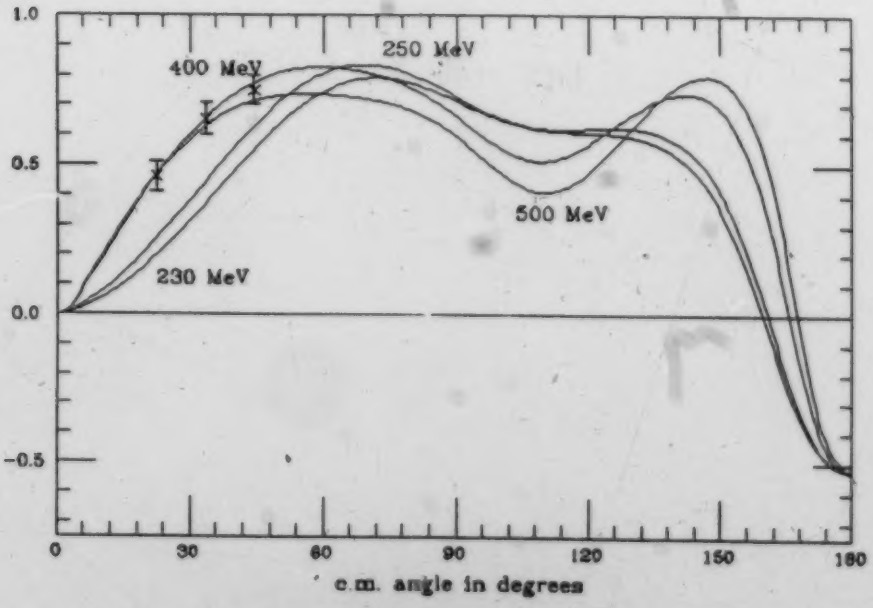

Figure III.5. The parameter A for np scattering (× 500 MeV (MA86)).

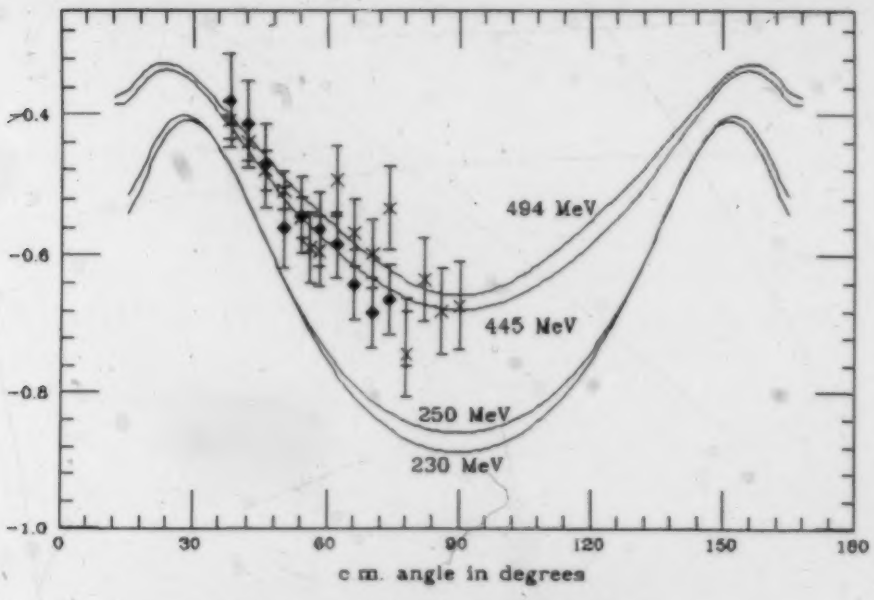

Figure III.6. The parameter A_{xx} for pp scattering (× for 445 MeV (APb83) and • for 494 MeV (APb83)).

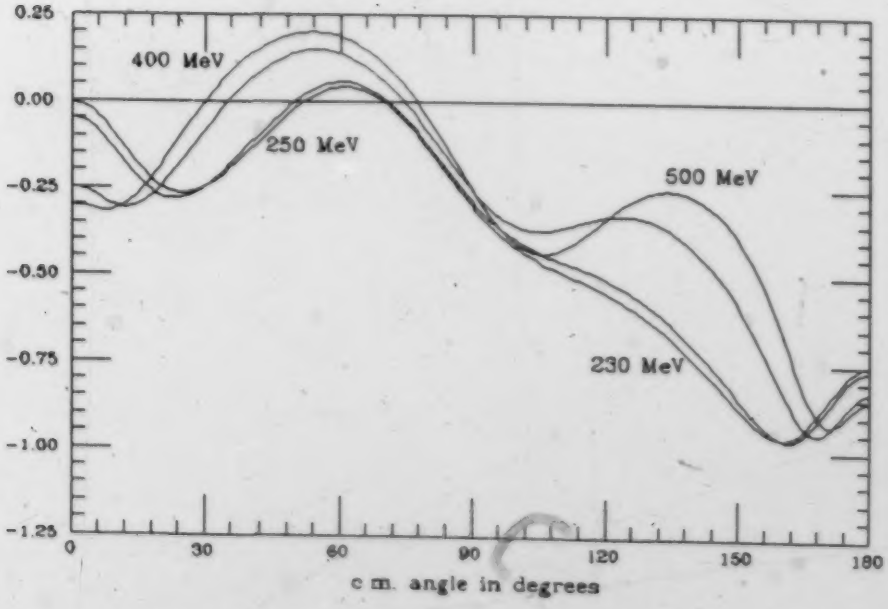

Figure III.7. The parameter A_{xx} for np scattering.

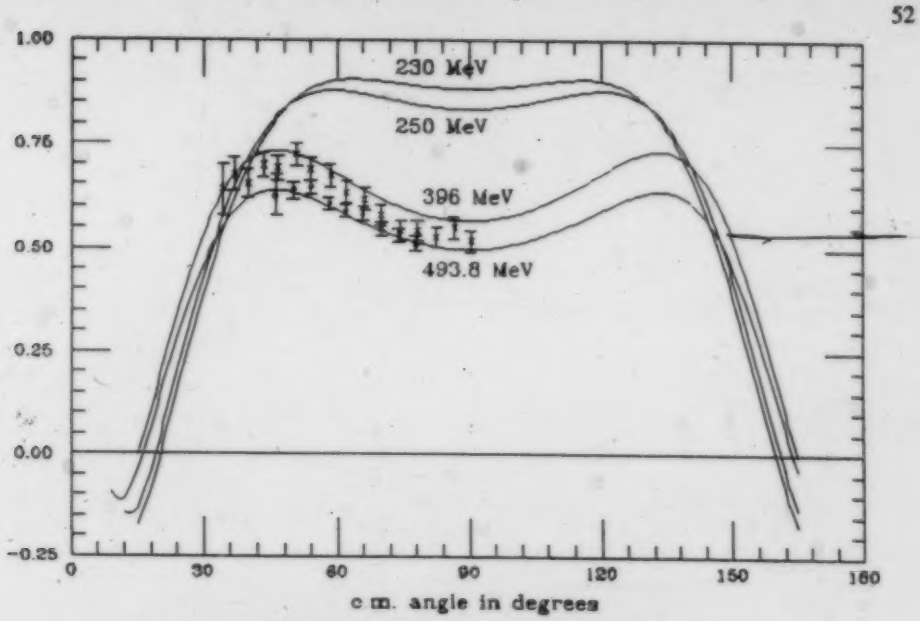

Figure III.8. The parameter A_{yy} for pp scattering (× for 396 MeV (BE80b) and • for 493.8 MeV (BY85)).

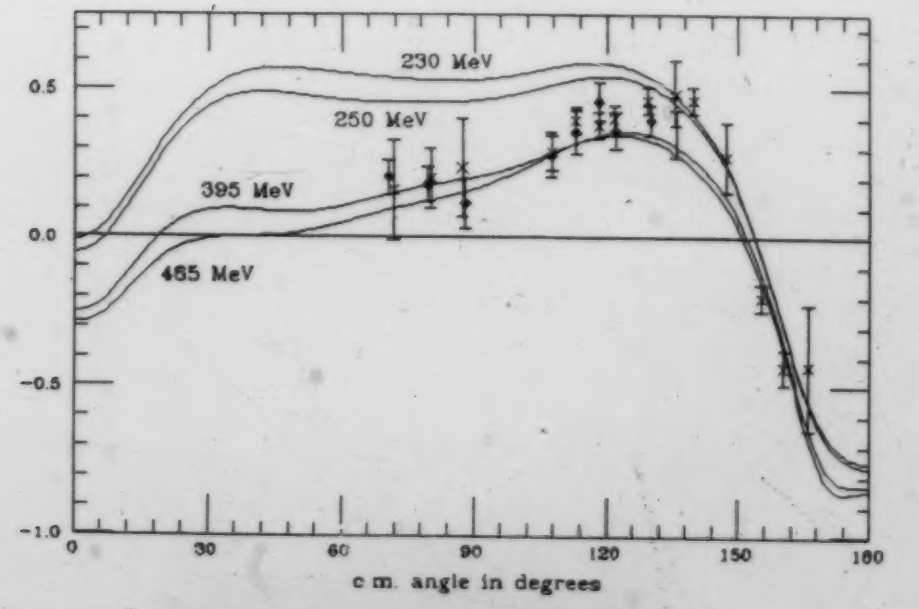

Figure III.9. The parameter A_{yy} for np scattering (× for 395 MeV (BH83) and • for 465 MeV (BH83)).

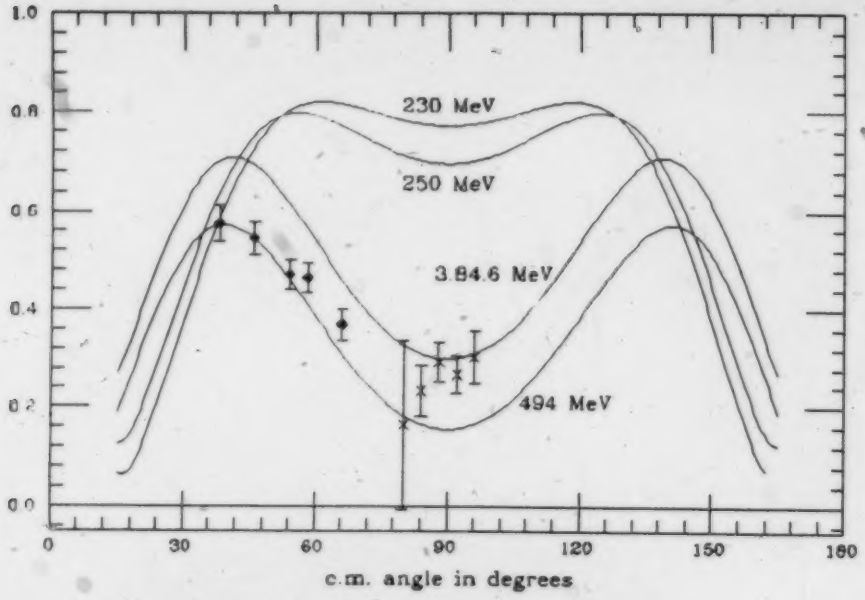

Figure III.10. The parameter A_{zz} for pp scattering (× for 392 MeV (AU84) and • for 494 MeV (APb83)).

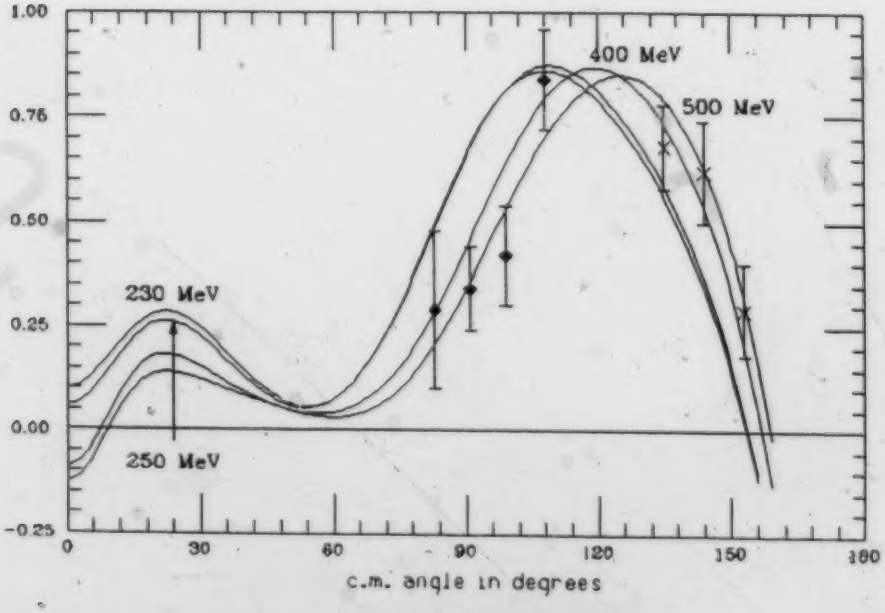

Figure III.11. The parameter A_{zz} for np scattering (× for and • are for 500 MeV (SP87)).

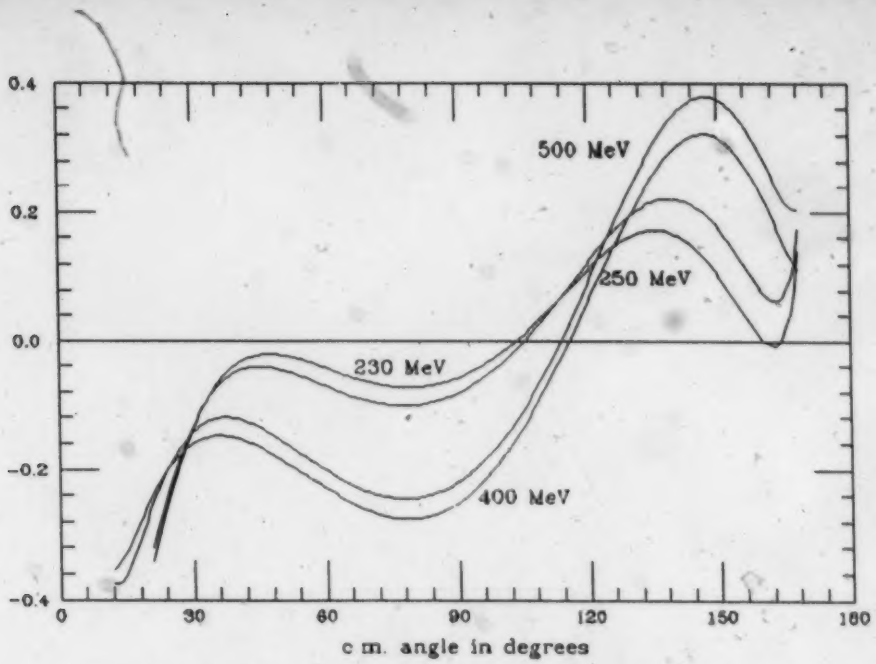

Figure III.12. The parameter C_{kk} for pp scattering.

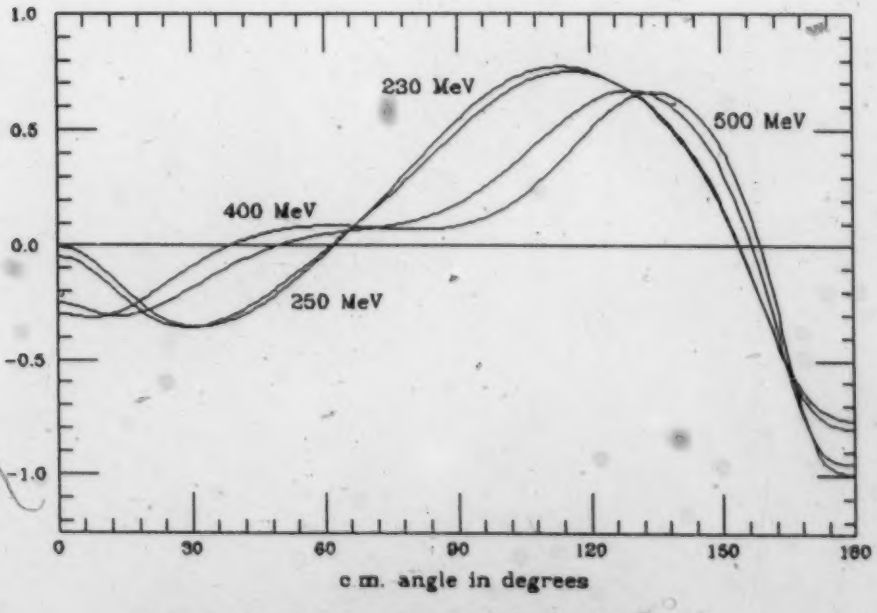

Figure III.13. The parameter C_{kk} for np scattering.

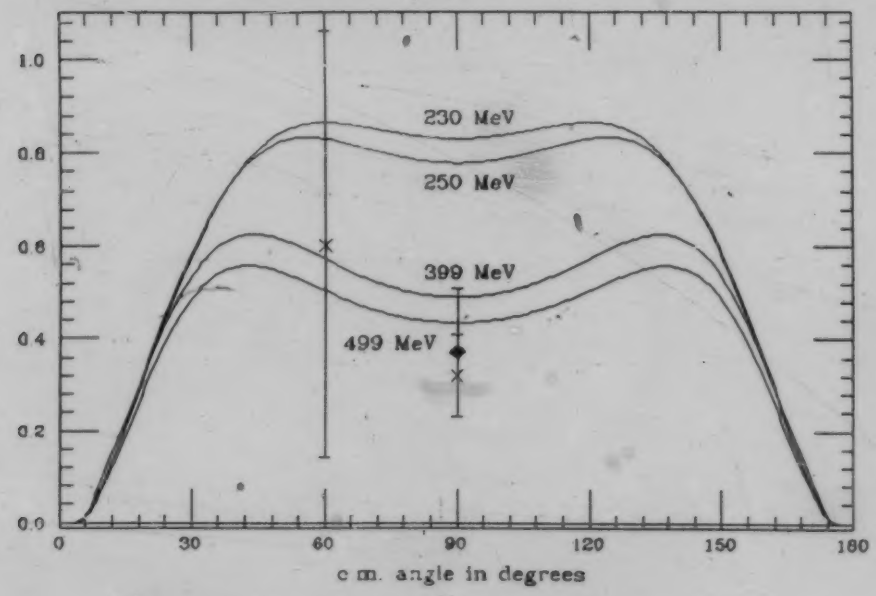

Figure III.14. The parameter C_{kp} for pp scattering (× for 399 MeV (EN63) and • for 449 MeV (EN63)).

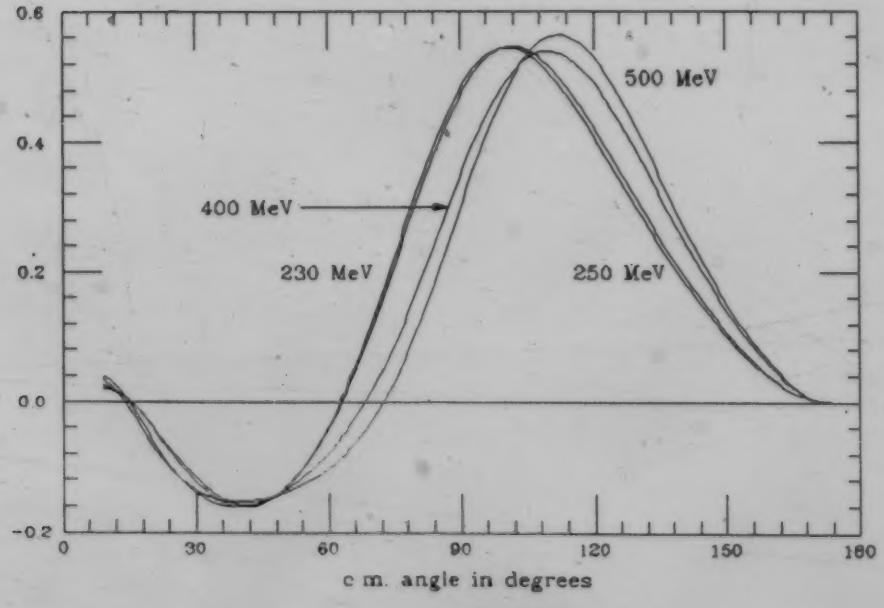

Figure III.15. The parameter C_{kp} for np scattering.

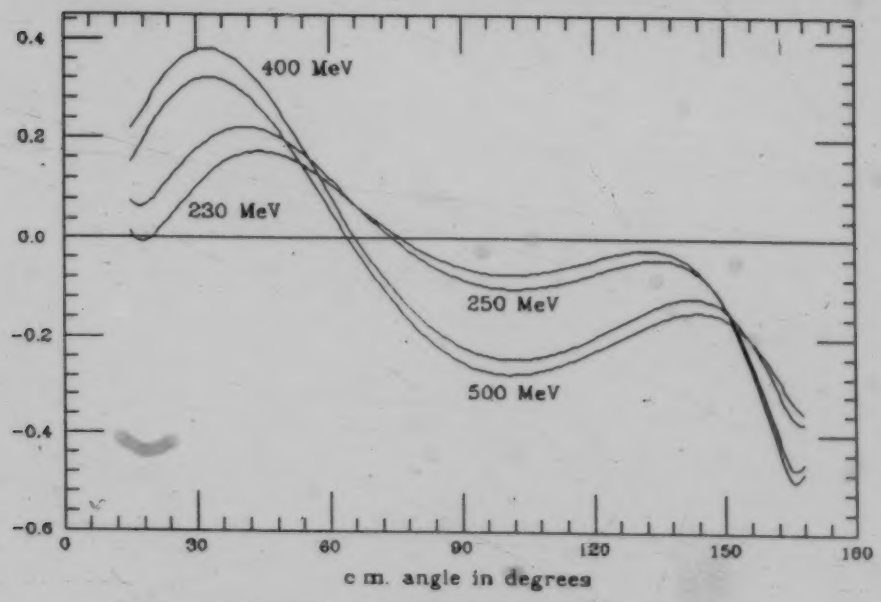

Figure III.16. The parameter C_{pp} for pp scattering.

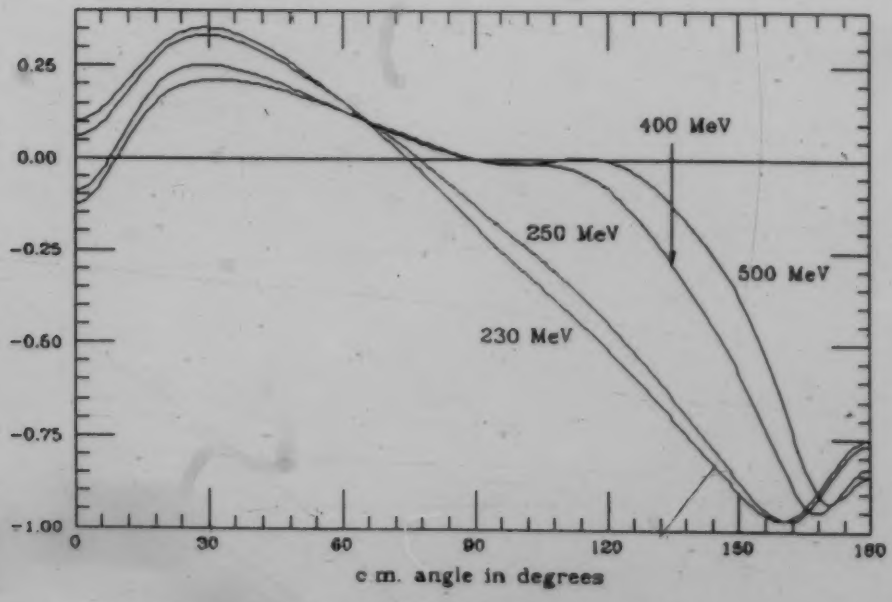

Figure III.17. The parameter C_{pp} for np scattering.

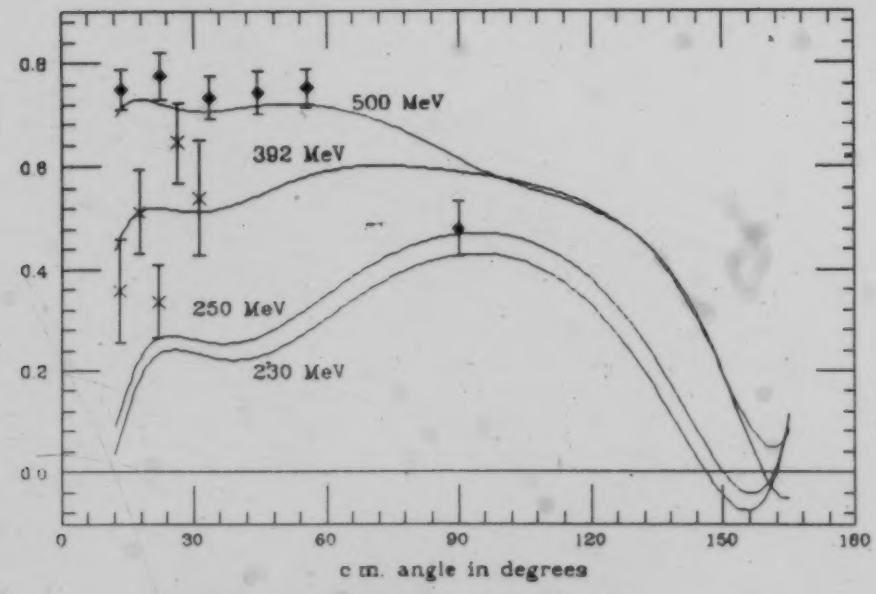

Figure III.18. The parameter D for pp scattering
(× for 392 MeV (BE80b) • for 500 MeV (MA86)).

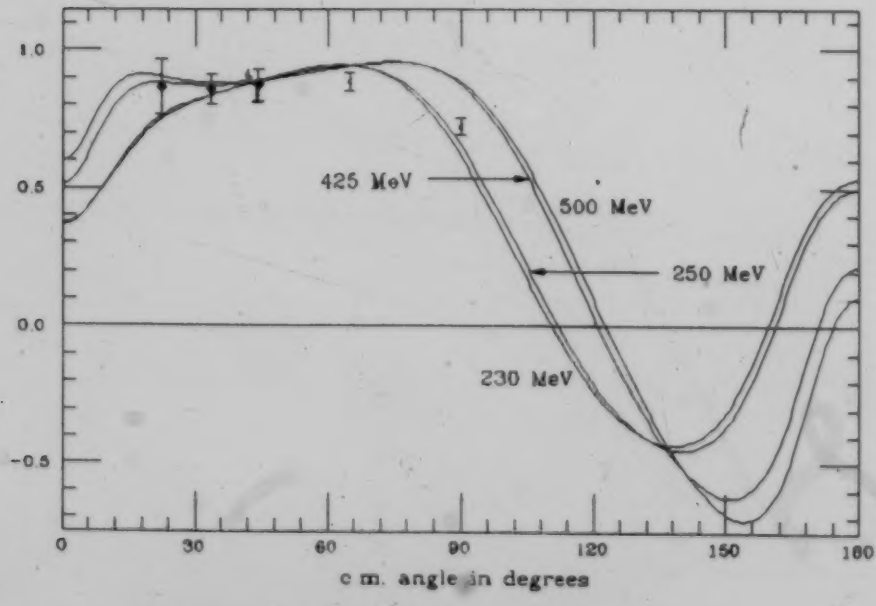

Figure III.19. The parameter D for np scattering
(× for 425 MeV (EN63) • for 500 MeV (MA86)).

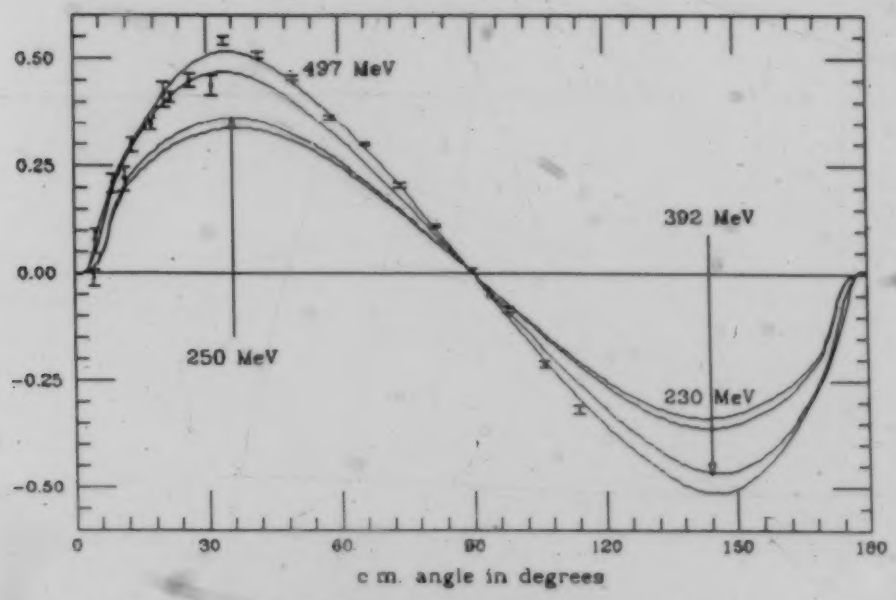

Figure III.20. The parameter P for pp scattering
(× for 392 MeV (BE80b) I for 497 MeV (AE77)).

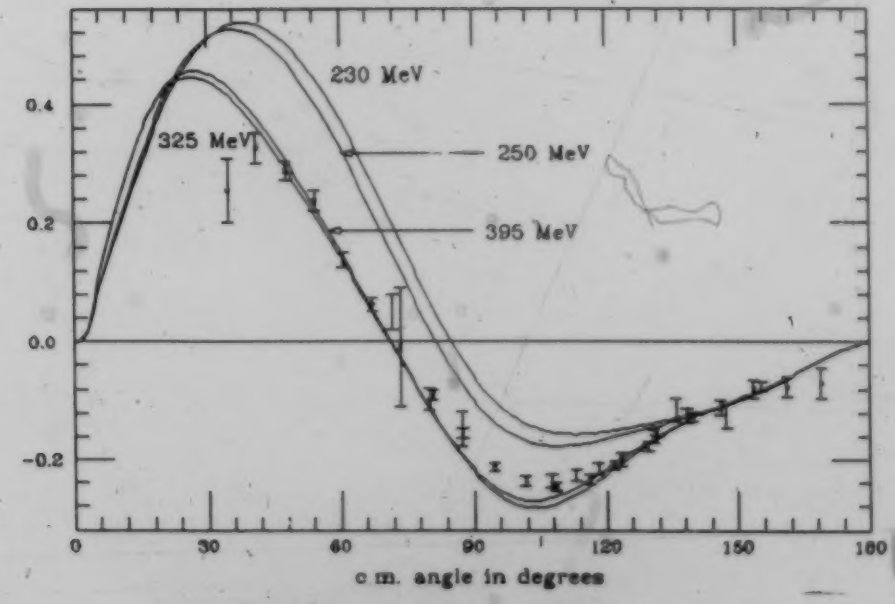

Figure III.21. The parameter P for np scattering
(× for 325 MeV (CL80) • for 495 MeV (BH83)).

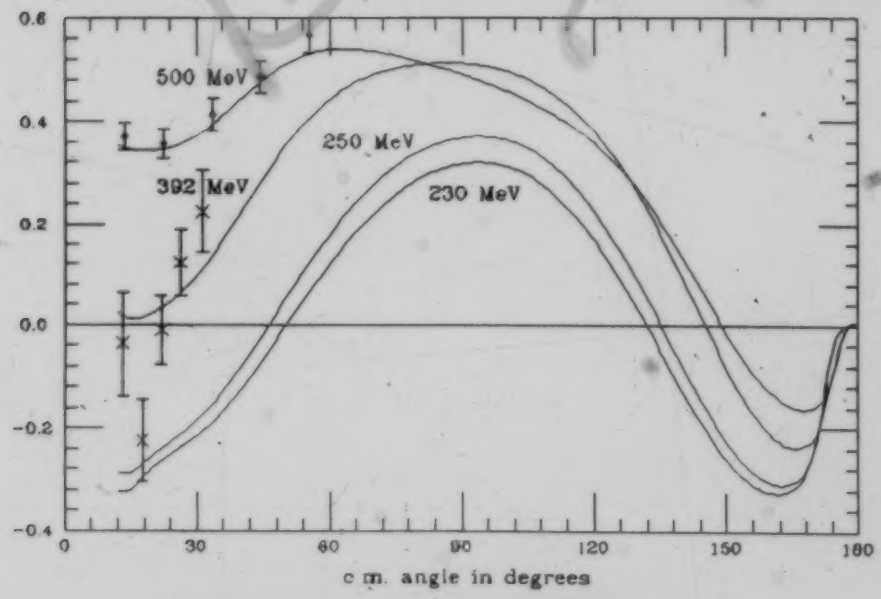

Figure III.22. The parameter R for pp scattering (× for 392 MeV (BE80b) • for 500 MeV (MA86)).

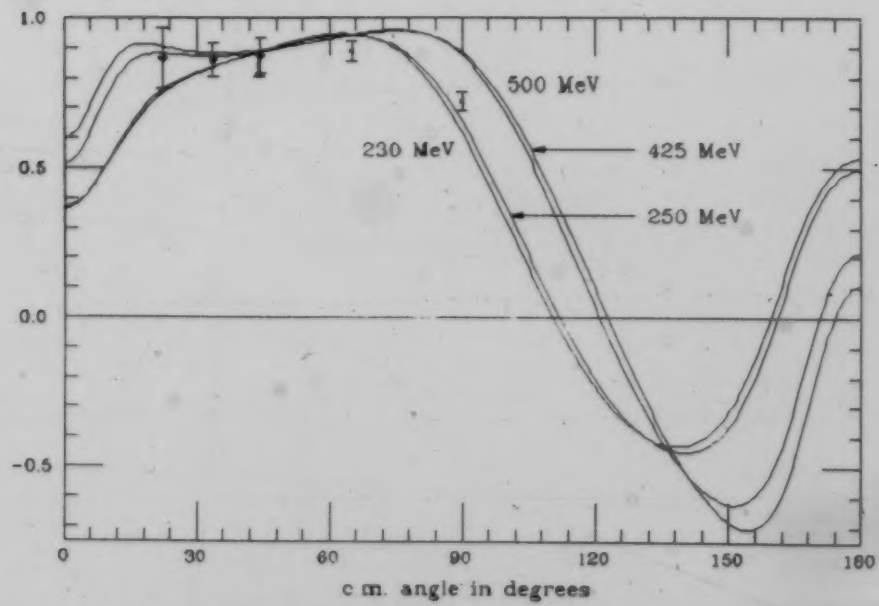

Figure III.23. The parameter R for pp scattering (× for 425 MeV (WR68) • for 500 MeV (MA86)).

CHAPTER IV

PARITY NONCONSERVATION IN PROTON-PROTON SCATTERING

The hypothesis of the existence of weak forces between nucleons which unlike ordinary nuclear forces, violate PC laws, was put forward since 1958 (FE58). The reason for looking at the effect of PNC forces in more detail-in experiments as well as in theoretical calculations is the idea that with the increasing accuracy of experiments as well as carefully performed theoretical investigation we should be able to learn more about the detailed form of the weak interaction.

At present two general trends can be distinguished in the description of the weak NN interaction with PNC: the "traditional" potential approach, which leads to an effective PNC NN potential, and the quark-nucleon approach, which essentially takes into account the quark structure of the nucleons and the formation of six-quark clusters at short distances. Both approaches, however, suffer from the fact that calculations by various authors differ significantly from each other even when the same approach is used (e.g. see KO81).

In the present work we shall discuss mainly the first appraoch and use the second one for comparison resons only.

The PNC nucleon-nucleon (NN) forces are in their simplest form delta functions, figure (IV.1a), which means that nucleon (1) can interact with nucleon (2)

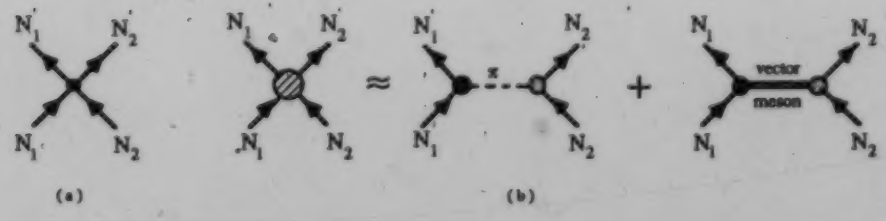

Figure **IV.1. Contribution to PNC NN forces: (a) point interaction, (b) NN interaction including one-boson-exchange (OBE).(dark and dotted circles represent strong and weak veticies respectively.**

only at the same point. Actually these types of forces are reduced in their effect due to the repulsive nature of the strong NN interaction at small relative distances (smaller than 1 fm), which restrict taking into account the present the use of meson theory along with the present understanding of the strong NN interactions (figure (IV.1b)).

IV.1. Parity Nonconserving Nucleon-Nucleon Potentials

In the conventional Cabibbo theory (CAa63) of weak interactions, the interaction currents consist of leptonic and hadronic components. The low-energy properties of the leptonic current are understood and the structure of the hadronic weak currents is obtained from studies of semileptonic processes. However, the empirical $\Delta I=1/2$ rule, which seems to hold true in the weak nonleptonic decays of strange baryons and mesons, does not follow from the simple Cabbibo theory. It is therefore necessary to generalize the Cabbibo theory to account for those new isospin changes, and this generalization could be achieved by either: (i) the addition of (neutral) currents or, (ii) dynamical octet enhancement (HE69a). The first of these, adds sufficient currents which account for the $\Delta I=1/2$ rule, whereas the second one assumes that the hadronic forces enhance the octet representation of the current-current interaction. Because the $\Delta I=3/2$ is contained, the representation of the octet enhancement suffices to give the desired result. There are differences between (i) and (ii) which can be tested experimentally, particularly in the weak forces between nucleons.

In the low energy regime (AD85), the hadronic weak interaction can be described by a phenomenological current-current Lagrangian

$$\mathcal{L} = \frac{1}{\sqrt{2}} G \, (J_W^{\dagger} J_W + J_Z^{\dagger} J_Z) + \text{h.c.} \, , \qquad \text{(IV.1)}$$

where J_w and J_z are the charged and neutral currents respectively. The charged current has two components

$$J_W = \cos\theta_c \, J_W^{\Delta S=0} + \sin\theta_c \, J_W^{\Delta S=1} \, , \qquad \text{(IV.2a)}$$

where θ_c is the Cabbibo angle ($\tan\theta_c \approx 0.22$) and the neutral current has two components

$$J_Z = J_Z^{\Delta I=0} + J_Z^{\Delta I=1} \ , \qquad \text{(IV.2b)}$$

and the effect of J_W's and J_Z's on the isospin and strangness are described in table IV.1.

Table IV.1
Effect of J_w's and J_z's on the Isospin and Strangness.

Current	Quark Transitions	Isospin Changes ΔI	Strangeness Changes ΔS
J_w^0	$u \to d$	1	0
J_w^1	$u \to s$	1/2	-1
J_z^0	neutral	0	0
J_z^1	neutral	1	0

The weak $\Delta S=0$ and $\Delta S=1$ NN interaction is then governed by the current-current Lagrangians

$$\mathcal{L}^{\Delta S=0} = \frac{1}{\sqrt{2}} G \left(\cos^2\theta_c J_W^{0\dagger} J_W^0 + \sin^2\theta_c J_W^{1\dagger} J_W^1 + J_Z^{0\dagger} J_Z^0 + J_Z^{1\dagger} J_Z^1 + J_z^{0\dagger} J_Z^1 + J_Z^{1\dagger} J_Z^0 \right) + \text{h.c.} \ , \qquad \text{(IV.3a)}$$

$$\mathcal{L}^{\Delta S=1} = \frac{1}{\sqrt{2}} G \left(J_W^{0\dagger} J_W^1 + J_W^0 J_W^{1\dagger} \right) \sin\theta_c \cos\theta_c \ . \qquad \text{(IV.3b)}$$

and the effect of the charged current-current terms on the isospin and strangeness is recorded in table IV.2.

In the low energy regime, the following prescription of the PNC NN interaction has proven to be useful (see table IV.3): (i) the PNC NN interaction is

written as a potential arising from single meson (π, ρ, ω), 2π-exchange where one meson-nucleon

Table IV.2
Effect of the Charged Current-Current Terms of the Lagrangian on the Isospin and Strangness.

Type	Isospin Changes (ΔI)	Weight
$J_w^{0\dagger} J_w^0$	0, 2	1
$J_w^{1\dagger} J_w^1$	1	$\tan^2\theta_c$

vertex is governed by the weak interaction and the other by the strong interaction (see figure IV.1b), (ii) the matrix elements of the NN interaction are expressed in terms of five elementary S-P amplitudes (SIa74).

IV.2. Meson Exchange PNC NN Potential

An obvious process which contributes to the PNC NN interaction is direct $W^{\pm}$ or Z^0 exchange between the nucleons. Because of the small Compton wavelengths of the bosons (≈0.002 fm), direct exchanges effectively occur only when two nucleons overlap. There is no adequate understanding of such short-range contributions to the PNC NN interaction. Fortunately, because of the energy characteristic of bound nucleons, the NN interaction takes place primarily at distances large compared to the nucleon size. This is due, in part, to the strong repulsion in the NN interaction at short distances. Thus we expect long-range contributions, which could be described without explicit reference to the structure of the nucleons, to dominate the low energy PNC interaction. We could also say that, in the NN interaction, all the physics of W and Z-exchanges between quarks is contained in the weak meson-nucleon vertex. At small center-of-mass energies, exchanges of light mesons dominate the PNC potential because the meson mass and the momentum transfer between

interacting nucleons appear in the static limit of the meson propagator $(q^2 + m_\pi^2)^{-1}$. The meson exchange description of the NN interaction becomes increasingly cumbersome at higher energies as a result of the proliferation of heavier mesons. In nuclei, the nucleons have $\langle p^2 \rangle_{ave.} = 3/5\ k^2_F \approx (200\ MeV)^2$ (we assume a Fermi energy of ε_F=37 MeV and an effective mass $m^*_N = 0.7 m_N$), so that a description of the PNC interaction that include light mesons should be adequate. We anticipate exchanges involving the isoscalers π(140 MeV), η(549 MeV), and η'(958 MeV), the scalers S(975 MeV) and δ^0(983 MeV), and the vector mesons ρ(769 MeV), ω(783 MeV), and ϕ(1020 MeV) along with 2π- exchange will determine the interaction of bound nucleons. Fortunately, the possible scaler and isoscaler exchanges are greatly restricted by Barton's theorem (BA61), which states that CP invariance forbids any coupling between neutral J=0 mesons and on-shell nucleons. Therefore π^0, η, η', S, and δ^0 exchanges are excluded to the extent that CP violation is negligible.

In order to describe the PNC NN interaction in terms of meson-exchange we have to classify the exchanges as:

i. The long-range part of the potential is well represented by π-exchange, whose parameters (coupling constants and form factors) are well determined.

ii. The short-range part of the potential is not well defined. Of course a sizeable ω-exchange would reproduce the well known fact that short range repulsive cores are supposed to be generated at distances (<1 fm) by interactions among quarks in nucleons, where the wavefunction mechanism is inoperative.

iii. The medium-range, is much more complicated (DE72) because the strong Hamiltonian is approximated by a phenomenological NN potential and not constructed by one-pion and two pion–exchange diagrams.

So that we can write the V_{PNC} as:

$$V^{NN}_{PNC} = V_\pi + V_\rho + V_\omega + V_{2\pi}\ , \qquad \text{(IV.4)}$$

In the next sections we shall discuss the recent developments for each of these contributions in terms of their corresponding isospin changes.

IV.2.a. π,ω,ρ Exchanges

The PNC NN potential for π, ρ, ω exchanges, could be written in the nonrelativistic limit as (see figure IV.1) (AD85)

$$V_{PNC}^{NN}(1,2) = \frac{i}{2}(\tau_1 \times \tau_2)^z (\sigma_1 + \sigma_2)\left[\left(\frac{P}{M}\right), \left(\frac{g_{NN\pi} f_\pi(r)}{\sqrt{2}} - g_\rho h_\rho^1 f_\rho(r)\right)\right] -$$

$$- g_\rho \left[h_\rho^0 \tau_1.\tau_2 + \frac{1}{2}h_\rho^1(\tau_1^z + \tau_2^z) + \frac{1}{2}\frac{h_\rho^2}{\sqrt{6}}(3\tau_1^z\tau_2^z - \tau_1.\tau_2)\right] x$$

$$x\left[(\sigma_1 - \sigma_2)\{\left(\frac{P}{M}\right), f_\rho(r)\} + i(1+\mu_v)(\sigma_1 \times \sigma_2)[\left(\frac{P}{M}\right), f_\rho(r)]\right]$$

$$- g_\omega\left[h_\omega^0 + \frac{1}{2}h_\omega^1(\tau_1^z + \tau_2^z)\right]\left[(\sigma_1 - \sigma_2)\{\left(\frac{P}{M}\right), f_\omega(r)\} + i(1+\mu_s)(\sigma_1 \times \sigma_2)[\left(\frac{P}{M}\right), f_\omega(r)]\right] .$$

$$- \left[(g_\omega h_\omega^1 - g_\rho h_\rho^1)\frac{1}{2}(\tau_1^z - \tau_2^z)(\sigma_1 + \sigma_2)\{\left(\frac{P}{M}\right), f_{\rho,\omega}(r)\}\right] , \qquad \text{(IV.5a)}$$

where

$$P = \frac{P_1 - P_2}{2} , \quad f_\pi(r) = \frac{e^{-m_\pi r}}{4\pi r} , \quad f_\rho(r) = g_\omega(r) = \frac{e^{-m_{\rho,\omega} r}}{4\pi r} . \qquad \text{(IV.5b)}$$

In the above expression of the potential, the g's represent the strong meson-nucleon coupling constants. h's represents the weak meson-nucleon coupling constants (see table IV.3) in which h's are assumed to be negative (AD85). The {,} is an anticommutator and [,] is a commutator. The factors μ_v and μ_s, describe the strong tensor couplings and are often given the values 3.7 and -0.12 which result from an identification with the anomalous isovector and isoscaler magnetic moments of the nucleon. The other coupling constants which appear in equation (II.19) are $h_\rho^{0,1,2}$, $h_\rho'^1$ and $h_\omega^{0,1}$ which govern the short range part of the potential. The indices represent the isospin component of the weak interaction to which they refer and the vector meson from which they originate. $h_\rho'^1$ corresponds to an axial vector coupling.

Table IV.3
Weak Coupling Constants from "Best Value" and "Reasonable Range"

Coefficient	Best Value ($x10^{-6}$)	Reasonable Range ($x10^{-6}$)
$(F_\pi=)\ g_{\pi NN} f_\pi/\sqrt{32}$	1.08	0 : 2.71
$(F_0=)\ -g_\rho h_\rho^0/2$	1.59	- 1.59 : 4.29
$(F_1=)\ -g_\rho h_\rho 1/2$	0.027	0 : 0.053
$(F_2=)\ -g_\rho h_\rho^2/2$	1.33	- 1.06 : 1.54
$(G_0=)\ -g_\omega h_\omega^0/2$	0.80	- 2.39 : 4.29
$(G_1=)\ -g_\omega h_\omega^1/2$	0.48	0.32 : 0.8

Note that π-exchange plays a dominant role in the ΔI=1 interaction. Both ρ and ω exchanges contribute to the ΔI=0 interaction, while the ΔI=2 interaction arises from ρ-exchange.

Among different PNC meson-nucleon coupling constants which appear in equation (IV.5a), the πNN coupling constant, f_π, has certainly received the most attention until now. On one hand it is the part of the PNC nuclear force which has the longest range. Because of this property, the corresponding contribution may be enhanced relative to other contributions. While this is confirmed by calculations of the PNC effect at low energy (<46 MeV), part of the advantage is lost at higher energies and in complex nuclei, due to the exchange character of this force. On the other hand, since its contribution from the charged current, which contains the factor $\sin^2\theta_c \approx 0.05$, is small, it essentially depends on the properties of the neutral current whose contribution which contains factors $\sin^2\theta_w \approx 0.25$ and $(1-2\sin^2\theta_w) \approx 0.5$ (where θ_w is Weinberg angle); is not similarly suppressed.

IV.2.b. Two-Pion Exchange

In figure (IV.2b) we can see the possible 2π-exchange contributions which were calculated by Blin-Stoyle (BL60a). He calculated the contribution of the 2π-exchange to the total asymmetry and concluded that it does not exceed $< 8 \times 10^{-8}$.

The diagrams (IV.2.a) express PNC weak NNπ vertex which has ΔI=1 when CP is conserved (DE72). Therefore, they contribute to ΔI=1 potential as one-pion exchange potential. This effect was calculated assuming the contribution of π, ρ and 2π-exchanges which gives ≈4.3 x 10^{-8}.

Priner and Resika (PI73) considered in their calculations the contribution from figure (IV.2a) and figure (IV.2b.ii), and it was concluded that the 2π-exchange has to be taken into account. Later another group (BR74) investigated the same thing using the Hamada-Johnston potential, and concluded that it has to be included in calculating the total asymmetry (see figure IV.7). They stated that care has to be taken concerning double counting and the uncertainties in evaluating off-mass-shell contributions, which are required for the 2π-exchange potential. Another calculation (CH74), concluded that the 2π-exchange effects are not intrinsically small, as they apper in a significant way in components of the potential where π-exchange effects are excluded, they would provide 10 ~ 50 % enhancement in the magnitude of the ρ-exchange contributions.

Recently another analysis has been done (MU86), in which the diagram of figure (IV.2.c) has been considered. They considered contributions from regions

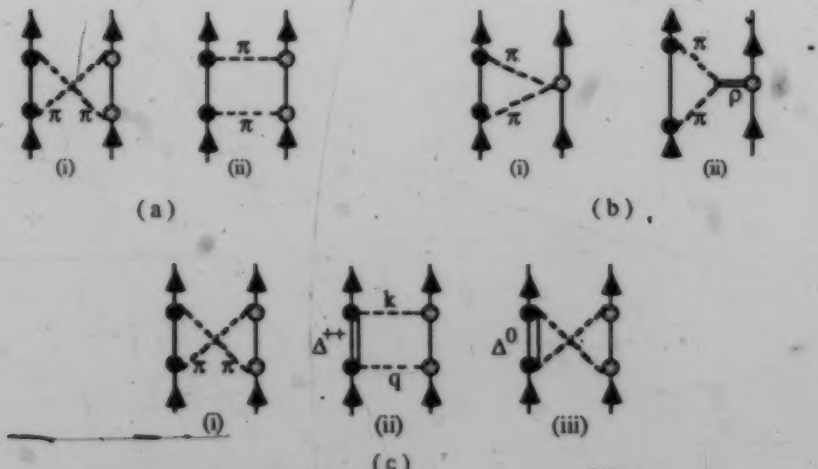

Figure **IV.2. 2π-exchange diagrams (a) ΔI=0, 2 (BLa60), (b) ΔI=1 (DE72), (c) ΔI=0 and other possibilities (MU86). Dark and dotted circles are the strong and weak verticies respectively.**

where the internucleon separations are larger than those where the ρ and ω exchange contribution's dominate. The calculations were based on the cloudy bag model (LEb79), (TH81) and different bag radii were used (0.4-1.0 fm). The authors concluded that the contribution of ρ and ω is concentrated in the range $0.5\text{-}0.6 < r < 1.5\text{ -}1.6$ fm depending on the strong potential used, and the 2π-exchange is concentrated mainly at $r > 0.8$ - 1.0 fm. The second diagram in figure (IV.2c) contributes 50 - 70 % with positive sign, the first diagram contribution is ≈ 20 % with positive sign and the third one contributes 7 - 9 % with negative sign.

There may be some ambiguity in using the PNC 2π-exchange potential in nuclear calculations where the strong Hamiltonian is approximated by a phenomenological NN potential and not constructed from one-pion or 2π-exchange diagrams.

IV.3. Two-Nucleon S-P Amplitudes

An analysis of PNC effects which does not rely on meson exchange models of the weak interaction has been performed for the NN system at very low energy. Since it is not subject to the uncertainties inherent in potential model calculations, it was believed that such approach is more appropriate for comparing PNC effects (DE78). The weak PNC potential could be written in terms of five zero-range elementary S-P amplitudes, summarized in table IV.3. In addition to these, it is customary to include a sixth long range parameter due to one-pion exchange, which is the significant part of $^3S_1 \rightarrow {}^3P_1$ amplitude and produces a sizable $^3P\text{-}^3D$ and $^3D\text{-}^3F$ transition amplitudes as well.

In terms of the transition amplitudes, the weak NN scattering amplitudes are

$$\mathcal{F}_w^{NN} = \frac{1}{2} v^{NN}(P^2)\left[(\sigma_1 - \sigma_2)\cdot(p_f + p_i) + i(\sigma_1 \times \sigma_2)\cdot(p_f - p_i)\right], \qquad \text{(IV.6a)}$$

and

$$\mathcal{F}_w^{pn} = \frac{1}{2} v^{pn}(p^2)\,[(\sigma_p - \sigma_n)\cdot(p_f + p_i) + i\,(\sigma_n \times \sigma_p)\cdot(p_f - p_i)] +$$

$$+ \frac{1}{2} u(p^2)\,\{(\sigma_p - \sigma_n)\cdot(p_f + p_i) - i\,(\sigma_n \times \sigma_p)\cdot(p_f - p_i)\} +$$

$$+ w(p^2)(\sigma_p + \sigma_n)\cdot(p_f + p_i)\,, \qquad \text{(IV.6b)}$$

Table IV.4
Nucleon-Nucleon S-P Weak Amplitudes and Meson-Exchange Equivlants

Transitions	I→I'	ΔI	NN State	Exchanged	Range Particle	Potential Term
$^3S_1 \rightarrow {}^1P_1$	0 → 0	0	pn	ρ,ω	Short	$u(p^2)$
$^1S_0 \rightarrow {}^3P_0$	1 → 1	0	pp, nn, pn	ρ,ω	Short	$v(p^2)$
		1	pp, nn, pn	ρ	Short	$v(p^2)$
		2	pp, nn, pn	ρ	Short	$v(p^2)$
$^3S_1 \rightarrow {}^3P_1$	0 → 1	1	pn	π	Long	$w(p^2)$
		1	pn	ρ	Short	$w(p^2)$

In the plane wave Born approximation (PWBA) the $^1S_0 \rightarrow {}^3P_0$ amplitudes v's are given by

$$v^{NN} \approx \frac{1}{m_\rho^2}\left[\left(F_0 \pm F_1 + \frac{F_2}{\sqrt{6}}\right)(2 + \mu_v) + (G_0 \pm G_1)(2 + \mu_s)\right], \qquad \text{(IV.7a)}$$

$$v^{pn} \approx \frac{1}{m_\rho^2}\left[\left(F_0 - \sqrt{\frac{2}{3}}\,F_2\right)(2 + \mu_v) + G_0(2 + \mu_s)\right], \qquad \text{(IV.7b)}$$

while the $^3S_1 \rightarrow {}^3P_1$ amplitude w^{pn} is given by

$$w^{pn} \approx \frac{1}{m_\rho^2}\left[2\,F_\pi\left(\frac{m_\rho}{m_\pi}\right)^2 + 2\,H_1 + G_1 - F_1\right], \qquad \text{(IV.7c)}$$

and the $^3S_1 \rightarrow {}^1P_1$ amplitudes is

$$u^{pn} \approx \frac{1}{m_\rho^2}(G_0 \mu_s - 3 F_0 \mu_v) , \qquad \text{(IV.7d)}$$

where we have taken $m_\omega \approx m_\rho$, and the F's, G's and H's are the same as in table IV.3.

Ideally one would perform at least five low energy experiments in the NN system to determine independent combinations of the five partial-wave amplitudes, including one experiment in which the dependence of the observable on the center of mass energy could be exploited to separate the pion-exchange contribution to the $^3S_1 \rightarrow {}^3P_1$ amplitude from the shorter range contributions.

IV.4. PNC ASYMMETRY IN P-P SCATTERING

The high-intensity accelerators make investigation of weak NN scattering experiments feasible. In these investigations one can observe the nonvanishing expectation values $\langle \sigma_1 \cdot P \rangle$, $\langle \sigma_2 , P \rangle$, or $\langle \sigma_1 \cdot \sigma_2 \times q \rangle$. A particularly effective method is the observation of the $\langle \sigma_1 \cdot P \rangle$ in measurements of the total cross section for the scattering of unpolarized nucleons by polarized ones (BR74). Such studies would allow one to investigate the weak nonleptonic force in some detail, and thus hopefully to distinguish between various proposed models (HE69a).

The computed asymmetry for what is plotted as a function of scattering angle at various energies in figure (IV.3). It is surprising that $A_z(\theta)$ (see equations II.26 and II.33b) remains small with increasing energy (it is maximum roughly at 50 MeV), and it was expected that the asymmetry would increase linearly with p, the incident momentum, since the Fourier transform (Born-approximation amplitude) increases in this manner over the range of energies considered here (BR73). The decrease at higher energies appears to be caused in large measure by the effects of the strong repulsive core between nucleons, If we write $f = \Sigma_J f(J)$, where J is the total angular momentum, then we find that f(0), in particular, is strongly reduced by distortions caused by the hadronic forces (it was suggested that this decrease was due to the

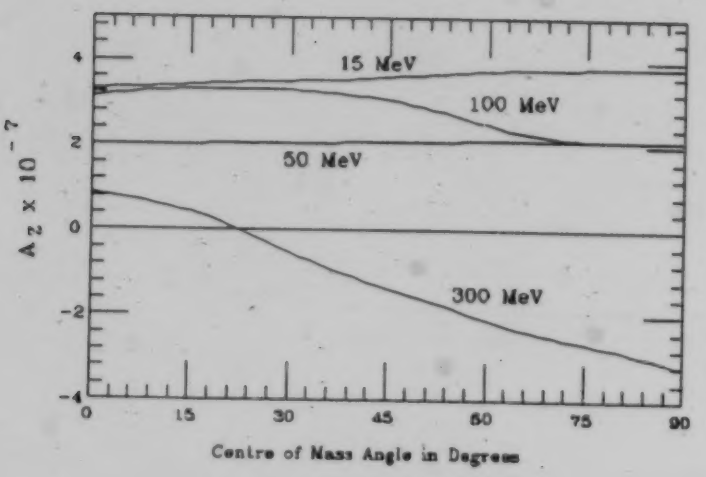

Figure IV.3. The total asymmetry as a function of the center of mass angle.

short-range repulsion between nucleons). Because of this reduction, f(2) which increases with energy and has the opposite sign, cancels a large part of f(0) at higher energies. This is the reason that the asymmetry remains small.

In actual measurements with the beam polarization between ≈0.7 and 1 and a detection system extending over a large solid angle Ω to increase statistics, one measures P. A_L rather than $A_L(\theta)$ (which is the total scattered asymmetry) where

$$A_L = \frac{\int (\frac{d\sigma}{d\Omega})\, A_L\, d\Omega}{\int (\frac{d\sigma}{d\Omega})\, d\Omega} \qquad \text{(IV.8)}$$

is the intensity weighted average analyzing power, and it is well known that $A_L(\theta)\neq 0$ violates parity in reactions with two body final state.

We can write down a formula for A_L using the phase shift method in which the case it has the form (SIa74)

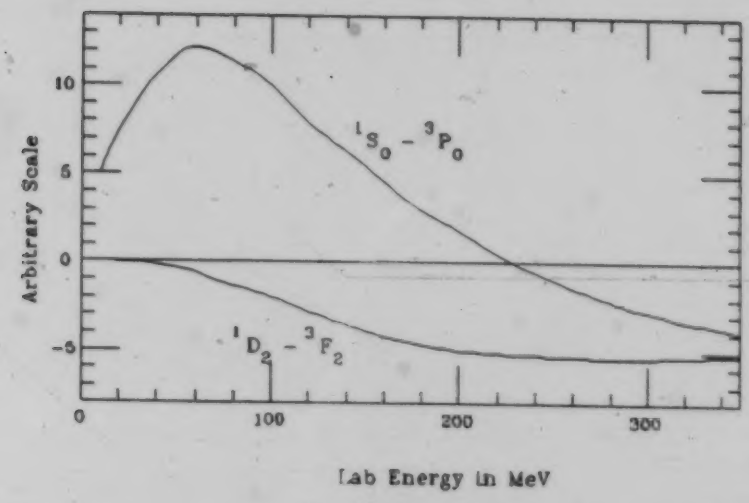

Figure IV.4. The two main contributions to the scattering asymmetry at low energies (the vertical scale is arbitrary).

$$A_L = \frac{2\, f(^1S_0 \rightarrow {}^3P_0)\, \sin[\delta(^1S_0) + \delta(^3P_0)]}{\sum_{\Delta J} (2J+1) \sin^2 \delta_{\Delta J}} \qquad \text{(IV.9)}$$

There is another form A_L (SIa86 and SIa87a) in which A_L can expressed as a sum of partial wave contributions

$$A_L(\theta) = A_L(^1S_0 - {}^3P_0) + A_L(^3P_2 - {}^1D_2) + A_L(^1D_2 - {}^3F_2) + \ldots , \qquad \text{(IV.10a)}$$

where each term is a combination of

$$\left[\text{Combination of } h_\rho \,\&\, h_\omega\right] \times \left[\text{Matrix elements of the weak meson exchange interaction}\right] \times \left[\text{Angular distribution from pp phase shift analysis (strong interaction)}\right] . \qquad \text{(IV.10b)}$$

We can write the PNC pp potential (SI86) for low energies, ignoring the 2π-exchange, in the form

$$V_{PNC}^{PP} = -(h_\rho^{PP} g_\rho + h_\omega^{PP} g_\omega)(\sigma_1 - \sigma_2)\{P, F_{m_\rho(m_\omega)}(r)\} -$$
$$-(h_\rho^{PP} g_\rho (1+\mu_v) + h_\omega^{PP} g_\omega (1+\mu_s))\, i(\sigma_1 x \sigma_2)[P, F_{m_\rho(m_\omega)}(r)], \qquad \text{(IV.11a)}$$

where the constants here are connected to the usual DDH parameters (see table IV.5) as (Sla83a)

Table IV.5
The Values of Five Parameters for the Weak NN Vertex

Authors	h_ρ^0	h_ρ^1	h_ρ^2	h_ω^0	h_ω^1	h_ρ^{PP}	h_ω^{PP}	$h_\rho^{PP}+h_\omega^{PP}$
DDH (AD85)	- 15.90	- 0.27	- 13.3	- 0.80	- 0.48	-21.60	-1.28	-16.35
OKA (OK81)	23.49	0.54	- 8.82	- 35.19	-9.50	20.43	44.69	-10.93
DZ (DU83)	- 8.30	-0.39	- 6.70	- 3.90	- 2.20	-10.05	-6.10	-16.35

$$h_\rho^{PP} = h_\rho^0 + h_\rho^1 + \frac{h_\rho^2}{\sqrt{6}}, \qquad \text{(IV.11b)}$$

$$h_\omega^{PP} = h_\omega^0 + h_\omega^1. \qquad \text{(IV.11c)}$$

In table IV.5 we see different representations for the weak coupling constants and the figure (IV.12) represents the different ways of measuring and estimating equations (IV.11b) and (IV.11c). Using the fact that the spin matrix elements obey

$$<\text{triplet}|(\sigma_1 - \sigma_2)|\text{singlet}> = <\text{triplet}|i(\sigma_1 x \sigma_2)|\text{singlet}>, \qquad \text{(IV.12)}$$

it is convenient to split the f in equation (IV.9) and use equation (IV.11a) to write

$$f_J^s \propto <J\ \ell=J\pm1\ s=1|(\sigma_1 - \sigma_2)F_m(r)\,P|J\ \ell=J\ s=0>, \qquad \text{(IV.13a)}$$

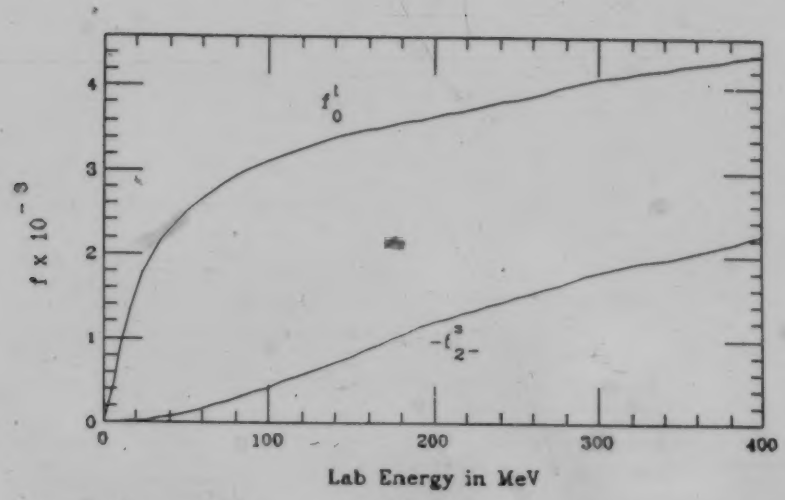

Figure IV.5. **Energy dependence of the dominating amplitudes calculated with Paris potential.**

$$f_J^t \propto \langle J\, \ell=J\pm1\, s=1 | (\sigma_1 - \sigma_2)\, P\, F_m(r) | J\, \ell=J\, s=0 \rangle \quad , \tag{IV.13b}$$

which represents the difference (proportional to μ's) and sum (proportional to $2+\mu$) of the anticommutator (notice the approximation that $m_\rho=m_\omega$) and the commutator parts respectively, of the matrix elements of the PNC potential. The superscripts **s** and **t** stand for singlet ($\ell=J$) and triplet ($\ell=J\pm1$) side of the matrix element respectively. Now P is responsible for the transition between different values of ℓ and since $F_m(r)$ has a short range ($m^{-1}\approx0.25$ fm), its matrix element in the lowest possible ℓ state dominates at low energies (<250 MeV see SIa86). For a semiquantitative analysis we therefore find

$$\begin{aligned} f(^1S_0 - {}^3P_0) &\approx \left[h_\rho^{pp} g_\rho (2+\mu_v) + h_\omega^{pp} g_\omega (2+\mu_s) \right] f_0^t \\ &\approx 15\, (h_\rho^{pp} + h_\omega^{pp})\, f_0^t \quad , \end{aligned} \tag{IV.14b}$$

and

$$f(^3P_2 - {}^1D_2) \approx -\left[h_\rho^{pp} g_\rho \mu_v + h_\omega^{pp} g_\omega \mu_s\right] f_2^s$$
$$\approx -\,(9.7\, h_\rho^{pp} - 0.94\, h_\omega^{pp})\, f_2^s \,. \qquad \text{(IV.14b)}$$

Figure (IV.5) shows new calculations of f's done using the Paris potential to describe the pp scattering states.

In figure (IV.10) the energy dependence of the amplitudes and their contribution to the asymmetry of the total nuclear cross sections are shown for the two lowest possible PNC partial wave transitions $^1S_0 \rightarrow {}^3P_0$, $^3P_2 \rightarrow {}^1D_2$ and $^1D_2 \rightarrow {}^3F_2$ (considering that only ρ and ω exchange contribute to p-p scattering) (PA86). The energy dependence is essentially model independent and is given in an essentially model independent way by kinametics and fixed by pp phase shifts. The relative strength of the two contributions shown corresponds to pure ρ^0 exchange (calculated with wavefunction obtained from Reid soft core). For ω-exchange the $^3P_2 \rightarrow {}^1D_2$ transition is strongly suppressed since to a good approximation it is proportional to the anomalous magnetic moment coupling for the ω which is much smaller than for ρ. Thus measurements above about 200 MeV, which are sensitive to this difference would be of great interest because (SIa83b) (of course one has to take into account higher transition amplitudes as well as the fact that A_L in not angular independent anymore): (i) it contains practically no ω contribution (information complentary to the one at low energy is herefore obtained), (ii) it is more peripheral (due to the "centrifugal barrier") and thus less sensitive to detalis of the short range NN interaction than the low energy results. Thus measurements in the 200-300 MeV region would be of great interes

IV.5. Scattering Asymmetry from 10 MeV and 5.3 GeV

Figure (IV.8) shows a plot of the different calculations introduced for the total asymmetry. The general shape of the curve could be explained in the low energy regime as follows: for E_L<50 MeV the weak interaction amplitudes $\mathfrak{F}_{01}(0)$ and $\mathfrak{F}_{10}(0)$ of the protons are monotonically decreasing functions of energy. The strong

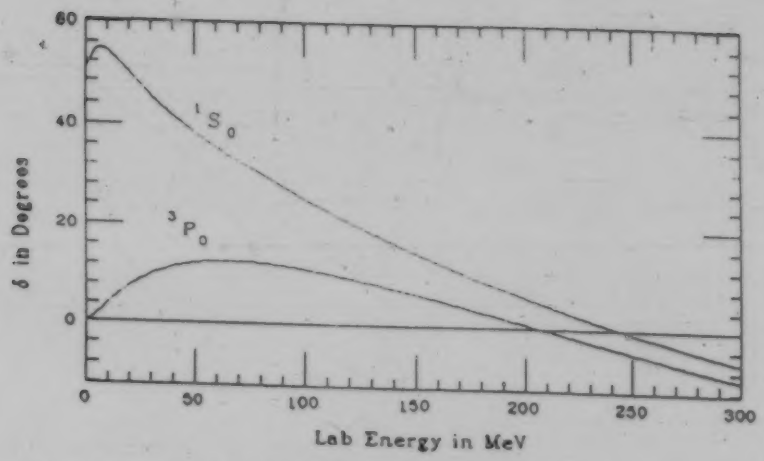

***Figure* IV.6. Shape of the major two phase shifts affecting the scattering asymmetry at low energy.**

interaction amplitudes $\mathcal{G}_{00}(0)$ and $\mathcal{G}_{10}(0)$ (see equation II.33b) are proportional to $\sin\delta(^1S_0)$ and $\sin\delta(^3P_0)$ as in equation (IV.9). The energy dependence of δ phases is shown in figure (IV.6). Thus, the part of the numerator in equation (II.33b) corresponding to J=0 decreases with increasing E_L, reaches a minimum, and then passes through zero near E_L ≈220 MeV. The denominator in equation (II.33b) in this case does not vanish. For higher partial waves, especially J=2 and 4, the contributions increase with energy, and since they have opposite signs relative to the contribution of t J=0, they partially compensate for this contribution. The effect can be observed in the shift of the minimum of the asymmetry towards the proton energy E_L=50 MeV, and of the zero towards E_L<220 MeV. In case of high energy there is a discreipancy between theory and experiment, which reflects difficulties in explaining the high energy data as will be discussed later in this section. In this section we shall review theoretical attempts in historical order.

An early attempt was that by Henley (HE75) devoted to the energy range 100 MeV to 10 GeV. As can be seen from table IV.6 the results are in complete disagreement with experiment. The predicted asymmetry has a slope of opposite sign to those shown in figure (IV.8). Another calculation by Epstein (EP75) using the Reid soft core and hard core potentials for the contribution of $^1S_0$-$^3P_0$ amplitude only, also (table IV.x) does not agree with experiment even as far as the sign of the asymmetry is concerned.

In 1981, four calculations were carried out by different authors. The first one was by Lobov (LOb81), using Reid soft core and Hamada-Johnstone potentials for the low energy range, showed that both differ by <20% (the number shown in table IV.6 is for Reid soft core calculations). It colud be seen from table (IV.6) that the 15 MeV calculations agree with the experiment within the error bars, which is not true for the 45 MeV case. The second calculation, carried out by Dubovik *et al* (DU81) using the QCD model disagreed with experiment. It was concluded that the difference is due to difficulties in calculating the matrix element and/or unsatisfactory knowledge of the strong potentials at short distances. The third attempt was introduced by Oka (OK81). Oka's calculations for the 15 MeV showed an excellent agreement with experiment using Z-boson exchange but failed at 45 MeV. His 800 MeV result was obtained using the DDH parameters. On the other hand, he failed to explain the 5.3 GeV data. Oka concluded that there may be several reasons for the small theoretical values obtained for the asymmetry. Among them he pointed out the importance of inelastic channels. He expected that the intermediate inelastic channels to have contributions similar to those of the intermediate elastic channels in magnitude and he expected an enhancement by a factor of 16 at this energy range (see figure IV.10). Although such an argument is too crude to draw anything definite, Oka suggested that one must consider these effects when evaluating the calculations. The fourth

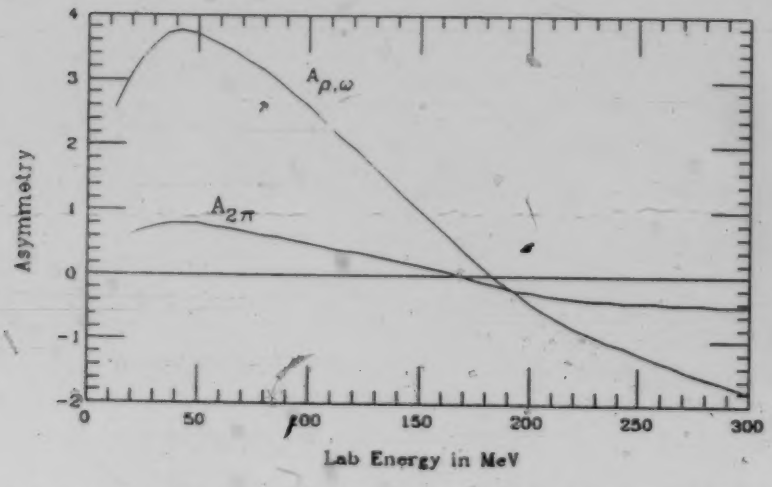

***Figure* IV.7. Comparison between ρ,ω contributions and 2π exchanges to the total asymmetry (vertical scale is arbitrary).**

Table IV.6

Comparison between experimental results and calculations for the asymmetry over the energy range from 10 MeV to 5.3 GeV (R. s.c. is Reid soft core, z iis for z-boson exchange, I without considering two pion contribution and II with considering two pion contribution.

Lab Energy In Mev	Experiment	Theory													
						OK81			BAb81		NA83a	NA83b		NAb84	
		HE75	EP75 R. s.c.	DU81	LOb81	DDH	QCD	Z	I	II	I	II	MIa84	I	II
15	-1.7±0.8 (NA78)		= 0.75		-2.40	-1.20	-0.50	-1.70					-1.50		
25															
45	-1.5±0.2 (KI87)		= 1.3	-0.32	-3.90	-4.00	-1.50	-5.00					-1.80		
50															
100		-1.50	= 1.45		-2.60	-4.50	= -2.50	-8.80					= -1.95		
250		0.30	= -0.30		1.30								= -1.25		
300		-1.00	= -4.00		2.40	2.90	= 0.80	= 8.50			8.00		= -1.10	8.00	
800	2.4±1.1 (YUa86)	-1.60				= 2.80	= 1.10	8.10			9.00	2.00	= -0.20	9.00	2.00
1000		-1.50				2.30	0.80	7.00			= 9.40	= 3.60		= 9.40	= 3.60
5300	26.5±6.00 (LOc84)	-1.20				1.20	1.10	8.00	1.04	0.96	11.60	= 10.20		11.60	= 10.20

Lab Energy In Mev	Experiment	Theory												
				MU86										
				DDH				ZD						
				Reid s.c.		Paris		Reid s.c.		Paris			Sla87a	
		SIb84	MU85	I	II	I	II	I	II	I	II	GO86	Reid s.c.	Paris	Sla87b
15	-1.7±0.8 (NA78)			-1.00	-0.69	-1.39	-1.08	-0.87	-0.78	-1.21	-1.12		1.10	1.50	
25			-2.20												
45	-1.5±0.2 (KI87)			-2.06	-1.59	-2.96	-2.48	-1.79	-1.66	-2.51	-2.37		1.80	2.40	
50			-2.30												
100													2.20	3.10	
250													2.70	3.90	
300												2.00			
800	2.4±1.1 (YUa86)											= 2.20			
1000												3.00			
5300	26.5±6.00 (LOc84)	0.49										25.00			< 2.00

calculation was introduced by Barroso and Tadic' (BAb81), for the high energy range, using the meson exchange method taking into account the 2π-exchange contribution. They obtained a value which disagrees with experiment. It was concluded that some of the factors affecting the calculations are the unceratinties in evaluating the scattering amplitude at high energies, and also the use of uncertain weak coupling constants (they have used weak coupling constants different from those of the DDH ones). Also they expected that the asymmetry will decrease with increasing the energy.

In 1984 three attempts were introduced. The first one was by Miller (MIb84) based on the quark model, but these results were opposite in sign comparison to the the experimental results. Calculations by Nardulli and Prestone, including 2π-exchange, were normalized to agree with the experimental data in this range. The third calculations were introduced by Singh and Ahmed (SIb84). It was carried out using Glauber theory and meson exchange potential model with the use of two different sets of weak coupling constants, for the high energy range (the number introduced in table IV.6 was calculated using DDH parameters). Their result disagrees with the experimental value and they expected that this discripancydue to the need of including the electromagnetic and strong distortions and the inelastic channels as well.

In 1985 another calculation were carried out by Musakhanov and Israliov

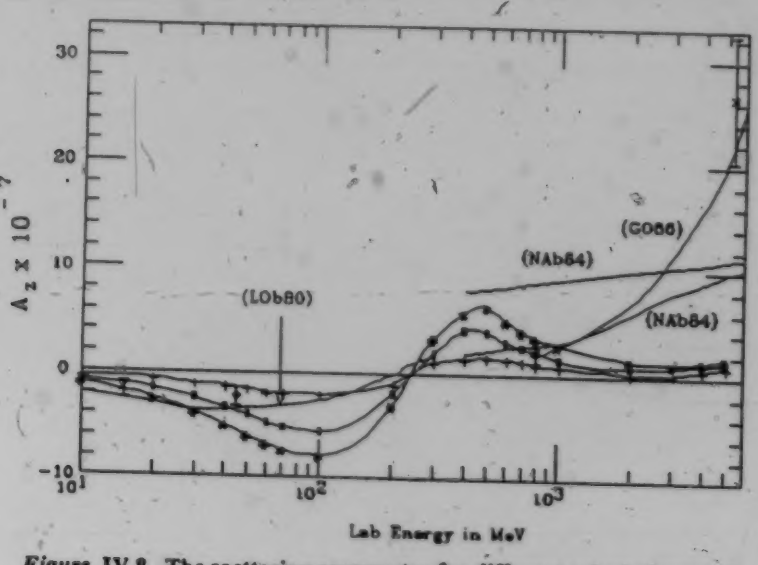

***Figure* IV.8. The sacttering asymmetry for different calculations and experiments. * for the Z-boson exchange (Ok81), • for the use of DDH parameters (OK81), and + for the QCD model (OK81).**

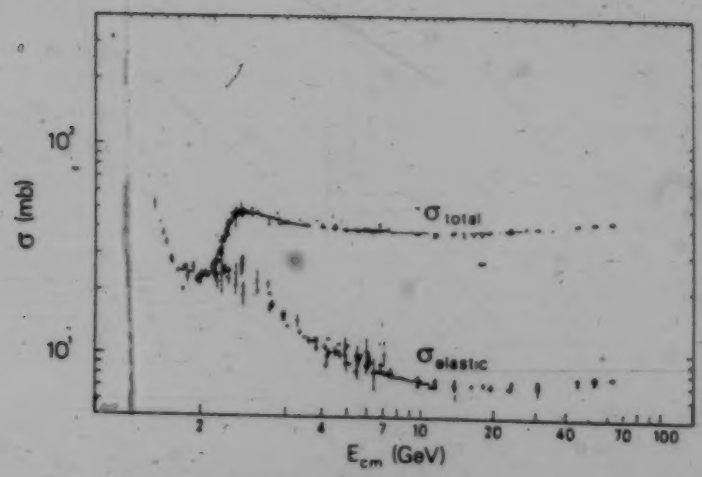

***Figure* IV.9. Comparison between elastic and total cross sections contributions for the pp interaction (AG86).**

(MU85) for the energies 25 MeV and 50 MeV (see table IV.x) using a field theoretic approaches.

In 1986 two different calculations were reported. The first one were by Musakhanov (MU86) using two different potentials and two different sets of weak coupling constants were reported in (AD85) and (ZD83) (see table IV.5). The results achieved have a good agreement with experiment for the 15 MeV data by using the Paris potential and the DDH parameters and without including the 2π-exchange. The 45 MeV has the best agreement with the experiment, which was obtained using the Paris potential and DDH or DZ parameters, including 2π-exchange. The second set of calculations were introduced by Goldmann and Preston (GO86) using the quark model, and they have normalized their calculations to agree with the experimental results agree. Their results disagrees with the experimental result and they concluded that this may be because of ignoring the contribution of the inelastic channels. They also expected that the asymmetry will increase with increasing energy.

In 1987 two calculations were reported. The first one was performed by Simonius (SIa87a) introduced calculations using Reid soft core and the Paris potentials,for the low energy range, including only the scattering amplitudes $^1S_0$-$^3P_0$ and $^3P_2$-$^1D_2$. He achieved the second best agreement with the experiment for the 15 MeV and 45 MeV with the use of the Paris potential. Calculations by Simonius and Unger (SIa87b) for the high energy range, were based on the quark-diquark model.

Table IV.7
Contributions of 2π and $2\pi+\rho+\omega$ exchanges to the asymmetry $A_{pp}.10^{-7}$

Potential and Lab Energy	Bag radius	DDH Parametrs 2π Bag model I*	2π Bag model II**	$2\pi+\rho+\omega$ Bag model I	$2\pi+\rho+\omega$ Bag model II	DZ Parameters 2π Bage model I	2π Bage model II	$2\pi+\rho+\omega$ Bag model I	$2\pi+\rho+\omega$ Bag model II
Reid s.c.	1.0	0.31	0.58	-0.69	-0.42	0.09	0.17	-0.78	-0.70
15 MeV	0.8	0.54	0.94	-0.46	-0.06	0.15	0.27	-0.72	-0.60
	0.6	0.97	1.30	-0.03	0.30	0.28	0.37	-0.59	-0.50
	0.4	1.57	1.66	0.57	0.66	0.45	0.47	-0.42	-0.40
Paris	1.0	0.31	0.60	-1.08	-0.79	0.09	0.17	-1.12	-1.04
15 MeV	0.8	0.55	0.98	-0.84	-0.41	0.16	0.28	-1.05	-0.93
	0.6	1.02	1.42	-0.37	0.03	0.29	0.40	-0.92	-0.81
	0.4	1.75	2.00	0.36	0.61	0.50	0.60	-0.71	-0.61
Reid s.c.	1.0	0.47	1.01	-1.59	-1.05	0.13	0.29	-1.66	-1.50
45 MeV	0.8	0.91	1.76	-1.15	-0.30	0.26	0.50	-1.53	-1.29
	0.6	1.78	2.53	-0.28	0.47	0.51	0.72	-1.28	-1.07
	0.4	3.09	3.32	1.03	1.26	0.88	0.96	-0.91	-0.83
Paris	1.0	0.48	1.04	-2.48	-1.92	0.14	0.30	-2.37	2.21
45 MeV	0.8	0.96	1.83	-2.00	-1.13	0.27	0.52	-2.24	-1.99
	0.6	1.88	2.77	-1.08	-0.19	0.54	0.79	-1.97	-1.72
	0.4	3.47	4.04	0.51	1.08	0.99	1.15	-1.52	-1.36

* without including two-pion-exchange.
** with including two-pion-exchange.

The results reported disagrees with the experimental value. Those authors concluded that the total asymmetry will decrease with increasing energy.

IV.6. The Scattering Asymmetry and the Weak Coupling Constants

Table IV.5 shows three different sets of the weak coupling constants. The first is deriven from field theory, and it was claimed that all of them should have a negative sign. The second set was introduced in 1981 and it could be seen that they have different signs and they differ in magnitude from the first set. In 1983 a second set was introduced again derived from field theory. These, however, have the same sign as the first set but differ in magnitude.

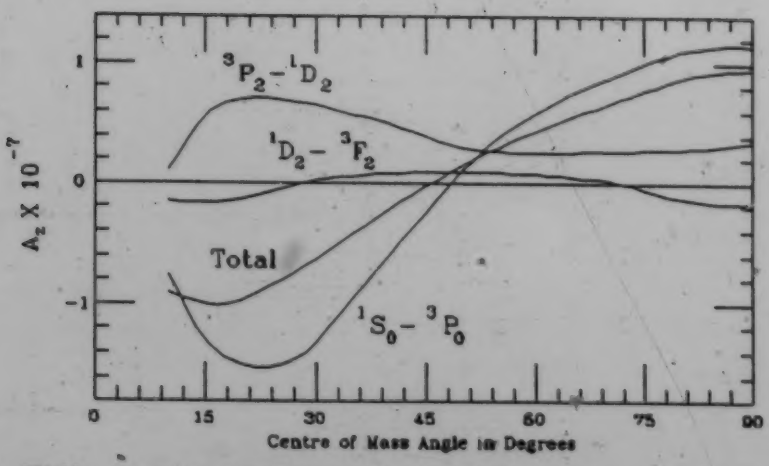

Figure IV.10. Angular distribution for the scattering asymmetry at 230 MeV for the major contributions to the asymmetry.

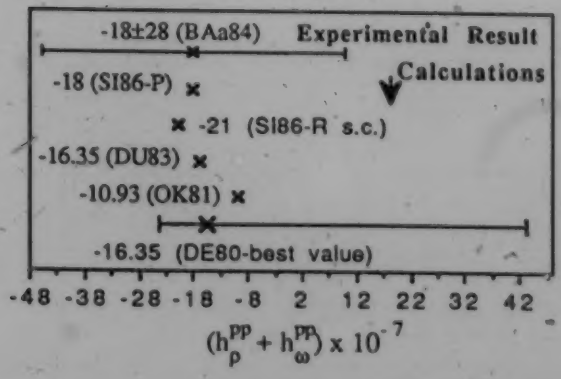

Figure IV.11. Comparison between experimental results ans calculations for the weak coupling constants satisfying equations (IV.11b and c) (see table IV.6).

In figure (IV.11) we show a comparison between the additive coupling constants $h_\rho^{pp} + h_\omega^{pp}$ resulting from these sets (which satisfy equations (V.11b and c)) and results by Simonius (using the first two scattering amplitudes only). It seems that all of them are in agreement with each other and with the experimental value with the error bars. From table IV.6 and equation (IV.11a) we can see that it does not matter what the individual values of parameters (for pp scattering) are, or even their

individual additive behavior (i.e. h_ρ^{pp} or h_ω^{pp} alone), since they add finally to a number agreeing in sign and approximately in magnitude and giving the same accuracy for the measured scattering asymmetry. We should note that the results that Simonius had were based on the experimental result $A_z=(-1.3\pm2.3)\times10^{-7}$ (BAa84), a new result (KI87) was published recently for the same experiment and gives $A_z=(-1.5\pm0.22)\times10^{-7}$.

CHAPTER V

CONCLUSION

Based on the previous discussion, one can classify theoretical methods for calculating the PNC effects into two different classes, the first one is microscopic approach which starts from the field theory of weak interactions, and the second one is via phenomenological approach based on the theoretical fits to experimental data.

Currently, I am carrying out calculations for such pp interaction at intermediate energies range using plane wave approximation. But their are many difficulties to clear first, e.g., first, the coupling constants, in which there are three sets use, it was concluded that the DZ ones are tricky because of the quark masses that have been used to deducted those coupling constants (HA87), second, the two pion exchange and what amount of contribution they will have for such a reaction (may be 10~20% SIa87a).

REFERENCES

(AD75) Adelberger, E. G. et al., Phy. Rev. Lett. 34 (1975) 402.

(AD85) Adelberger, E. G. and Haxton, W. C., Ann. Rev. Nucl. Part. Sc., 35 (1985) 501.

(AE77) Aebischer, D. et al., Nucl. Phys. A276 (1977) 445.

(AG86) Aguilar-Benitez, M. et al., Phys. Lett. 170B (1986) 89.

(APa76) Apagyi, B. et al., Nucl. Phys. A272 (1976) 303, 317.

(APb83) Aprile, E. et al., Phys. Rev. D 28 (1983) 21.

(APb86) Aprile, E. et al., Phys. Rev. D 34 (1986) 2566.

(AR87) Arndt, R. A. et al., Phys. Rev. D 35 (1987) 128.

(AU84) Auer, I. P. et al., Phys. Rev. D 29 (1984) 2435.

(BAa84) Balzer, R. et al., Phys. Rev. C 30 (1984) 1409.

(BAb81) Barroso, A. and Tadic', D., Nucl. Phys. A364 (1981) 194.

(BAc61) Barton, G., Nuvo Cimento, 19 (1961) 512.

(BE80a) Besset, D. et al., Phys. Rev. D 21 (1980) 580.

(BE80b) Besset, D et al., Nucl. Phys. A345 (1980) 435.

(BH83) Bhatia, T. S., Preprint Lampf LA-UR-84-675, pp. 27, 1983.

(BL60a) Blin-Stoyle, R. J., Phys. Rev. 118 (1961) 286.

(BL60b) Blin-Stoyle, R. J., Phys. Rev. 120 (1961) 184.

(BO76a) Box, M. A. et al., J. Phys. G. 2 (1976) L107.

(BO76b) Box, M. A. et al., Nucl. Phys. A271 (1976) 412.

(BR73) Brown, V. R. et al., Phys. Rev. Lett. 30 (1973) 770.

(BR74) Brown, V. R. et al., Phys. Rev. C 9 (1974) 935.

(BY78) Bystricky, J. et al., I. Phys. 39 (1987) 1.

(BY85) Bystricky, J. et al., Nucl. Phys. B262 (1985) 727.

(CAa63) Cabibbo, N., Phys. Rev. Lett. 10 (1963) 531.

(CAb77) Cavaignac, J. F. et al., Phys. Lett. 67B (1977) 148.

(CH74) Chemtob, M. and Desplanques, B., Nucl. Phys. B78 (1974) 139.

(CL80) Clough, A. S. et al., Phys. Rev. C 21 (1980) 988.

(CR76) Craver, B. A. et al., Phys. Rev. D 13 (1976) 1376.

(CU77) Cung, V. K. and Kim, C. W., Phys. Lett. 68B (1977) 169.

(DA65) Danilov, G. S., Phys. Lett. 18 (1965) 40.

(DA71) Danilov, G. S., Phys. Lett. 35B (1971) 579.

(DA72) Danilov, G. S., Sov. J. Nucl. Phys. 14 (1972) 443.

(DE72) Desplanques, B., Phys. Lett. 41B (1972) 461.

(DE73) Desplanques, B., Phys. Lett. 47B (1973) 1614.

(DE78) Desplanques, B. and Missimer, J., Nucl. Phys. A300 (1978) 286.

(DE79) Desplanques, B. and Missimer, J., Phys. Lett. 84B (1979) 363.

(DE80) Desplanques, B., Donoghue, J. F. and Holstein, B. R., Ann. Phys. 124 (1980) 449.

(DU81) Dubovik, V. M. et al., Nucl. Phys. B182 (1981) 52.

(DU83) Reference no.6 in (MU86).

(EN63) Engles, E. Phys. Rev 129 (1963) 1858.

(EP75) Epstein, G. N. Phys. Lett. 55B (1975) 249.

(FE58) Feynmann, R. P. and Gell-Mann, M., Phys. Rev. 109 (1958) 193.

(GA73) Gari, M., Phys. Rep. 6C (1973) 317.

(GO86) Goldman, T. and Preston, D., Phys. Lett. 168B (1986) 415.

(HA87) Haxton, W., Symposium/workshop, On Parity Violation in Hadronic Systems, Tuimf, vancouver, 1987, to be published.

(HE69a) Henley, E. M., Ann. Rev. Nucl.Sc. 19 (1969) 367.

(HE69b) Henley, E. M. et al., Phys. Rev. Lett. 23 (1969) 941.

(HE75) Henley, E. M. et al., Phys. Rev. D 11 (1975) 605.

(HE78) Henley, E. M., J. Phys. Soc. Japan Supp. 44 (1978) 812.

(HO69) Hoshizaki, N., Prog. Theo. Phys. Supp. 42 (1969) 107.

(KI87) Kistryn, S. et al., Phys. Rev. Lett. 58 (1987) 1616.

(KO81) Kopeliovich, V. B., Sov. J. Usp. 24 (1981) 717.

(LA74) Lassey, K. R. and McKellar, B. H. J, Aus. J. Phys. 27 (1974) 637.

(LEa56) Lee, T. P. and Yang, C. N., Phys. Rev. 104 (1956) 254.

(LEb79) Levinger, J. S., Phys. Lett. 82B (1979) 181.

(LOa72) Lobashov, V. M. et al., Nucl. Phys. A197 (1972) 241.

(LOb81) Lobov, G. A., IETP lett. 32 (1981) 65.

(LOc84) Lockyer, N. et al., Phys. Rev. D 30 (1984) 860.

(MA86) Marshall, J. A. et al., Phys. Rev. C 34 (1986) 1433.

(MIa81) Miller, G. A., Int. Rev. of Nucl. Phys., ed. Weise, W., 1 (1984) 273.

(MIb76) Missimer, J. Phys. Rev. C 14 (1976) 347.

(MU85) Musakhanov, M. M. and Israilov, Z. Z., Z. Phys. C. 27 (1985) 501.

(MU86) Musakhanov, N. M., Sov. J. Nucl. Phys. 44 (1986) 459.

(NAa78) Nagel, D. et al., AIP Conf. Proc. 51 (1978) 224.

(NAb84) Nardulii, G. et al., Phys. Lett. 137B (1984) 111.

(NE74) Neubeck, K. et al., Phys. Rev. C 10 (1974) 320.

(OK81) Oka, T., Prog. Theo. Phys. 66 (1981) 977.

(PA87) Page, S., Proc. 24th Western Regional Nucl. Phys. Conf., Alberta, canada, 1987.

(SIa72) Simonius, M., Phys. Lett. 41B (1972) 415.

(SIa74) Simonius, M., Nucl. Phys. A220 (1974) 269.

(SIa81) Simonius, M., Proc. of the 1980 Inter. Sympo., Lausanne, eds. Joseph c., and Soffer J., (1981) 335.

(SIa83a) Simonius, M., AIP Conf. Proc. 95 (1983) 139.

(SIa83b) Simonius, M., Nucl. Phys. A396 (1983) 203c.

(SIa86) Simonius, M., AIP Conf. Lake Louise, Alberta, 1986, to be published.

(SIa87a) Simonius, M., Symposium/workshop, On Parity Violation in Hadronic Systems, Tuimf, vancouver, 1987, to be published.

(SIa87b) Simonius, M. and Unger, L., Phys. Lett. 198B (1987) 547.

(SIb84) Singh, S. K. and Ahmed, I., Phys. Lett. 143B (1984) 10.

(PI73) Pirner, H. J. and Resika, D. O., Phys. Lett. 44B (1973) 151.

(SP87) Spinka , S., Preprint, Lampf LA-UR-84-2031, pp. 12, 1987.

(ST57) Stapp, H. P. et al., Phys. Rev 105 (1957) 302.

(TA78) Tadic', D. and Barroso, A., Nucl. Phys. A294 (1978) 376.

(TH81) Thomas, A. W. and Theberge, S., Phys. Rev. D. 24 (1981) 216.

(WI58) Wilkinson, D. H., Phys. Rev. 109 (1958) 1603, 1610, 1614.

(WO52) Wolfenstein, L. and Askin, S., Phys. Rev. 85 (1952) 947.

(WO54) Wolfenstein, L., Phys. Rev. 96 (1954) 1654.

(WO56) Wolfenstein, L., Ann. Rev. Nucl. Sc. 6 (1956) 43.

(WR68) Wright, S. C. et al., Phys. Rev. 175 (1968) 1704.

(YUa86) Yuan, V. et al., Phys. Rev. Lett. 57 (1986) 1680.

(YUb35) Yukawa, H., Prog. Phys. Math. Soc. Japan 17 (1935) 48.

VITA

NAME: Khaled Ezzat Ahmed Negm

PLACE OF BIRTH: Cairo, Egypt.

YEAR OF BIRTH: 1962.

POST-SECONDARY EDUCATION:

1. May 1983: Honour B.Sc. in Physics, Department of Physics, Faculty of Science, Ain Shams University, Cairo, Egypt.
2. Dec. 1987: M.Sc. in Nuclear Physics, Department of Physics, University of Alberta, Alberta, Canada.

HONOURS AND AWARDS:

1. June 1973: First Honour Excellence Degree in Mathematics, Ministry of Education, Cairo, Egypt.
2. June 1976: First Honour Excellence degree in Mathematics, Ministry of Education, Cairo, Egypt.
3. Sept. 1979 to May 1983: Ain Shams University Undergraduate Scholarship.
4. Dec. 1980: First Honour Medal Prize in Science Competition, Faculty of Science, Ain Shams University, Cairo, Egypt.
5. Dec. 1981: First Honour Medal Prize in Science Competition, Faculty of Science, Ain Shams University, Cairo, Egypt.
6. Dec. 1982: First Honour Medal Prize in Science Competition, Faculty of Science, Ain Shams University, Cairo, Egypt.

7. April 1983: Honour Excellent Award for the B.Sc. Graduating Research, Faculty of Science, Cairo, Egypt.
8. Sept. 1983: Ain Shams University Graduate Fellowship, Ain Shams University, Cairo, Egypt.
9. Dec. 1983: First Honour Medal Prize in Science Competition, Faculty of Science, Ain Shams University, Cairo, Egypt.
10. Jan 1985: D.S.M. Ministry of Defense, Cairo, Egypt.

RELATED WORK EXPERIENCE:

1. June 1982 to Sept. 1982: Traineeship in Institute fur Angewadte Physik der Universtat Munster (Institute of Solid State Physics, University of Munster), Munster, West Germany.
2. Sept. 1983: Appointed as a Research and Teaching Instructor (Staff Memeber), Physics Department, Faculty of Science, Ain Shams University, Cairo, Egypt.
3. Oct. 1983 to Jan. 1985: Teaching Assistant, Department of Physics, Military Technical Collage, Cairo, Egypt (part of Military Service).
4. Oct. 1983 to Jan. 1985: Part-Time Research Assistant, Department of Metallurgy, Military Technical Collage, Cairo, Egypt (part of Military Service).
5. Sept. 1985: Research and Teaching Assistant, Department of Physics and Nuclear Research Centre, University of Alberta, Alberta, Canada.